TECHNISCHE UNIVERSITÄT MÜNCHEN
TUM School of Engineering and Design

Methodology for Enabling Active Vibration Control Systems of Machine Tools for Industrial Use

Robin Karl-Hermann Kleinwort

Vollständiger Abdruck der von der Fakultät für Maschinenwesen der Technischen Universität München zur Erlangung des akademischen Grades eines

Doktors der Ingenieurwissenschaften (Dr.-Ing.)

genehmigten Dissertation.

Vorsitzender: Prof. Dr. ir. Daniel J. Rixen

Prüfer der Dissertation:

1. Prof. Dr.-Ing. Michael F. Zäh
2. Prof. Kaan Erkorkmaz, Ph.D.

Die Dissertation wurde am 22.07.2021 bei der Technischen Universität München eingereicht und durch die TUM School of Engineering and Design am 29.11.2021 angenommen.

Contents

Notation, Symbols and Abbreviations

Abbreviations

ADC	analogue to digital converter
AMB	active magnetic bearing
ANC	active noise cancellation
AVC	active vibration control
CNC	computerized numerical control
CSSV	continuous spindle speed variation
DAC	digital to analogue converter
DAF	direct acceleration feedback
DDE	delayed differential equation
DelPF	delayed position feedback
DelAF	delayed acceleration feedback
DOC	depth of cut
DPF	direct position feedback
DSP	digital signal processor
DVF	direct velocity feedback
e.g.	abbreviation for the Latin phrase "exempli gratia", meaning “for example”
Eq.	equation
FAAC	frequency amplitude assurance criterion
FE	Finite Element
Fig.	figure
FIR	finite impulse response
FRAC	frequency response assurance criterion
FRF	frequency response function
FxLMS	filtered-x least mean squares
i.e.	short for the Latin phrase "id est", meaning “that is”
IEPE	Integrated Electronics Piezo Electric
LMS	least mean squares
LTI	linear time invariant
LTV	linear time variant
MbVF	model-based velocity feedback

MDOF	multiple-degree-of-freedom
MICA	moving iron controllable actuator
MIMO	multi-input-multi-output
LQG	linear-quadratic-Gaussian (regulator)
PID	proportional-integral-derivative
PLC	programmable logic controller
PRBS	pseudo random binary signal
PSO	particle swarm optimization
PZT	piezoelectric lead zirconate titanate
RLS	recursive least squares
SDOF	single-degree-of-freedom
Sec.	section
SISO	single-input-single-output
SLD	stability lobe diagram
SSS	spindle speed selection
Tab.	table
TCP	tool center point
TMD	tuned mass damper
TRL	technology readiness level
VDI	abbreviation for the association of German engineers (Verein Deutscher Ingenieure)

Notation

s	scalar
$\boldsymbol{v}$	vector
$\boldsymbol{M}$	matrix
$\mathbf{0}$	zero vector
$\boldsymbol{v}^T;\boldsymbol{M}^T$	transposed vector or matrix
$\boldsymbol{v}^*;\boldsymbol{M}^*$	conjugated complex vector or matrix
$\boldsymbol{M}^{-1}$	inverse matrix
$\frac{\partial}{\partial \boldsymbol{w}(n)}$	first derivative after $\boldsymbol{w}$
$\dot{x}(t)$	first time derivative of $x(t)$
$\ddot{x}(t)$	second time derivative of $x(t)$
$\lvert\ \rvert$	absolute value
$\lVert\ \rVert_2$	euclidean norm

$\| \|_\infty$	infinity norm, also known as uniform norm or supremum norm
$\mu(\ )$	structured singular value μ
max	maximum value

Symbols[1]

Latin Symbols

$\hat{\boldsymbol{A}}$	system matrix of a state space system
A_m	gain margin
a_{notch}	frequency band of a notch filter in $\mathrm{rad\,s^{-1}}$
a_p	depth of cut in m
$a_{p,lim}$	maximum stable depth of cut in m
$\hat{\boldsymbol{B}}$	input matrix of a state space system
$\boldsymbol{B_m}$	modal input matrix
$\boldsymbol{C}$	controller feedback matrix
$\hat{\boldsymbol{C}}$	output matrix of a state space system
$C(s)$	controller transfer function
C_{AVC}	investment costs for the hardware of an active vibration control system in €
C_{setup}	setup/commissioning costs in €
C_{total}	production costs per workpiece in €
$\boldsymbol{D}$	damping matrix in $\mathrm{N\,m^{-1}}$
$\hat{\boldsymbol{D}}$	feedthrough matrix of a state space system
$\boldsymbol{D_m}$	modal damping matrix in $\mathrm{N\,s\,m^{-1}}$
d	damping of a damping element in $\mathrm{N\,s\,m^{-1}}$
d_A	damping of an actuator damping element in $\mathrm{N\,s\,m^{-1}}$
$d_i(t)$	disturbance signal at the system input
$\tilde{d}_i(t)$	performance channel input related to the disturbance signal at the system input
$d_o(t)$	disturbance signal at the system output
$\boldsymbol{E}$	influence matrix describing the nodal degrees of freedom
$e(n)$	time-discrete error signal in $\mathrm{m\,s^{-2}}$ or V

[1] The units usually refer to the translational direction.

$e(t)$	error signal in $\mathrm{m\,s^{-2}}$ or V
$\tilde{e}(t)$	performance channel output related to the error signal in $\mathrm{m\,s^{-2}}$ or V
$\boldsymbol{F}(t)$	force vector in N
F_A	actuator force in N
F_f	cutting force in feed direction in N
F_L	Lorentz force in N
F_o	open-loop transfer function
F_r	cutting force in radial direction in N
F_t	cutting force in tangential direction in N
$\hat{\boldsymbol{f}}$	vector of the nodal degrees of freedom at the actuator position
f_a	frequency at the first half-power point in Hz
f_b	frequency at the second half-power point in Hz
f_c	chatter frequency in Hz
f_m	modeled natural frequency in Hz
Δf_{max}	maximum frequency band in Hz
Δf_{min}	minimum frequency band in Hz
f_n	natural frequency in Hz
f_{TCP}	cutting force at the TCP in x, y, or z direction in N
f_z	tooth passing frequency in Hz
$G(s)$	transfer function of a controlled system
$\hat{G}(s)$	measured perturbations of $G(s)$
$G(z)$	time-discrete transfer function of a controlled system
$\hat{G}(z)$	time-discrete estimation of $G(z)$
$G_A(s)$	actuator transfer function in $\mathrm{N\,V^{-1}}$
$G_{AComp}(s)$	compensation filter for an actuator's transfer function
G_{HP}	transfer function of a high pass filter
$G_n(s)$	nominal transfer function of a controlled system
G_{notch}	transfer function of a notch filter
G_{ref}	measured frequency response function
G_{sys}	synthesized frequency response function
g_A	cumulated gain of an actuator and power amplifier
g_C	controller gain
$H(s)$	frequency response function of a mechanical structure in $\mathrm{m\,N^{-1}}$ or $\mathrm{m\,N^{-1}\,s^{-2}}$
$h(t)$	dynamic chip thickness in m
h_0	constant chip thickness in m

$\boldsymbol{I}$	identity matrix
i	electric current in A
J	cost function of a linear quadratic regulator
j	imaginary unit
k	stiffness of a spring in $\mathrm{N\,m^{-1}}$
k_A	stiffness of an actuator spring in $\mathrm{N\,m^{-1}}$
$\boldsymbol{K}$	controller feedback matrix
K_{fc}	cutting force coefficient in feed direction in $\mathrm{N\,mm^{-2}}$
K_{rc}	cutting force coefficient in radial direction in $\mathrm{N\,mm^{-2}}$
K_{tc}	cutting force coefficient in tangential direction in $\mathrm{N\,mm^{-2}}$
K_{fe}	edge force coefficient in feed direction in $\mathrm{N\,mm^{-1}}$
K_{re}	edge force coefficient in radial direction in $\mathrm{N\,mm^{-1}}$
K_{te}	edge force coefficient in tangential direction in $\mathrm{N\,mm^{-1}}$
$K_{f1.1}$	specific cutting force coefficient for $a_p = 1$ mm and $h = 1$ mm in feed direction in $\mathrm{N\,mm^{-2}}$
$K_{r1.1}$	specific cutting force coefficient for $a_p = 1$ mm and $h = 1$ mm in radial direction in $\mathrm{N\,mm^{-2}}$
$K_{t1.1}$	specific cutting force coefficient for $a_p = 1$ mm and $h = 1$ mm in tangential direction in $\mathrm{N\,mm^{-2}}$
$\boldsymbol{K}$	stiffness matrix in $\mathrm{N\,m^{-1}}$
$\boldsymbol{K_m}$	modal stiffness matrix in $\mathrm{N\,m^{-1}}$
$\boldsymbol{L}$	Kalman filter feedback matrix
l	number of FIR filter coefficients
$\boldsymbol{M}$	mass matrix in kg
m	mass in kg
m_A	inertial mass of an actuator in kg
m_f	power value of the specific cutting force in feed direction
m_r	power value of the specific cutting force in radial direction
m_t	power value of the specific cutting force in tangential direction
N	rotational spindle speed in $\mathrm{min^{-1}}$ (rpm-rate)
n	discrete time sample
n_d	number of physical degrees of freedom
$\boldsymbol{P}$	matrix containing the algebraic solution of the Ricatti equation
$\boldsymbol{P_r}(s)$	weighted transfer function matrix with the performance specifications
p_{leak}	leaking integrator variable
$\boldsymbol{Q}$	weighting matrix of the states

$\boldsymbol{q_m}(t)$	displacement vector in modal coordinates
q_1	columns of M_{11} and M_{21}
q_2	columns of M_{12} and M_{22}
$\boldsymbol{R}$	weighting matrix of the inputs
$r(n)$	time-discrete control reference in $\mathrm{m\,s^{-2}}$ or V
$r(t)$	control reference in $\mathrm{m\,s^{-2}}$ or V
$\tilde{r}(t)$	performance channel input related to the control reference signal in $\mathrm{m\,s^{-2}}$ or V
$r(j\omega)$	uncertainty radius within the Nyquist plot
$\boldsymbol{S}$	substitution matrix
$S_c(s)$	sensitivity function
s	Laplace variable
T	delay time in s
T_A	delay time of the AVC hardware in s
$T_c(s)$	complementary sensitivity function
$\boldsymbol{T_{zw}}(s)$	performance channel transfer function matrix
t	time in s
t_{be}	time until breakeven is reached in s
t_{cot}	change-over time between two workpieces in s
t_{tct}	total cycle time of a workpiece in s
$t_{tct,AVC}$	total cycle time of a workpiece produced with active vibration control in s
$u(t)$	control output in V
$\hat{\boldsymbol{u}}(t)$	input vector of a state space system
$\tilde{u}(t)$	performance channel output related to the control output in V
$u(n)$	time-discrete control output in $\mathrm{m\,s^{-2}}$ or V
$u'(n)$	time-discrete modified control output in $\mathrm{m\,s^{-2}}$ or V
$W_d(s)$	weighting transfer function for the disturbance signal $\tilde{d}_i(t)$
$W_e(s)$	weighting transfer function for the error signal $\tilde{e}(t)$
$W_m(s)$	weighting transfer function of the unstructured multiplicative uncertainties
$W_r(s)$	weighting transfer function for the control reference $\tilde{r}(t)$
$W_u(s)$	weighting transfer function for the control output $\tilde{u}(t)$
$W(z)$	time-discrete FIR filter
$\boldsymbol{w}(n)$	time-discrete FIR coefficient vector
$\boldsymbol{w}(t)$	performance channel input vector
$w_i(n)$	time-discrete element of the FIR coefficient vector

$x(n)$	time-discrete reference signal
$x(t)$	displacement in m
$\dot{x}(t)$	velocity in $\mathrm{m\,s^{-1}}$
$\ddot{x}(t)$	acceleration in $\mathrm{m\,s^{-2}}$
$\hat{\boldsymbol{x}}(t)$	state vector of a state space system
$\dot{\hat{\boldsymbol{x}}}(t)$	state vector of a state space system derived with respect to time
$\hat{\boldsymbol{x}}_{\boldsymbol{0}}$	starting value of the state vector $\hat{\boldsymbol{x}}(t)$
$x_f(n)$	time-discrete reference signal filtered by an estimation of the controlled system's transfer function
$\hat{\boldsymbol{x}}_{\boldsymbol{K}}(t)$	estimated state vector of a state space system
$\dot{\hat{\boldsymbol{x}}}_{\boldsymbol{K}}(t)$	estimated state vector of a state space system derived with respect to time
$\boldsymbol{x}_{\boldsymbol{TCP}}$	displacement vector at the TCP in m
x_{TCP}	displacement at the TCP in x, y, or z direction in m
$y(t)$	output of the controlled system in $\mathrm{m\,s^{-2}}$ or V
$\hat{\boldsymbol{y}}(t)$	output vector of a state space system
$y_K(t)$	estimated output of the controlled system in $\mathrm{m\,s^{-2}}$ or V
$y_u(n)$	time-discrete control output filtered by the transfer function of the controlled system in $\mathrm{m\,s^{-2}}$ or V
$y_v(n)$	time-discrete modeling signal filtered by the transfer function of the controlled system in $\mathrm{m\,s^{-2}}$ or V
$y_{u,v}(n)$	time-discrete modified control output filtered by the transfer function of the controlled system in $\mathrm{m\,s^{-2}}$ or V
$\hat{y}_v(n)$	time-discrete modeling output filtered by the estimated transfer function of the controlled system in $\mathrm{m\,s^{-2}}$ or V
$\hat{y}_u(n)$	time-discrete estimation of $y_u(n)$ in V
$y_x(n)$	time-discrete distortion signal in $\mathrm{m\,s^{-2}}$ or V
$\hat{y}_x(n)$	time-discrete estimation of $y_x(n)$ in V
Z	number of teeth of a tool
$\boldsymbol{Z_m}$	modal damping matrix
z	discrete time variable
$\boldsymbol{z}(t)$	performance channel output vector

Greek Symbols

γ	coherence
$\boldsymbol{\Delta}$	uncertainty matrix

$\Delta(s)$	normalized, stable, unstructured uncertainty transfer function
$\Delta_m(s)$	multiplicative uncertainty
ζ_i	modal damping value of mode i
ζ_A	damping ratio of an actuator
ζ_{Anew}	new damping ratio of an actuator with compensation filter
η	forgetting factor of the adaptive step size
$\eta^*(\rho)$	optimum forgetting factor of the adaptive step size
μ	step size of the LMS algorithm
ν	leakage factor of the LMS algorithm
ρ	adaptation parameter of the adaptive step size
$\upsilon(n)$	modeling signal for online identification
$\mathbf{\Phi}$	modal matrix
$\{\phi_i\}$	eigenvector of mode i
ϕ_m	phase margin in °
Ω	matrix of the natural frequencies in rad s^{-1}
ω	angular frequency in rad s^{-1}
ω_A	angular natural frequency of an actuator in rad s^{-1}
ω_{Anew}	new angular natural frequency of an actuator with compensation filter in rad s^{-1}
ω_c	angular chatter frequency in rad s^{-1}
ω_{hp}	angular cut-off frequency of a high-pass filter in rad s^{-1}
ω_{notch}	angular cut-off frequency of a notch filter in rad s^{-1}

Indices

A	actuator
c	chatter
G	controlled system
K	Kalman filter
k	run variable
TCP	tool center point
i	run variable
x	x direction
y	y direction
z	z direction

1 Introduction

1.1 Motivation and Objective

Driven by an increasing scarcity of resources as well as the change in climate and social values, the topic of sustainability now increasingly determines the thinking and actions of European companies (REITHOFER 2010). This is also shown by the European Commission's strategy for a more sustainable economy, which was announced at the beginning of 2020. The *European Green Deal* targets "a modern, resource-efficient and competitive economy, where there will be no net emissions of greenhouse gases in 2050 and where economic growth will be decoupled from resource use" (EUROPEAN COMMISSION 2019, p. 2). For the machine tool industry this leads to an increased demand for energy efficient machines. The energy efficiency of machine tools can be improved by lightweight design as well as by a reduction in machining times. Lightweight design reduces the mass of components and thus the kinematic energy required for acceleration (ZULAIKA ET AL. 2011). Unfortunately, consistent lightweight design also leads to lower damping values of the machine tool structure (SIMNOFSKE 2009; ZULAIKA ET AL. 2011). The machining time is governed by the maximum material removal rate, which is often not limited by the installed drive power, but by the dynamic compliance of the machine structure (HAASE 2005). Insufficient damping of the machine tool structure leads to process instabilities, so-called chatter vibrations (ALTINTAS 2012), which in turn cause significantly increased tool wear (KAYHAN & BUDAK 2016), high noise pollution (CHENG 2009), and damage to the workpiece and machine components (ALTINTAS 2012). To improve process stability, the damping behavior of the machine structure must be increased (MERRIT 1965). Having high damping values of the machine elements that carry the load of the cutting force is also desirable in order to achieve high machining quality (WECK & BRECHER 2006a; ALTINTAS 2012). Hence, both measures for energy efficiency improvement, lightweight design and machining time reduction, are competing with each other. A possible solution to this conflict is active vibration control (AVC), which can increase the chatter stability by significantly improving the damping behavior of machine tools (SIMNOFSKE 2009; ZULAIKA ET AL. 2011).

Besides the avoidance of greenhouse gas emissions, further targets of the European Green Deal are reduced waste and resource use. Hence, the *circular economy action plan* focuses on measures to encourage businesses to offer sustainable products (EUROPEAN COMMISSION 2020). One possibility to achieve these goals is to retrofit existing machines with upgrades to enhance their life span and performance. By using AVC systems, some of these targets can be achieved, since existing machines often do not fully utilize the installed drive power. Consequently, an unproductive or noncompetitive machine can be made competitive again by implementing an AVC system (BOLDERING 2015). Using an AVC system to restore the competitiveness of

an existing machine instead of purchasing a new one reduces resource consumption and waste.

Despite major research efforts and their promising results, very few commercial machine tool systems have integrated AVC so far (NEUGEBAUER ET AL. 2007; PARK ET AL. 2007; MUNOA ET AL. 2016a). Entry barriers for industrial use are the high costs for the development of active systems and a lack of the multidisciplinary expert knowledge required for design and commissioning (SIMNOFSKE 2009; BAUR 2014; BOLDERING 2015). In particular serial and parallel actuators, which are integrated in the force flux, require extensive adjustments of the machine design during integration (EHMANN 2004). Proof-mass actuators, on the other hand, are characterized by their simple attachment to the structure which is to be damped (WAIBEL 2012). To reduce development and commissioning costs even further, BAUR (2014) and JALIZI (2015) advised using commercially available components. Past research focused on the hardware and software design of AVC systems, proof of functionality, and comprehensive investigation of the operating behavior. Industrial use (DANOBATGROUP 2017, 2019) proves that AVC systems can achieve high robustness and reliability. Nevertheless, the efforts needed for design and commissioning of AVC systems must be further reduced, especially to enable a simple retrofit solution for end users. Up to today, these tasks require, among others, a great deal of expertise in the areas of machine dynamics, measurement, and control engineering, which is not always available to machine tool manufacturers and, even less likely, end users (BOLDERING 2015).

The objective of this thesis is to develop a methodology that reduces the effort needed for the design and commissioning of AVC systems in order to simplify their application to machine tools. Due to their simple installation and flexible applicability, this research work focuses on the use of proof-mass actuators, which have been successfully applied by several researchers and have demonstrated their robustness in industrial application (MUNOA ET AL. 2016a).

The present work is a publication-based dissertation comprising seven publications with the main research results. In Chapter 2, a literature review is presented first, from which the objectives and the methodology are derived in Chapter 3. Summaries of the publications are presented in Chapter 4. Afterwards, the results are evaluated in Chapter 5. This dissertation concludes with a summary and an outlook in Chapter 6.

2 Background and Literature Review

2.1 Machine Tool Vibrations and Process Stability

During machining, dynamic vibrations often limit the achievable quality and productivity. This section will give an overview of the different vibration types and briefly present the theory of process stability in machining.

2.1.1 Classification of Machine Tool Vibrations

The different kinds of vibrations that occur during machining can be classified into *forced* and *self-excited vibrations*.

An external excitation of the machine tool causes *forced vibrations*. These are separated into *free* and *periodic vibrations*. *Free vibrations* are caused by an impulse excitation and occur, for example, due to high acceleration and jerk of the feed drives or external forces that act on the machine tool structure through the foundation (WECK & BRECHER 2006c). Another characteristic of free vibrations is that their response contains all natural frequencies. Since the mechanical structure is damped, free vibrations always decay. Tooth-passing in milling and shaft runout of the spindle and tool cause periodic excitation forces (WECK & BRECHER 2006c). These lead to a *periodic vibration* response at the excitation frequency. The closer the excitation frequency is to a natural frequency of the system, the higher is the vibration response amplitude.

The interaction of the machining process with the structural dynamics of a machine tool and a workpiece can lead to *self-excited vibrations*, also called *chatter*. This results in a vibration response at one or more natural frequencies of the mechanical structure. According to ALTINTAS (2012), there are two main mechanisms that lead to chatter: the *regenerative effect* and *mode-coupling*. The regenerative effect occurs more often and can easily be modeled. However, if the cross-coupling of vibration modes is considered within the cross-diagonal elements of the dynamic matrices, the regenerative effect model inherently covers mode-coupling, too (ALTINTAS 2012). Hence, the following section will briefly summarize the most commonly applied stability model for regenerative chatter vibrations.

2.1.2 Regenerative Chatter

The famous researcher Frederick Winslow Taylor described chatter as “the most obscure and delicate of all problems facing the machinist” (TAYLOR 1907, p. 148). In 1955, LYSEN (1955) already recognized that instability in machining processes is based

on the dependence of cutting speed and depth of cut, as well as on the regenerative effect. Using slow motion recordings, EISELE & SADOWY (1955) also identified that the relationship between the tool and the workpiece movement affect the process stability. They could prove that the vibration mode during chatter corresponds to a natural vibration mode of the machine tool and that the chatter frequency is constant under the same cutting conditions. The first mathematical descriptions of the regenerative effect were developed by TOBIAS & FISHWICK (1958) and TLUSTY & POLACEK (1963) independently of each other. Both models describe the relation between the depth of cut (DOC) a_p, the structural dynamics of the machine tool, and the cutting coefficients. For the most simple case, the model for regenerative

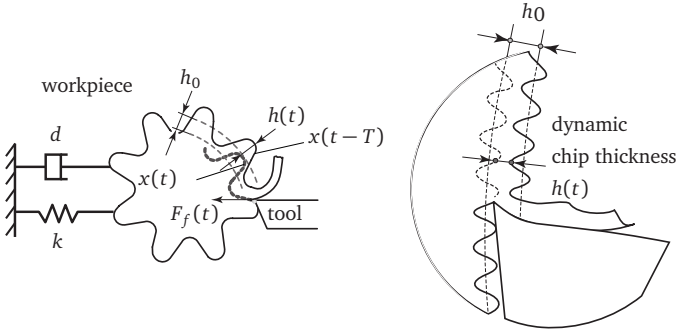

Fig. 2.1: Regenerative chatter vibrations in orthogonal cutting based on ALTINTAS (2012)

chatter is shown in Fig. 2.1. Assuming that a flat-faced orthogonal grooving tool is fed perpendicular to the axis of a rotating cylindrical shaft and vibrates in the feed direction, the resulting differential equation of motion can be expressed as

$$m\ddot{x}(t) + d\dot{x}(t) + kx(t) = F_f(t) = K_{fc} a_p \underbrace{[h_0 + x(t-T) - x(t)]}_{h(t)}. \tag{2.1}$$

The cutting force F_f in feed direction, which may contain perturbations, causes the tool to vibrate, which leaves a wavy surface on the workpiece behind. The tool is described by a single-degree-of-freedom (SDOF) system with the mass m, damping d, and stiffness k. The resulting dynamic chip thickness $h(t)$ depends on the constant chip thickness h_0, the current tool position $x(t)$, and the tool position during the previous revolution of cut $x(t-T)$. The cutting force in feed direction $F_f(t)$ is a function of the dynamic chip thickness $h(t)$, the cutting force coefficient in the feed direction K_{fc}, and the DOC a_p. The delay time T corresponds to one spindle revolution period. In a more general case, T refers to the period between the previous

and present tooth of the cutting tool and depends on the number of teeth Z as well as the rotational spindle speed N:

$$T = \frac{60\,\frac{s}{\mathrm{min}}}{NZ} \,. \tag{2.2}$$

If the delayed differential equation (DDE) for the simple case presented in Eq. 2.1 is solved, the maximum stable DOC $a_{p,lim}$ for the chatter frequency ω_c is

$$a_{p,lim} = \frac{-1}{2K_f H(s=\omega_c)} \,. \tag{2.3}$$

Here, $H(s)$ is the compliance frequency response function (FRF) of the SDOF system. Since the DOC is a physical quantity, the solution of Eq. 2.3 is valid only for negative values of the real part of $H(s)$ (ALTINTAS 2012). Using the above equation, a so-called stability lobe diagram (SLD) can be calculated, which displays the maximum stable DOC as a function of the rotational spindle speed N. An exemplary SLD is shown in Fig. 2.2.

Each parameter of the DDE influences the maximum stable DOC $a_{p,lim}$. Hence, several measures for increasing the chatter stability exist, as will be explained in the following section.

2.2 Chatter Suppression Techniques

Measures for the reduction of chatter vibrations increase the machine's productivity by improving the surface finishes and by prolonging the life of tools and mechanical components (MUNOA ET AL. 2016a). Increased productivity, production quality, and machine availability also lead to an improved overall equipment effectiveness (HANSEN 2001). Depending on the parameters of Eq. 2.1, MESCHKE (1995) and MUNOA ET AL. (2016a) classify the chatter suppression techniques in metal cutting into

- improved process parameter selection (a_p, T),
- regeneration disturbance (T),
- design optimization (m, k), and
- system damping enhancement (d).

Each of the measures presented in the following can be effective, and it is the relative position of the unstable process in the SLD that determines which measure should be preferred (MUNOA ET AL. 2016a). The relative position in the SLD is defined by the ratio between the chatter frequency f_c and the tooth passing frequency f_z:

$$\frac{f_c}{f_z} = \frac{60 f_c}{ZN} \,. \tag{2.4}$$

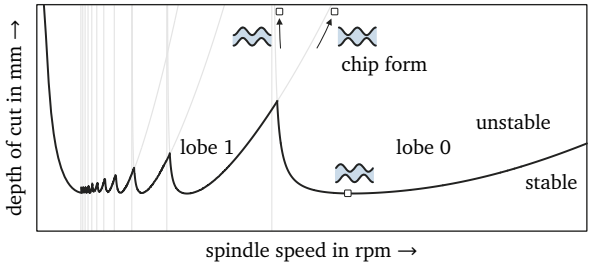

Fig. 2.2: Example of an SLD based on MUNOA ET AL. (2016a)

The tooth passing frequency f_z depends on the spindle speed N and the number of teeth Z on the tool. Physically, this ratio defines the number of complete waves per revolution produced on the workpiece surface. Hence, the first digit of this ratio also determines the stability lobe order. However, this ratio is only applicable if just one dominant mode exists that causes chatter. On a real system, several dominant eigenmodes can exist and for each eigenmode, a relative position on the SLD can be calculated (MUNOA ET AL. 2016a).

Recently, several authors have compared different chatter suppression techniques (JALIZI 2015; MUNOA ET AL. 2016a; ZHU & LIU 2020). The following sections will give a short overview of the different chatter suppression techniques, focusing on their applications and limitations.

2.2.1 Process Parameter Selection

The main idea of improved process parameter selection, in the following shortly called *process parameter selection*, is to choose a spindle speed N with a high but chatter-free depth of cut based on the SLD (URBIKAIN ET AL. 2015). This way, the resulting delay time T ensures that the chip thickness stays constant. Most popular is a measure called *spindle speed selection*, which is applied during the process planning phase (SMITH & TLUSTY 1992) and can also be easily automated for online process control (ALTINTAS & CHAN 1992; SMITH & TLUSTY 1992). Online spindle speed selection is also called *discrete spindle speed tuning* and is based on the assumption that only one dominant mode causes chatter (QUINTANA & CIURANA 2011). Based on a measured microphone or accelerometer signal, the chatter frequency f_c is determined. Then, the spindle speed N is changed accordingly to synchronize one of the harmonics of the tooth passing frequency with the chatter frequency. Several commercial solutions applying this measure exist, such as CHATTERPRO from MAL Inc., HARMONIZER from MLI, and BESTSPEED SYSTEM from KENNAMETAL.

Process parameter selection performs well in spindle speed ranges, where clear lobes appear when one dominant mode is present (MUNOA ET AL. 2016a). However, EYNIAN

(2014) states, that the calculation of the natural frequency from the measured chatter frequency is a challenging task. Milling experiments showed that even a 1 % error in the calculation of the natural frequency severely limits the usefulness of the predicted SLD.

Instead of choosing an optimum delay time T, the following section summarizes measures on how to vary this value in order to increase chatter stability.

2.2.2 Regeneration Disturbance

The regeneration effect can be disturbed by varying the delay T with the help of *special tool geometries* or *continuous spindle speed variation* (DOHNER ET AL. 2004).

Special Tool Geometries directly affect the time period between subsequent cutting edges of a milling process (MUNOA ET AL. 2016a). The most popular measures can be further classified into tools with *variable pitch angles*, *serrated profiles*, and different *helix angle variations* (see Fig. 2.3).

Variable pitch angles alter the phase between the past and the present vibration by creating multiple discrete delays depending on the actual edge position and the number of teeth (ALTINTAS ET AL. 1999). Hence, they do not increase the absolute stability limit, but are able to move the zone with clearly separated lobes to lower spindle speeds in order to obtain optimal stability and machinability in the same spindle speed range. Since chatter suppression is not assured with any arbitrary pitch distribution, a proper tuning of the pitch angle(s) is required for every process (ALTINTAS ET AL. 1999).

The wavy flutes of serrated cutters produce periodic variations in the local cutting edge radii and lead angle. Due to this special profile, serrated tools produce high surface roughness and cannot be used for finishing but for roughing operations only. The chatter stability increases if the chip thickness is smaller than the peak-to-peak amplitude of the serration profile (MERDOL & ALTINTAS 2004). In that case, some sections of the flutes do not have contact with the material and, as a result, the serrations attenuate the regeneration effect.

Non-constant or alternating helix angles lead to continuous changes in the local pitch angles along the tool axis, which varies the delay between the flutes and disturbs the regenerative effect (DOMBOVARI & STEPAN 2012). According to MUNOA ET AL. (2016a), variable helix tools can significantly increase the stability in high order stability lobes.

Continuous Spindle Speed Variation (CSSV) is another method of disturbing the regenerative effect and was first introduced by GRAB (1973). The nominal spindle speed N can be varied by a sinusoidal, triangular, rectangular, random, or continuous linear perturbation. In practice, the sinusoidal signal with a simple harmonic variation

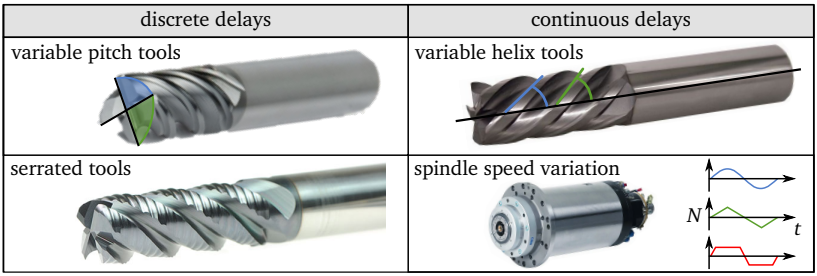

Fig. 2.3: Regeneration disturbance strategies based on MUNOA ET AL. (2016a)(image sources: CALLOYTOOL (2020); GMN (2020); LINK (2020); TRAVERSTOOL (2020))

is most often used (MERINO ET AL. 2019). To set up this technique, the amplitude and frequency of the perturbation signal need to be tuned. Both parameters are constrained by the power and dynamics of the spindle (ZATARAIN ET AL. 2008). For an optimal tuning, AL-REGIB ET AL. (2003) proposed a simple formula, but more exact solutions can be gained by complex simulation models (YAMATO ET AL. 2018; DONG & ZHANG 2019). The biggest advantage of CSSV, compared to the above measures for regeneration disturbance, is its flexibility because the parameters can be adapted easily for every new process (MUNOA ET AL. 2016a). According to ZATARAIN ET AL. (2008), CSSV is most effective at low spindle speed ranges, where small amplitudes of the perturbation signal can create large variations in the delay between successive waves. Hence, this methodology is mainly used in machining operations that run at low spindle speeds, such as turning and boring operations (MUNOA ET AL. 2016a), but it can also be applied to grinding (INASAKI ET AL. 2001) or milling operations at very low spindle speeds (BEDIAGA ET AL. 2011). At higher spindle speeds, CSSV is usually not applicable due to limited spindle power and dynamics (FAASEN 2007). Furthermore, CSSV introduces uneven patterns in the surface roughness caused by the rotational speed variation, which is not acceptable in some accurate finishing processes (INASAKI ET AL. 2001).

Besides the delay time T, the machine tool's compliance $H(s)$ has a significant effect on the chatter stability. The following section summarizes how the machine tool design can be optimized in order to increase chatter stability.

2.2.3 Design Optimization

During the design phase of a machine tool structure, its chatter stability properties can be mainly influenced by the damping behavior, which strongly depends on the joint design (WECK & BRECHER 2006a) and the material selection (MESCHKE 1995). As an example, sandwich structures with highly damped aluminum foam can be advantageous (MÖHRING ET AL. 2015). Using simulation tools, it is even possible to optimize

the structural properties of the machine to be developed. Numerical optimizations of machine tool designs are often based on Finite Element (FE) models (ALTINTAS ET AL. 2005), which allow for dynamic properties such as natural frequencies and mode shapes to be estimated with reasonable accuracy. However, the estimation of damping parameters is still challenging (SCHWARZ 2015). As a result, "machine designers mainly focus on increasing the static stiffness; and the result can lead to a rigid but poorly damped machine tool" (MUNOA ET AL. 2016a, p. 786). To overcome this drawback, SEMM ET AL. (2020) introduced an optimization methodology which considers local damping effects by using flexible multibody models. Due to the local damping models, damping- as well as stiffness-based optimization potentials are considered, enabling a holistic, numerical optimization of the dynamic behavior in arbitrary axis positions.

If design optimization is exhausted or already existing machine tools are to be improved, one last option can be the integration of dynamic auxiliary systems for damping enhancement, which are presented in the following section.

2.2.4 System Damping Enhancement

With Eq. 2.3, MERRIT (1965) showed that the stability limit is inversely proportional to the compliance of the machine tool structure for turning operations. Hence, *dynamic auxiliary systems* can be applied to the machine tool, the tool, or the workpiece in order to increase the chatter stability by damping the structure's critical eigenmode and thereby reducing the maximum compliance. Dynamic auxiliary systems can be classified into *passive*, *semi-active*, and *active* systems (BRECHER ET AL. 2013). Fig. 2.4 shows such systems attached to a SDOF system to be damped which possesses the parameters of mass m_1, stiffness k_1, and damping d_1.

Passive Systems achieve the damping effect by means of energy conversion into heat or relative movement between bodies (WECK & BRECHER 2006a). Thus, these systems do not require any external energy supply (MESCHKE 1995). *Impact dampers*, *friction dampers*, and *tuned mass dampers* (TMD) are an example for passive systems and are most often used in the field of machine tools (TELLBÜSCHER 1986; MESCHKE 1995).

Impact dampers are based on an increase or change in material damping. Energy dissipation occurs when the individual masses of an impact damper collide. Friction dampers extract vibration energy from the system by means of the friction between two solid bodies moving relatively to each other. Friction dampers have proven to be successful in chatter suppression when integrated in an end mill (KIM ET AL. 2006; MADOLIAT ET AL. 2011). The disadvantage is that the friction damper is integrated into a monolithic tool, which is disposed of at the end of its service life. Current research, however, attempts to increase the energy dissipation and thus chatter

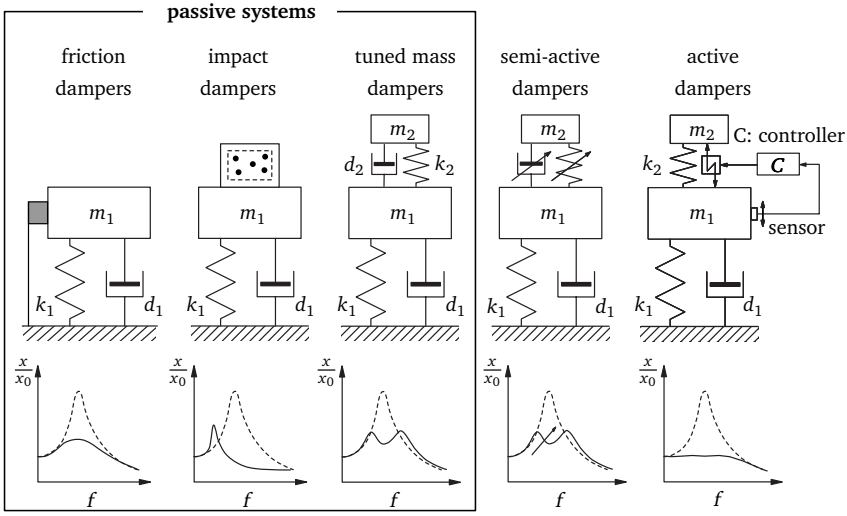

Fig. 2.4: Passive, semi-active, and active auxiliary systems for system damping enhancement based on WECK & BRECHER (2006a) and SIMNOFSKE (2009)

stability of additively manufactured tools and tool holders by introducing hollow elements or truss-like structures (VOGEL ET AL. 2019).

According to VDI 2062-1 (2011), a TMD consists of a mass m_2 which is connected to a mechanical structure by a linear spring of stiffness k_2 and damping d_2. These parameters are tuned in such a way that the damper's natural frequency matches the critical natural frequency of the system to be damped. Mode coupling transfers the kinematic energy from the main structure to the highly damped TMD and increases the overall damping (WECK & BRECHER 2006a). Consequently, the original mode is split up into two modes. According to SIMS (2007), the basics for the design of TMDs have already been described in the first half of the last century by ORMONDROYD & DEN HARTOG (1928), BROCK (1946), and DEN HARTOG (1947). These works aimed at reducing the maximum compliance of the oscillating system. Since the chatter stability depends on the negative real part of the compliance FRF (see Sec. 2.1.2), SIMS (2007) presented an approach showing how to minimize this quantity. YANG ET AL. (2010) picked up a similar idea, but extended it for an optimization of multiple TMDs, which can damp several natural modes. TMDs are occasionally used by machine tool builders in new designs (FLADERER 2007) if they can be tuned without a large increase in mass and the associated deterioration of feed drive dynamics. They are also already in industrial use for the damping of tools with a long overhang, such as boring bars (MAPAL 2018; SANDVIK COROMANT 2020). However, they can

only be applied if the dynamic behavior of the structural element to be damped does not change (WECK & BRECHER 2006a).

Semi-active Systems have been developed in the 1990s by integrating electronics into originally passive systems in order to change the damping characteristics and increase their application flexibility (SIMNOFSKE 2009; ROTH 2009). The energy demand of such semi-active systems is limited to signal processing and adjusting the passive system components (MESCHKE 1995).

Electrorheological (e.g. MESCHKE (1995)) or magnetorheological fluids (e.g. KERSTING (2009)) are mainly used for semi-active systems, because their viscous properties can be quickly and reversibly adjusted by an externally applied electric or magnetic field. Another concept was introduced by MUNOA ET AL. (2016b), who used a variable stiffness TMD on a modular workpiece fixture. The automatic optimal tuning methodology developed varies the stiffness via a rotary spring, while damping is provided by eddy currents.

Active Systems increase damping of the structure by using external energy (MESCHKE 1995). With their high bandwidth compared to passive and semi-active systems, the requirements of machine tools are better met because active systems can adapt to changes in the dynamic behavior during machining operations (SIMNOFSKE 2009). Active systems consist of a sensor, a controller, and an actuator, as illustrated in Fig. 2.4 (WECK & BRECHER 2006a). Based on the structural vibrations measured by the sensor, the controller usually generates a control signal with the aim of achieving a counter-vibration through an actuator. This way, dynamic auxiliary systems are able to enhance the damping of critical eigenmodes and thereby increase the absolute stability limit (DOHNER ET AL. 2004).

2.2.5 Conclusion

In Sec. 2.2, different existing techniques for chatter mitigation have been explained and summarized. *Design optimization* is only applicable for new machine tool developments and does not offer a sufficient solution for concept-conditioned weak spots (see Sec. 2.3.1). Measures for *process parameter selection* as well as *regeneration disturbance* are simple and cost-effective, since no machine tool design changes or additional hardware are needed. This is why these methods have been most widely used in the industry so far. However, each of these methods has only a limited field of application within the SLD.

In contrast, *dynamic auxiliary systems* work efficiently in all the zones of the SLD (MUNOA ET AL. 2016a). They are especially useful when the low machinability of the material does not permit any change in the process parameters (BAUR 2014). *Passive systems* are characterized by a simple design, high reliability, and low costs due to the absence of electronic components. Since they must always be precisely tuned to match the critical natural frequency of the structure to be damped, their

effect decreases significantly as soon as the dynamics of the machine tool change. To reduce this drawback of purely passive systems, *semi-active systems* have been developed. However, an adaptation to changing natural frequencies is still only possible to a limited extent. In addition, both passive and semi-active systems are accompanied by large additional masses, which can have a negative effect on the feed drive dynamics (HAASE 2005). *Active systems* enable the generation of large damping forces over a wide bandwidth with low additional mass. Due to their small space requirements, they can be placed on the machine structure easily. However, the advantages mentioned above come at the expense of a comparatively complex and costly system, which has to be applied in a hostile environment (MUNOA ET AL. 2016a). In addition, an active system can become unstable due to the closed feedback loop. Nevertheless, since several researchers have already proven the high performance of active systems in chatter suppression, this dissertation also focuses on such systems. The following section will provide a closer overview of the applications that can be found in the literature.

2.3 Active Systems in Machine Tools

WAIBEL (2012) classifies active systems by their way of integration within the force flux into *serial*, *parallel*, and *absolute*, as illustrated in Fig. 2.5:

For **Serial Integration**, the actuator is located inside of the force flux of the machine and has to withstand the cutting forces. Therefore, high stiffness is required for these elements and any breakage of the actuator will result in a machine stop (MUNOA ET AL. 2016a). Because of these drawbacks, this way of integration is rarely used in machine tools (MANOHARAN 2012).

Parallel Integration increases the stiffness due to an additional parallel force flux (WAIBEL 2012). The actuator has to be integrated at a location where the targeted mode has a large displacement amplitude (EHMANN 2004).

Absolute Integration describes an active system that is not placed within the force flux (WAIBEL 2012). This way of integration can only be achieved by *proof-mass actuators*, which are also called *inertial actuators*, *active vibration absorbers*, or *active tuned mass absorbers*. Based on *Newton's second law of motion*, these actuators generate forces by accelerating a suspended mass that is coupled to the main structure. SIMNOFSKE (2009) criticizes the high additional mass compared to a serial or parallel integration. On the contrary, EHMANN (2004), WAIBEL (2012), MUNOA ET AL. (2013), and BAUR (2014) mainly emphasize the simple installation as the actuator does not require complex design changes.

While active systems with absolute integration can only suppress vibrations, serial and parallel integrations are also capable of modulating the static stiffness and hence reduce static deflections (WAIBEL 2012). However, following Eq. 2.3, chatter stability

is strongly influenced by the compliance FRF. Furthermore, drawbacks of lightweight design mainly lead to increased peaks in the compliance FRF, but not to a reduced static stiffness (ZULAIKA ET AL. 2011). Therefore, this dissertation focuses on systems with the ability to reduce the peaks of the compliance FRF by damping enhancement only. In a technical-scientific context, the term *active damping* is commonly used for such systems. This might originate from the widely used control strategy *direct velocity feedback (DVF)* (see Sec. 2.4.6.3), which adds an actuator force proportional to the measured vibration velocity and acts as a viscous damper. BAUR (2014) points out that according to VDI 3833-1 (2014), *damping* is defined as the irreversible transformation of mechanical energy into another energy form – most often thermal energy – which is no longer available for exciting or sustaining an oscillation. This process is also called energy dissipation. Consequently, the term "active damping" is actually incorrect, since energy is supplied to the vibrating system and does not dissipate. In the literature, the term *active vibration control* (AVC) is also commonly used and more accurate. When presenting the state of the art in the following section, both terms are used synonymously.

According to NEUGEBAUER ET AL. (2007), piezoelectric, electrodynamic, and electromagnetic actuators are mainly used for AVC of machine tools. The reason for this is the working bandwidth, which should be in the range of the dominant eigenmodes which cause chatter. Accordingly, WAIBEL (2012) names a working bandwidth of approximately 20 to 400 Hz if damping the machine tool structure is the focus of interest. In contrast, local modes associated with the flexibility of the spindle and the tool can show high natural frequencies in the range from 500 Hz to 10 kHz (ALTINTAS & KO 2006) and, hence, these elements require a higher bandwidth. In the following, the three physical effects for generating an actuator force are briefly summarized. More detailed information about actuators for AVC can be found in ISERMANN (2008).

Piezoelectric Actuators offer high actuating forces and high positioning accuracy at frequencies up to the ultrasonic range, but their strokes are only in the sub-millimeter range (TELLBÜSCHER 1986; HUBER ET AL. 1997). The force generation is based on

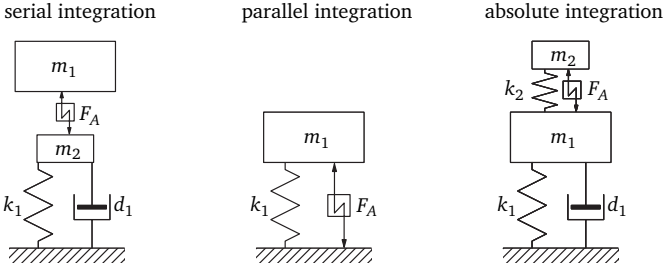

Fig. 2.5: Serial, parallel, and absolute integration based on WAIBEL (2012)

the piezoelectric effect. Due to their high stiffness, piezoelectric stack actuators in particular are well suited for an integration within the force flux (SIMNOFSKE 2009). Area transducers allow much larger amplitudes than stack actuators and can also be used as sensors (JANOCHA 2007). However, due to the very high operating voltages required (up to 1000 V), expensive high-voltage amplifiers are needed for piezoelectric actuators (EHMANN & NORDMANN 2002; BAUR 2014).

Electrodynamic and Electromagnetic Actuators are widely used as “shakers” to excite mechanical structures in modal analysis. BAUR (2014) states that cheap amplifiers are available due to the low operating voltage, which is also advantageous for operational safety. While electrodynamic actuators are based on the Lorentz force, which describes the magnetic force on a current-carrying wire, electromagnetic actuators generate forces based on the magnetic flux, which occurs between areas of different permeability (JALIZI 2015). Both actuator principles show good linear behavior and high forces for a wide frequency bandwidth up to the kilohertz range (ISERMANN 2008). It should be noted that in many publications electrodynamic and electromagnetic working principles are not separated. In standard text books, the electrodynamic actuator is sometimes defined as a subgroup of electromagnetic actuators (JANOCHA 1992).

The origins of AVC can be found in the area of acoustics as well as in the areas of automotive and civil engineering. In the 1980s, *adaptronic*[2] concepts for vibration reduction in the aerospace industry were developed (HESSELBACH ET AL. 2010). A lead project on adaptronics for industrial applications was funded by the German Federal Ministry of Education and Research in the early 1990s, in which mainly structure-integrated actuators and sensors were developed and tested (BOLDERING 2015). The European Commission funded first research projects in the field of AVC for machine tools from the end of the 1990s onwards (e.g. IMPACT, Smartools, DEMAT, Chameleon). From 2003 to 2009, the German Research Foundation funded the priority program SPP 1156 "Adaptronics for machine tools", whose results are summarized by HESSELBACH (2011). Within this program, 28 projects investigated the increase in performance of machine tools by adaptronic components. All in all, several publications for AVC of machine tools exist, which differ mainly in the machine element damped, the types of sensor and actuator used, and the implemented control strategy. Before a comprehensive overview of the literature on AVC is given, various weak spots of machine tools are presented first. The weak spots define the origin of compliance for the machine tool sub-structures to be damped and are used in this dissertation in order to categorize the literature, as depicted in Fig. 2.6.

[2] adaptronic is a word combination consisting of "adaptive structures" and "electronics" (PAHL ET AL. 2007). Sometimes the terms "smart structures", "smart materials", or "intelligent systems" are used synonymously (SIMNOFSKE 2009).

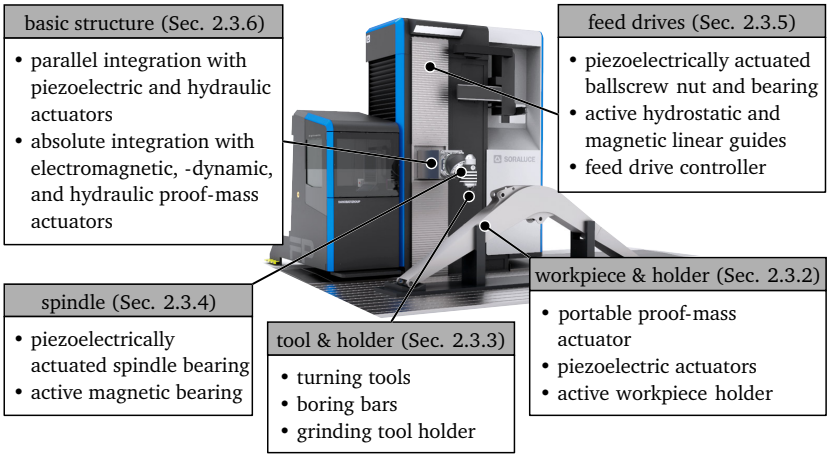

Fig. 2.6: Application areas of AVC in machine tools (image source: SORALUCE (2020))

2.3.1 Weak Spot Analysis

The weak spot of the system that causes the stability limiting natural frequency is chosen as the machine element to be damped (MANOHARAN 2012). However, it is not the mechanical structure alone that needs to be analyzed, but its interaction with the machining process (see Sec. 2.1.2). Eigenmodes of a machine tool's basic structure are usually located below 500 Hz (NIEHUES 2016) and often cause chatter in heavy duty machining operations due to the low tooth-passing frequency (MUNOA ET AL. 2016a). In contrast, high tooth-passing frequencies, which for example occur during the machining of aerospace structural parts made of aluminum, are often way above the absolute stable region related to the basic structure's eigenmodes, but can cause an excitation of the tool or spindle shaft. That is why the literature offers a variety of approaches for AVC for each potential weak spot element within the force flux.

The highest damping performance is always generated when the actuator is integrated close to the mode shape's highest deflection amplitude (see Sec. 2.4.4.2). When implementing AVC in machine tools, a comprehensive weak spot analysis should therefore be carried out first. MANOHARAN (2012) implements a coupled mechatronic simulation representing the structural dynamics by flexible multibody elements. Such a simulation model takes some effort to be built up and calibrated and is therefore usually used for new machine designs. In contrast, BAUR (2014) suggests detailed FRF measurements for the weak spot analysis of existing machines, which requires less effort. In the latter approach, however, the influence of the machining process is neglected. MANOHARAN (2012) also carried out FRF measurements on various exemplary machine concepts for an initial weak spot analysis and focused the

investigations on the eigenmodes of the basic structure. The results show that critical natural frequencies depend on the arrangement of the basic structure's components, the mass distribution of the structures, and the type of coupling. In many cases, there is a coupling of the eigenmodes of several components. MANOHARAN (2012) calls this a "concept-conditioned weak spot", because such cases cannot be solved constructively and economically. A weak spot analysis performed by BRECHER ET AL. (2008) for portal milling machines showed that over 40 % of the deformation rate at the tool center point (TCP) is caused by the static and dynamic stiffness of the z-slide. In a statistical evaluation, WECK & BRECHER (2006c) found that for column type milling machines, chatter vibrations occur in over 25 % of the investigated processes due to the high compliance of the basic structure. The reason why weak spots are often found within the basic structure is because its structural components always lie within the force flux and, thus, make a decisive contribution to the resulting static and dynamic compliance at the TCP (MANOHARAN 2012). Furthermore, the low natural frequencies of large machine components are likely to be excited by heavy duty machining operations (MUNOA ET AL. 2016a), which often exploit the stability limit. This holds especially for machine tool designs with high projection lengths, such as portal, column, gantry, or ram type machining centers (MANOHARAN 2012; ZULAIKA ET AL. 2011). Significant productivity increases can be expected by compensating such weak spots with AVC systems.

Therefore, the following literature review will focus on approaches for damping the machine's basic structure and only briefly summarize applications to other components. Please note that the following sections will only name the various sensors, actuators, and control strategies in order to give an overview of the different concepts used in the literature. A more theoretical background about the final concept chosen and the control strategies implemented in this dissertation is given in Sec. 2.4.

2.3.2 Workpiece and Workpiece Holder

The workpiece and its holder are the elements closest to the process on the workpiece side and therefore have a direct influence on the machining process. Applications of AVC exist mainly for milling machines due to the easier implementation on a stationary structure (HAASE 2005; JALIZI 2015). The literature in this section can be categorized into applications for the workpiece and for the workpiece holder.

Workpiece
Suppressing high frequency chatter vibrations resulting from flexible workpieces is a challenging task because the dynamics change strongly with the ongoing material removal (TUYSUZ & ALTINTAS 2017). BEUDAERT ET AL. (2019) applied a model-free DVF controller, which shows high robustness against changing dynamics, in a portable AVC system with a proof-mass actuator. Flexible workpieces can also be damped by integrating piezoelectric lead zirconate titanate (PZT) actuators and implementing model-free (ZHANG & SIMS 2005), model-based (PARUS ET AL. 2013), or harmonic

excitation (WEREMCZUK ET AL. 2015) control. With this way of integration, however, the actuators have to be applied and adapted to each new workpiece, which entails considerable effort.

Workpiece Holder
An active workpiece holder has the advantage that it can be easily retrofitted to machine tools without the need for a design change to the initial system (WAIBEL 2012; JALIZI 2015). Another advantage is the capability to control all occurring vibrations, meaning that the eigenmodes of all components within the force flux can be damped (MANOHARAN 2012). The following approaches are especially used for damping tool vibrations.

HAASE (2005) introduced a concept based on piezoelectric actuators that is capable of suppressing vibrations in two directions. Several authors have employed similar concepts: While HAASE (2005), RASHID & MIHAI NICOLESCU (2006), ABELE ET AL. (2008), and FORD ET AL. (2013) implemented an adaptive controller, BRECHER ET AL. (2010) applied model-free position control and SALLESE ET AL. (2017) introduced a novel strategy based on harmonic excitation. To date, however, there have been no industrial applications of these approaches. The reasons for this might be the reduced working space of the workpiece table as well as challenging cable routing for 5-axis machine tools with rotary tables. Furthermore, the control of such systems is quite demanding due to the high delay times of the controlled system: vibrations of the machine tool structure first lead to higher cutting forces before resulting in higher vibration amplitudes at the table, where they can finally be controlled by the AVC system.

2.3.3 Tool and Tool Holder

The tool and tool holder are the machine elements closest to the process on the tool side. There, all vibrations affecting the machining process can be theoretically suppressed. However, due to the limited assembly space, small piezoelectric actuators with small strokes are often used, which are not able to sufficiently damp the eigenmodes of the basic structure. Hence, most of the applications found in the literature focus on damping a stationary tool only.

Tools
One of the earliest publications in this field is the one by SHIRAISHI ET AL. (1991), who used a model-based controller, an eddy current type transducer attached to the turning tool post to measure the relative motion between the workpiece and the tool, and a highly dynamic stepping motor for actuation. Another concept was introduced by TEWANI ET AL. (1995), who integrated a proof-mass actuator, accelerated by piezoelectric stacks, into a boring bar. The maximum chatter free DOC achieved with a model-based controller was significantly higher compared to a plain boring bar and a boring bar with a TMD. Due to their compact design, parallel applications are

most commonly used for AVC of boring bars nowadays: CLAESSON & HÅKANSSON (1998) designed a boring bar with an embedded piezoelectric actuator, which was controlled by an adaptive controller. Similar approaches are presented in WORONKO ET AL. (2003), HARMS ET AL. (2004), HASHEMI & OHADIR (2007), ÅKESSON ET AL. (2007), and HEISEL & KANG (2012).

Tool Holder
BOLDERING (2015) introduced an actively damped grinding tool holder actuated by piezoelectric stacks. Self-excited vibrations were controlled by an automatically tuned model-based controller, while forced vibrations caused by the grinding spindle and a cooling fan were compensated by an adaptive finite impulse response (FIR) filter.

2.3.4 Main Spindle

The large overhang length of the spindle shaft is an unavoidable dynamic weakness of machine tool structures. Concepts for actively damped spindles can be further divided into using piezoelectric or electromagnetic actuators.

Piezoelectric Actuators
TÖNSHOFF ET AL. (2002) increased the process stability by varying the preload of the spindle bearings. These were actuated by piezoelectric stacks. DOHNER ET AL. (2004) integrated four piezoelectric stacks around the spindle housing to damp the spindle unit. Stress gauges at the tool measured vibrations which were suppressed by a model-based controller (KWAN ET AL. 1997). An actively supported spindle bearing system was introduced by RIES ET AL. (2006), who integrated piezoelectric stacks at the lower bearing of a motor spindle. Similar approaches were used by several authors implementing model-based controllers (ALIZADEH ET AL. 2003; MONNIN ET AL. 2014a, b) and harmonic excitation control (DENKENA & GÜMMER 2012).

Electromagnetic Actuators
Active magnetic bearings (AMB) are non-contact bearings that control the air gap between the outer ring and the spindle shaft using magnetic forces (NEUGEBAUER ET AL. 2007). STEPHENS (1996) and KNOSPE (2007) evaluated the performance of AMBs for chatter suppression implementing model-based control on a simplified test bench. Similar approaches can be found in KERN (2009), VAN DIJK ET AL. (2012), and HUANG ET AL. (2015). A new design approach with a spindle integrated magnetic actuator was introduced in BICKEL ET AL. (2014). The active component of the spindle motor was axially divided into two parts and the actuator coil windings were placed into the resulting gap in the form of three separately controlled sub-actuators in sectors of 120° around the spindle shaft. A Kalman filter was used to decompose the measured vibration signal into the individual parts of the natural frequencies and only damp the ones that cause chatter. The design was enhanced further by KÖNIGSBERG ET AL. (2018) in order to increase the achievable spindle motor torque.

Several manufacturers, being involved in research projects, have built prototypes of actively damped spindles. However, due to the reduced maintainability and static stiffness of such modified systems, as well as high manufacturing costs, no serial product is available so far. Nevertheless, AMBs as well as permanent magnet synchronous motors are commercially available (SKF 2020) and their use in main spindles is a promising research approach.

2.3.5 Feed Drives

Feed drives transmit process forces and convert the nominal path governed by the computerized numerical control (CNC) into a relative movement between the tool and the workpiece in order to generate the nominal shape of the workpiece (WECK & BRECHER 2006b). Hence, the compliance FRF, positioning accuracy, and dynamics of the feed drives have a direct influence on the achievable manufacturing accuracy and quality. The most popular approaches for AVC of feed drives can be categorized into the following three areas.

Ballscrew
NEUGEBAUER ET AL. (2010) compensated axial vibrations through the integration of a piezoelectric actuator-sensor unit between the ballscrew nut and the table. Piezofibre sensors measured the load, and two control strategies were tested: a model-free acceleration feedback controller led to increased stiffness, while a model-free DVF controller improved the damping behavior. PRITSCHOW & CROON (2013) controlled the preload of an axial ballscrew bearing in order to damp the first eigenmode of the feed drive by applying velocity feedback. An active system for vibration reduction in centerless grinding was developed by ALBIZURI ET AL. (2007). The piezoelectric actuator in the ballscrew nut successfully suppressed chatter vibrations and reduced roundness errors while being controlled by an acceleration feedback controller. The actuator was redesigned by GARITAONANDIA ET AL. (2013).

Linear Guides
Most applications in the field of active linear guides focus on the compensation of static deflections. However, a few approaches exist that damp vibrations. KYTKA ET AL. (2007) applied a model-free proportional-integral-derivative (PID) and a model-based control to active hydrostatic linear guides, while DENKENA ET AL. (2004) implemented model-based control in active magnetic linear guides.

Feed Drive Controller
Adapting the feed drive controller to suppress chatter is a low investment solution (BEUDAERT ET AL. 2017). The feed drive motor is used as an actuator, while the vibrations to be damped are measured by the feed drive's linear encoder (ALTINTAS ET AL. 2011), a Ferraris acceleration sensor (PRITSCHOW ET AL. 2003), or an accelerometer at the TCP (ZATARAIN ET AL. 2005; MUNOA ET AL. 2015). CNC providers

are also already working in this field (HEIDENHAIN 2013). Various closed-loop control techniques have been demonstrated to damp the vibrations by using position, velocity, acceleration, current, and force feedback (ALTINTAS ET AL. 2011). However, due to the high masses to be moved, feed drive controller approaches for AVC are always limited to the bandwidth of the feed drives (MUNOA ET AL. 2015; JALIZI 2015). Furthermore, a setup based on a proof-mass actuator which is located close to the TCP – as will be described in the following section – often delivers a better damping performance (MUNOA ET AL. 2015).

2.3.6 Basic Structure

For AVC systems integrated in the basic structure, usually more assembly space is available compared to the tool and the spindle (JALIZI 2015). This offers the possibility to use both parallel and absolute integration.

Parallel Integration
MICHELS (1999) introduced an approach to stabilize grinding processes with piezoelectric actuators integrated within the bearing of a grinding spindle and in the center. Two control strategies were implemented. The first generates an additional artificial resonance in order to damp the critical eigenmode with the new anti-resonance, and the second disturbs the regenerative effect by a harmonic excitation. SIMNOFSKE (2009) increased the static and dynamic stiffness of a plane grinding machine by means of structure-integrated modules. The two piezoelectric stacks and the force sensor were positioned based on a simulation, which allows for a simplified integration of structure-integrated actuators. A model-based state controller takes the force sensor signal as well as three accelerometer signals into account. The setup achieved significant damping of the eigenmodes. For the reduction of forced vibrations, an adaptive FIR was implemented.

MANOHARAN (2012) integrated piezoelectric stacks in the z-axis of a portal machine tool to damp its bending mode. The active module, which uses a PID controller, compensates thermal, static, and dynamic deflections. Based on this work, BRECHER ET AL. (2016) also integrated four hydraulic actuators in order to suppress the bending mode of the z-slide in two directions with a multi-input-multi-output (MIMO) model-based controller.

EHMANN (2004) has developed important basics for the design and integration of AVC systems in machine tools and tested different actuators for AVC. The critical mode of the z-slide was damped on a laboratory model of a gantry type machine. After the theoretical evaluation of several actuator working principles, a piezoelectric and an electromagnetic actuator were developed. The piezoelectric stacks were integrated parallel to the force flux, while the proof-mass electromagnetic actuator was integrated close to the TCP. A theoretical comparison of different control approaches led to the selection of a model-based controller with an inner PID position

control loop for the moving mass of the electromagnetic actuator. WAIBEL (2012) also tested a parallel-integrated piezoelectric stack and an absolutely integrated electrodynamic proof-mass actuator. Both concepts were controlled by an adaptive controller. EHMANN (2004) and WAIBEL (2012) concluded that an absolutely integrated proof-mass actuator is much easier to integrate compared to parallel applications and achieves a comparable or even better performance in chatter suppression. More examples for absolute integration are summarized in the following.

Absolute Integration
KEMMERLING-LAMPARSKY (1987) introduced AVC for cylindrical plunge grinding using a piezoelectric proof-mass actuator attached to the tailstock and headstock center. A cascaded control design was proposed with an inner PID position controller for the moving mass of the actuator along with outer PD and least mean squares (LMS) controllers. The inner control loop compensates the non-linear behavior of the actuator and improves the tracking error. The control parameters of the main control loop were adapted to changes within the controlled system by means of an identification routine. However, no significant increase in chatter stability was achieved. CHUNG ET AL. (1997) designed an electrodynamic proof-mass actuator, which was also installed on the headstock of a demonstrator. A DVF controller significantly reduced the compliance of the system at its resonance. However, machining tests were not possible with this setup.

For a portal milling machine, ROTH (2009) designed a biaxial electromagnetic proof-mass actuator and implemented a DVF controller for chatter suppression. The actuator's moving mass position was controlled by a cascaded PID controller, similarly to the concept of EHMANN (2004). The actuator was placed around the lower end of the spindle housing, close to the TCP. Machining tests demonstrated the performance of the installed AVC system in chatter suppression and showed a significant improvement in surface roughness. BAUR (2014) applied a proof-mass actuator with a DVF controller to a similar machine tool. A model-based loop shaping controller with manually selected poles was also tested, but showed a worse performance. In order to lower market entry barriers, the usage of commercially available components was investigated and a methodology for a low-effort commissioning of AVC systems was presented. Extensive machining experiments with varying spindle speeds and feed rates were performed, which were conducted to show the robustness of the AVC system under different cutting conditions. A similar setup was used by JALIZI (2015), who evaluated different actuator concepts for small machine tools and finally designed an electrodynamic proof-mass actuator. Analogous to ROTH (2009), the actuator was placed close to the TCP and a cascaded controller was implemented. For the outer loop, a model-based controller was synthesized and tested during machining.

For large machine tools, SCHULZ (2010) designed a hydraulic proof-mass actuator which provides high forces at low frequencies. The performance of the AVC system, running with a DVF controller, was validated during cutting tests. However, compared

to electrodynamic or electromagnetic proof-mass actuators, the implementation effort increases due to the additional hydraulic lines that need to be integrated within the machine tool (BAUR 2014).

As explained in Chapter 1, lightweight design, which is required for high feed drive accelerations, contradicts the demand for highly damped machine tools. Therefore, ZULAIKA ET AL. (2011) presented an AVC-integrated lightweight design approach for machine tools. The result led to a lightweight ram for a big milling machine tool with a slot for embedding an actuator. This way, a significant increase in the chatter-free DOC, as well as a decrease of energy consumption due to the weight reduction, were achieved. For a similar setup, MUNOA ET AL. (2013) developed a biaxial electrodynamic actuator to suppress chatter during heavy duty milling operations. The authors tested the performance of the actuator with different model-free controllers and also presented a new control strategy that reduces the regenerative effect. In MANCISIDOR ET AL. (2018), an improved actuator design, which achieves a higher force density, was presented. A similar system was also applied to a centerless grinding machine (BARRENETXEA ET AL. 2018) and a vertical turning center with a long overhanging ram (MANCISIDOR ET AL. 2019a).

For industrial applications, the company Micromega offers a solution consisting of an electrodynamic proof-mass actuator, an integrated accelerometer, and an amplifier with a manually adjustable gain for the DVF controller (MICROMEGA DYNAMICS 2020). Despite many promising research results, currently only the works and results of MUNOA ET AL. (2013) and MANCISIDOR ET AL. (2018) have been implemented by SORALUCE on their ram type milling machines and are used in industry (DANOBATGROUP 2017).

2.3.7 Conclusion

An absolute application via proof-mass actuators is most suitable for retrofit solutions because series and parallel applications are associated with high design complexity. Furthermore, the use of a proof-mass actuator close to the TCP often delivers better results compared to parallel applications or the use of feed drives for active vibration control. Model-free control strategies, model-based control synthesis, and adaptive controllers have most commonly been used and have achieved a good chatter mitigation performance in several works. Hence, the following section focuses on the design, modeling, and commissioning of AVC systems with proof-mass actuators, and will present the different control strategies in more detail.

2.4 Design, Modeling, and Commissioning of Active Vibration Control Systems

This section starts with a presentation of the different hardware components of an AVC system with a proof-mass actuator as illustrated in Fig. 2.7, focusing on the design requirements for a simple retrofit solution and its industrial use. Afterwards, a commonly used coupled simulation approach for AVC systems is introduced, which is not only helpful for actuator placement and its dimensioning, but also required for virtual controller tuning and testing as well as model-based control synthesis. This section ends with an explanation and evaluation of the different control strategies existing in the literature, as well as a presentation of methodologies for simplifying the commissioning of AVC systems.

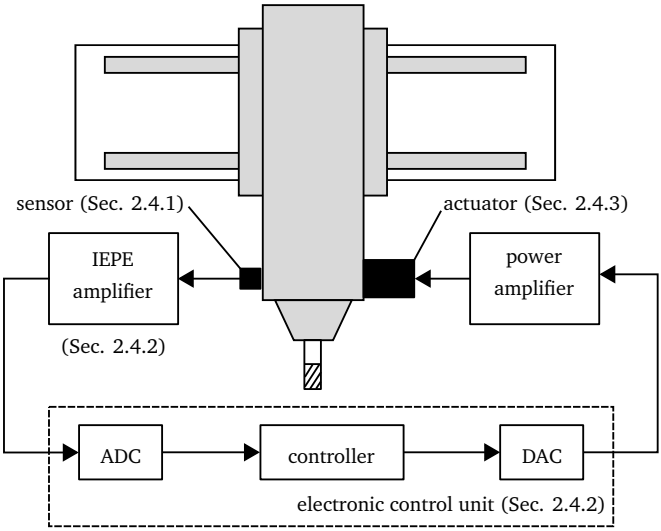

Fig. 2.7: Schematic structure of an AVC system with IEPE sensor

2.4.1 Sensor

The sensor measures the occurring vibrations which the AVC system is intended to suppress. If two or more actuators are installed in order to damp vibrations in different directions, each direction requires its own sensor (MUNOA ET AL. 2013; BAUR 2014). The comparably stiff cross-FRFs in machine tools usually prevent crosstalk between independently controlled AVC systems (BAUR 2014). The sensor should always be placed close to the actuator in order to achieve high controller

stability (see Sec. 2.4.6.3) (ZAEH & PIECZONA 2018). According to BAUR (2014), the sensors must be sealed and fulfill IP67 (DIN 60529 2000) in order to be protected against dust and strong jets of liquid (e.g. cooling lubricant, chips). A constant sensitivity in the working frequency range of 10 – 1000 Hz avoids problems during system identification and controller tuning (see Sec. 4.5). Absolutely integrated accelerometers based on the piezoelectric or capacitive principle have a small design and high robustness, and are preferable over speed sensors that operate with a wear sensitive plunger coil based on the electrodynamic principle (KUTTNER 2015). Within the scope of this research work, industrial accelerometers were used that operate based on the piezoelectric principle and are powered by an *Integrated Electronics Piezo Electric* (IEPE) amplifier, which is described in the following section.

2.4.2 IEPE Amplifier

IEPE sensors have the advantage that their sensitivity is not influenced by the length and type of the sensor cable. Hence, no expensive special cables have to be used (METRA MESS- UND FREQUENZTECHNIK 2017). Various manufacturers offer IEPE amplifiers, some of which are also equipped with analogue high-pass and low-pass filters. The high-pass and low-pass filters remove low- and high-frequency noise, respectively, and are of great importance for controller stability and performance (see Sec. 2.4.6.2). An analogue low-pass filter especially needs to be placed before the analogue to digital (ADC) converter to prevent aliasing[3] (EWINS 2000). In addition, a low-pass filter is useful for avoiding instabilities of model-based controllers due to non-modeled high-frequency modes (spillover effect) (PREUMONT 2002). The IEPE amplifier has to be grounded to the machine tool (sensor ground) in order to eliminate strong interference frequencies in the range of the electrical power supply frequency and its harmonics. Electronic control units exist in which the ADC already has an IEPE amplifier integrated (e.g. X20CM4810 from B&R AUTOMATION (2020c)).

2.4.3 Electronic Control Unit

The electronic control unit consists of an ADC, a digital signal processor (DSP), and a digital to analogue converter (DAC). Additional filters and the controller run on the DSP. For the AVC of machine tools, mainly rapid control prototyping platforms have been used in the literature (e.g. dSpace ds100x or NI CompactRIO). Such systems are very powerful, but also quite costly. Since the computational requirements for

[3] *Shannon's theorem* states that if the measured signal has frequency content above the *Nyquist frequency*, referring to half of the sampling frequency, those frequencies will be misinterpreted and appear as low frequencies instead. This effect is called *aliasing*. (EWINS 2000)

AVC are not very high, a cost-efficient programmable logic controller (PLC) may be sufficient as well. These systems are suitable for industrial use and nowadays offer computer-aided control engineering capabilities via a direct connection to MATLAB/SIMULINK® (e.g. B&R AUTOMATION (2020b)). This functionality allows for a simple controller implementation and test. The hardware needs to be powerful enough to enable real-time control at a specified sampling rate. The sampling rate varies in the literature from 2 kHz (MANCISIDOR ET AL. 2019b, a) to 10 kHz (BAUR 2014; BOLDERING 2015), and up to 50 kHz (MUNOA ET AL. 2013). In order to achieve a good time resolution of the vibration signal, the sampling rate should be at least ten times higher than the specified crossover frequency, which is the highest natural frequency to be damped (EWINS 2000). A very cost-efficient solution was introduced by EHMANN (2004), who designed a controller board based on analogue filters with switched capacity. However, this approach requires in-depth expert knowledge and implies that the controller transfer function is fixed.

2.4.4 Proof-mass Actuator

As a result of a literature review, it can be stated that piezoelectric, electromagnetic, and electrodynamic actuators have been the most commonly used as proof-mass actuators. Selecting the best proof-mass actuator concept depends greatly on the application. While the original concept of electrodynamic proof-mass actuators goes back to the actuation of a loudspeaker paper cone (voice coil) (JANOCHA 1992), recent research activities have focused on developing proof-mass actuators with an even higher power density.

KOSUB ET AL. (2012) introduced two measurement heads that can be attached directly to the spindle shaft via the HSK-interface. This so-called *high performance cutting measurement head* is based on an electrodynamic proof-mass actuator and excites a low frequency bandwidth, while the so-called *high speed cutting measurement head* uses a piezoelectric proof-mass actuator for high-frequency excitation. Both measurement heads show a high force density and are used for identifying the position-dependent dynamics of machine tools. A biaxial electrodynamic actuator was introduced by LOIX & VERSCHUEREN (2004). The actuator is a combination of a linear motor and a voice coil, that generates forces up to 1000 N in both directions. This actuator was successfully tested on a ram-type milling machine (MUNOA ET AL. 2013). A recently presented concept of a moving iron controllable actuator (MICA) achieved around ten times higher force densities compared to electrodynamic proof-mass actuators. The MICA is an electromagnetic actuator that polarizes the air gap using magnets. The symmetry of the polarized air gap is modified by the applied current. Due to the air gap's high induction magnitude, this working principle achieves high forces (MENEROUD ET AL. 2016).

All in all, electrodynamic proof-mass actuators have demonstrated their robustness in many applications and have been implemented commercially (DANOBATGROUP

2017, 2019). While different working principles describing how to accelerate the moving mass exist, the final dynamic behavior is always quite similar. Thus, the following section will, as an example, describe the working principle of an electrodynamic proof-mass actuator and show how it can be modeled.

2.4.4.1 Working Principle of Proof-mass Actuators

The working principle of an electrodynamic proof-mass actuator is shown in Fig. 2.8. The controller output $u(t)$ is amplified by the power amplifier to provide an electric

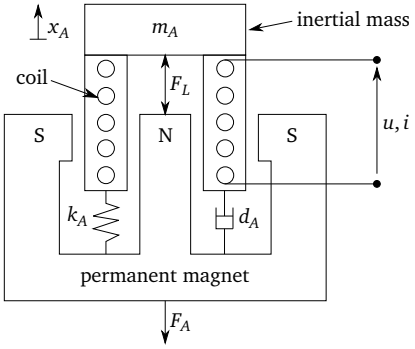

Fig. 2.8: Schematic working principle of an electrodynamic proof-mass actuator based on PREUMONT (2002)

current $i(t)$. The current-carrying wire generates a Lorentz force $F_L(t)$ between the permanent magnet and the coil. The coil is connected to a reaction mass m_A, which moves in parallel (coaxially) to the desired direction of the actuator force $F_A(t)$. A damper with the damping constant d_A and a spring with the stiffness k_A couple the coil and reaction mass unit to the permanent magnet, which is fixed to the housing (*moving-coil actuator*). Also actuator designs exist where the permanent magnet moves (*moving-magnet actuator*). Unless otherwise indicated, the following section is based on PREUMONT (2002).

Combining the differential equation of motion and the equation for the Lorentz force, the actuator transfer function is derived as

$$G_A(s) = \frac{F_A}{u} = g_A \frac{s^2}{s^2 + 2 \underbrace{\frac{d_A}{2\sqrt{m_A k_A}}}_{\zeta_A} \omega_A s + \omega_A^2}, \tag{2.5}$$

with g_A describing the combined gain of the actuator and power amplifier, while ζ_A and ω_A refer to the damping ratio and natural frequency of this SDOF system,

respectively. Hence, the actuator transfer function can be described by a double differentiated PT2 element. Fig. 2.9 shows an exemplary resulting magnitude and phase FRF. The model is in good agreement with the measurement, that was conducted with a MOOG SA10-V30 proof-mass actuator. Remaining deviations result mostly from a delay time T_A introduced by the actuator, the power amplifier, and the electronic control unit. This can be taken into account if Eq. 2.5 is multiplied by $e^{-T_A \cdot s}$ (MANCISIDOR ET AL. 2015).

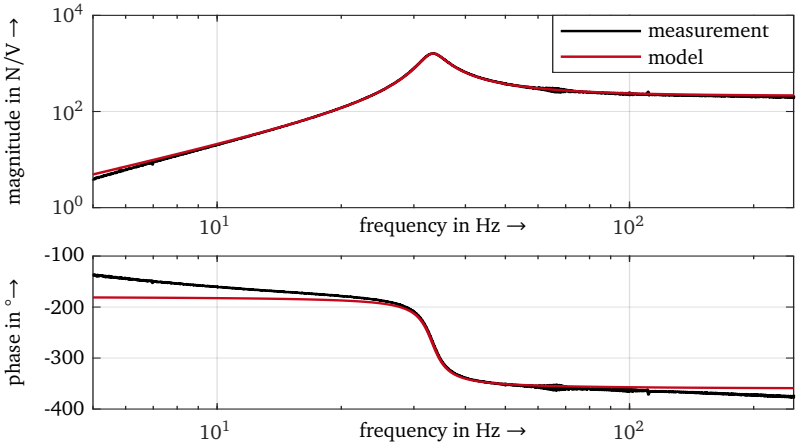

Fig. 2.9: Magnitude and phase FRF of a MOOG SA10-V30 proof-mass actuator

As can be seen in Fig. 2.9, the main disadvantage of proof-mass actuators is the presence of a weakly damped eigenmode. This means that the actuator only behaves as a linear force generator far above its natural frequency. This can lead to problems if a model-free controller is used and the eigenmodes to be damped are in the range of the actuator's natural frequency. Since the natural frequency of the actuator causes a phase shift of 180°, the actuator force being in counterphase with the vibration velocity is no longer safe (see Sec. 2.4.6.3) (BILBAO-GUILLERNA ET AL. 2012; BAUR 2014). Furthermore, high strokes occur in this area, which can lead to a non-linearity as a result of actuator saturation. In this case, a stable inverse of the actuator transfer function needs to be identified using pole placement and manual loop-shaping (BAUR 2014). The resulting compensation filter increases the working bandwidth of the AVC system. MANCISIDOR ET AL. (2015) tuned the following compensation filter to shift the actuator's natural frequency into a range that does not affect the controller performance:

$$G_{AComp} = \frac{s^2 + 2\omega_A \zeta_A s + \omega_A^2}{s^2 + 2\omega_{Anew} \zeta_{Anew} s + \omega_{Anew}^2} \,. \tag{2.6}$$

Here, ω_{Anew} and ζ_{Anew} define the actuator's new natural frequency and damping ratio. In addition to the force and stroke saturation explained above, the response at low frequencies is another disadvantage of proof-mass actuators. Independent of the application of a compensation filter, the actuator can only generate very little forces below its natural frequency due to the limited stroke (PEREIRA ET AL. 2014).

2.4.4.2 Actuator Placement

The actuator placement has a strong influence on the achievable controller performance (ZAEH ET AL. 2009; MANCISIDOR ET AL. 2015; ABELE ET AL. 2016). Furthermore, it is a comprehensive task because, in addition to considering the actuation efficiency, installation space restrictions have to be considered since the workspace of the machine tool must not be affected significantly (WAIBEL 2012; BAUR 2014).

EHMANN (2004) proved mathematically that the best controller performance is achieved at the position where the kinetic energy of the mode shape has its maximum, which is equivalent to the maximum vibration amplitude. ZAEH ET AL. (2009) optimized the actuator placement on a portal milling machine for both a parallel and an absolute integration by means of a computational approach. The introduced positioning index calculates the H_2 norm of the machine's compliance FRF at each potential actuator position in an FE model. ABELE ET AL. (2016) used the same positioning index to determine the position with maximum kinetic energy in order to achieve the highest possible controller performance. However, for retrofit solutions often no FE model exists. Hence, BAUR (2014) suggests to conduct operational vibration measurements and choose the position with the highest oscillation amplitudes, which is in agreement with the theoretical analyses of EHMANN (2004). MANCISIDOR ET AL. (2015) used a coupled mechatronic simulation, which is presented in Sec. 2.4.5, to evaluate the stability enhancement in milling at different actuator positions.

2.4.4.3 Actuator Dimensioning

Several authors have already investigated the design of proof-mass actuators (EHMANN & NORDMANN 2002; ROTH 2009; JALIZI 2015; MANCISIDOR ET AL. 2018). However, the individual actuator design is not within the scope of this dissertation. Instead, as already demanded by BAUR (2014), the focus is placed on a methodology for supporting the selection of commercially available components. Since the goal of a retrofit solution is often to increase the chatter-free DOC in order to utilize the full spindle power (HAASE 2005), the correct determination of the required actuator force for the AVC system is of great importance (BAUR 2014; MUNOA ET AL. 2016a).

EHMANN & NORDMANN (2002) and EHMANN (2004) carried out fundamental calculations of the required actuator force for a SDOF system by relating it to an external excitation force. Solving the extended differential equation for a SDOF system with

a proof-mass actuator, EHMANN (2004) obtained a formula that defines the required actuator force as a function of the modal parameters of the SDOF system and the excitation force. In the resonance case, the required actuator force corresponds exactly to the excitation force. When transferring this approach to a multiple-degree-of-freedom (MDOF) system, it was found that the corresponding actuator force is proportional to the excitation force and additionally depends on the velocity ratio between the TCP and the location of the actuator. Therefore, an important parameter for the determination of the required actuator force is the amplitude of the excitation force, i.e. the cutting forces. In an earlier publication, EHMANN ET AL. (2001) coupled the measured FRF of an actively damped machine tool structure with a simple cutting force model, as presented in Eq. 2.1, in order to evaluate the increase in chatter stability, but not for determining the dynamic actuator force.

According to ROTH (2009) and ABELE ET AL. (2016), the actuator must build up a force at the TCP that counteracts the increased cutting forces caused by chatter vibrations. For the actuator dimensioning, the cutting forces including the corresponding frequencies in unstable milling operations were measured. The maximum cutting forces were selected and increased by a safety factor of about 10 %.

MANOHARAN (2012) determined the required actuator forces for a parallel integration of piezoelectric actuators by means of an FE model. The focus of the analysis was placed on compensating the static displacement due to estimated disturbance forces. A flexible multibody simulation was set up to map the structural dynamics in combination with an active compensation module. This resulted in damped FRFs, which were coupled with a cutting force model. However, identical to EHMANN ET AL. (2001), this model was exclusively used for the simulative evaluation of the increase in chatter stability, but not for the actuator dimensioning. GARITAONANDIA ET AL. (2013) also used an FE model and dimensioned a piezoelectric actuator for a centerless grinding machine. Related to the approach of EHMANN (2004), the required force was determined using the cross transfer function between the TCP and the actuator position in combination with the excitation forces. The forces were estimated by simulating cutting conditions that produce strong chatter vibrations.

Based on the simulative stability analysis presented by EHMANN ET AL. (2001), a coupled time domain simulation considering the machine's structural dynamics, the AVC system, and the cutting forces was introduced by MUNOA ET AL. (2013) and further developed by MANCISIDOR ET AL. (2015). The analytical model allows for analyzing the AVC system during cutting operations and is, at the same time, used for studying the chatter stability. Hence, this model permits simulations of different control strategies and can be used to estimate the resulting actuator forces for a certain process and location.

In all approaches presented above, the occurring cutting forces, which form the basis for the dimensioning, result from a machining process defined by the authors. However, it cannot be excluded that other machining processes may result in even higher

required actuator forces that exceed the safety margins used in the dimensioning calculations. In this case, the actuator would saturate and the AVC system would not be able to stabilize the process.

2.4.5 Modeling of Active Vibration Control Systems

Several publications exist on how the behavior of AVC systems can be simulated. These will be briefly summarized below. Then, the simulation model used in this work for the purpose of controller tuning and testing, stability and energy demand analysis, and actuator dimensioning will be presented in more detail.

As described by ALTINTAS (2012) and explained in Sec. 2.1.2, EHMANN ET AL. (2001) coupled measured FRFs of a damped machine tool structure with a cutting force model to build a *regenerative cutting process model* for the evaluation of the stability enhancement in the frequency domain. ZULAIKA ET AL. (2011) used a similar approach to evaluate the chatter stability of an actively damped lightweight design. GANGULI (2005), too, calculated the stability lobes with AVC for a SDOF and a two-degree-of-freedom system in the frequency domain based on the DDE in Eq. 2.1. FERNANDES ET AL. (2009) applied an approach similar to the one in EHMANN ET AL. (2001), but used FRFs derived from an FE model instead of measured FRFs and coupled them with a model of the AVC system. The resulting simulation model was used for chatter stability analysis in the time domain for an actively damped grinding machine. MANOHARAN (2012) extended this approach by calculating the damped FRFs of a portal milling machine with the help of a flexible multibody simulation, which is linked to a model of the AVC system. Altogether, this results in a greater flexibility of the model. MUNOA ET AL. (2013) and MANCISIDOR ET AL. (2015) identified a state space model from an experimental modal analysis and coupled it with a cutting force model as well as a model of the AVC system. The last four publications presented holistic simulation approaches, which are able to reproduce the real machine's behavior with activated vibration control and, hence, can be used to test the performance of different control strategies under cutting conditions.

As already mentioned, this dissertation concentrates on simple retrofit solutions. Therefore, an approach that works with measured FRFs similarly to the one introduced by MANCISIDOR ET AL. (2015) is pursued in this work, which is presented in the following sections.

2.4.5.1 Structural Dynamics

GAWRONSKI (2004) describes how the dynamic behavior of a linear elastic mechanical structure can be represented with the help of the equation of motion:

$$\boldsymbol{M}\ddot{\boldsymbol{x}}(t) + \boldsymbol{D}\dot{\boldsymbol{x}}(t) + \boldsymbol{K}\boldsymbol{x}(t) = \boldsymbol{F}(t)\ . \tag{2.7}$$

Here, $\boldsymbol{M}$, $\boldsymbol{D}$, and $\boldsymbol{K}$ denote the mass, damping, and stiffness matrices of the structure, and $\boldsymbol{F}(t)$ represents the forces that act at the respective nodes. The nodal displacement vector $\boldsymbol{x}(t)$ directly relates to the n_d physical degrees of freedom of the individual nodes of the mechanical structure. In order to use the results of an experimental modal analysis for the model parameterization, the equation of motion (Eq. 2.7) needs to be transformed into *modal coordinates* $\boldsymbol{q_m}(t)$. The relationship between nodal and modal coordinates is defined by the modal transformation using the *modal matrix* $\boldsymbol{\Phi}$:

$$\boldsymbol{x}(t) = \boldsymbol{\Phi}\boldsymbol{q_m}(t). \tag{2.8}$$

The modal matrix $\boldsymbol{\Phi}$ contains as columns the n_d eigenvectors of the structure $\boldsymbol{\phi_i}$, while the rows refer to the modal coordinates:

$$\boldsymbol{\Phi} = \begin{bmatrix} \boldsymbol{\phi_1} & \boldsymbol{\phi_2} & \cdots & \boldsymbol{\phi_{n_d}} \end{bmatrix} = \begin{bmatrix} \phi_{11} & \phi_{21} & \cdots & \phi_{n_d 1} \\ \phi_{12} & \phi_{22} & \cdots & \phi_{n_d 2} \\ \cdots & \cdots & \cdots & \cdots \\ \phi_{1n_d} & \phi_{2n_d} & \cdots & \phi_{n_d n_d} \end{bmatrix}. \tag{2.9}$$

If the modal transformation (Eq. 2.8) is inserted into the equation of motion in nodal coordinates (Eq. 2.7) and additionally multiplied from the left by $\boldsymbol{\Phi}^T$, the equation of motion in modal coordinates yields

$$\underbrace{\boldsymbol{\Phi}^T\boldsymbol{M}\boldsymbol{\Phi}}_{\boldsymbol{M_m}}\ddot{\boldsymbol{q}}_m(t) + \underbrace{\boldsymbol{\Phi}^T\boldsymbol{D}\boldsymbol{\Phi}}_{\boldsymbol{D_m}}\dot{\boldsymbol{q}}_m(t) + \underbrace{\boldsymbol{\Phi}^T\boldsymbol{K}\boldsymbol{\Phi}}_{\boldsymbol{K_m}}\boldsymbol{q}_m(t) = \boldsymbol{\Phi}^T\boldsymbol{F}(t). \tag{2.10}$$

With the help of the modal matrix, the mass and stiffness matrices $\boldsymbol{M}$ and $\boldsymbol{K}$ are diagonalized. The same applies to the damping matrix $\boldsymbol{D}$ under the assumption of proportional damping (RAYLEIGH 1877). With the modal mass ($\boldsymbol{M_m}$), stiffness ($\boldsymbol{K_m}$), and damping matrix ($\boldsymbol{D_m}$), the equation of motion in modal coordinates is

$$\boldsymbol{M_m}\ddot{\boldsymbol{q}}_m(t) + \boldsymbol{D_m}\dot{\boldsymbol{q}}_m(t) + \boldsymbol{K_m}\boldsymbol{q}_m(t) = \boldsymbol{\Phi}^T\boldsymbol{F}(t). \tag{2.11}$$

Since only diagonal matrices appear on the left side of Eq. 2.11, each modal degree of freedom is decoupled from all other degrees of freedom and can be described by a second-order differential equation. The required modal parameters to describe the dynamic behavior of the mechanical structure in the form of Eq. 2.11 can be derived from an FE model or an experimental modal analysis. The latter was used in the context of this work.

In control theory, it is common to use a first-order state space representation. For linear time invariant (LTI) systems, the state differential equation (Eq. 2.12) and the output equation (Eq. 2.13) of a state space model representation are

$$\dot{\hat{\boldsymbol{x}}}(t) = \hat{\boldsymbol{A}}\hat{\boldsymbol{x}}(t) + \hat{\boldsymbol{B}}\hat{\boldsymbol{u}}(t), \tag{2.12}$$

$$\hat{\boldsymbol{y}}(t) = \hat{\boldsymbol{C}}\hat{\boldsymbol{x}}(t) + \hat{\boldsymbol{D}}\hat{\boldsymbol{u}}(t), \tag{2.13}$$

where $\hat{\boldsymbol{A}}$ is the system matrix defining the system's behavior depending on the states and $\hat{\boldsymbol{B}}$ is the input matrix linking the inputs $\hat{\boldsymbol{u}}$ to the system's states $\hat{\boldsymbol{x}}$. The output matrix $\hat{\boldsymbol{C}}$ translates the system's states to the resulting output $\hat{\boldsymbol{y}}$, and $\hat{\boldsymbol{D}}$ represents the feed-through matrix. In order to transform Eq. 2.11 into state space form, it first needs to be multiplied with $\boldsymbol{M}_m^{-1}$:

$$\ddot{\boldsymbol{q}}_m(t) + 2\boldsymbol{Z}_m\boldsymbol{\Omega}\dot{\boldsymbol{q}}_m(t) + \boldsymbol{\Omega}^2\boldsymbol{q}_m(t) = \boldsymbol{B}_m\boldsymbol{F}(t), \tag{2.14}$$

where $\boldsymbol{\Omega}^2$ and $\boldsymbol{Z}_m$ are diagonal matrices. While $\boldsymbol{\Omega}^2$ contains the squared natural frequencies of the system, $\boldsymbol{Z}_m$ has the modal damping values ζ_i of the individual eigenmodes as its main entries. Additionally, the modal input matrix is introduced for simplification reasons:

$$\boldsymbol{B}_m = \boldsymbol{M}_m^{-1}\boldsymbol{\Phi}^T. \tag{2.15}$$

When defining the state vector $\hat{\boldsymbol{x}}(t)$ as

$$\hat{\boldsymbol{x}}(t) = \begin{Bmatrix} \boldsymbol{q}_m(t) \\ \dot{\boldsymbol{q}}_m(t) \end{Bmatrix} \text{ and } \dot{\hat{\boldsymbol{x}}}(t) = \begin{Bmatrix} \dot{\boldsymbol{q}}_m(t) \\ \ddot{\boldsymbol{q}}_m(t) \end{Bmatrix}, \tag{2.16}$$

Eq. 2.14 is rearranged into state space form:

$$\dot{\hat{\boldsymbol{x}}}(t) = \underbrace{\begin{bmatrix} 0 & I \\ -\boldsymbol{\Omega}^2 & -2\boldsymbol{Z}_m\boldsymbol{\Omega} \end{bmatrix}}_{\hat{A}} \hat{\boldsymbol{x}}(t) + \underbrace{\begin{bmatrix} 0 \\ \boldsymbol{B}_m \end{bmatrix}}_{\hat{B}} \hat{\boldsymbol{u}}(t). \tag{2.17}$$

The output matrix $\hat{\boldsymbol{C}}$ and feed-through matrix $\hat{\boldsymbol{D}}$ depend on the type of output vector $\hat{\boldsymbol{y}}(t)$ desired and are introduced in Sec. 2.4.5.3 for the coupled simulation model. It should be noted that for a physical interpretation, the modal output vector needs to be transformed back into nodal coordinates.

2.4.5.2 Cutting Force Model

According to DENKENA & TÖNSHOFF (2011), three different kinds of models exist for cutting force simulation:

- empirical models,
- analytical models, and
- numerical models.

Empirical models are suitable to reproduce power and forces in a limited range of validity with good accuracy (DENKENA & TÖNSHOFF 2011). One difficulty is to determine the validity limits. Nevertheless, these models have proven to be useful in practice. Analytical models based on elementary plastomechanics generally do not provide exact results, but they have the great advantage of reproducing the

relationships of the forces to the most important input variables of a process in the form of equations (DENKENA & TÖNSHOFF 2011). They are thus suitable for sensitivity analyses of individual influencing variables. With the FE method (numerical models), power and forces - and also other quantities such as displacements, trajectory velocities, strains, stresses, and thermal quantities - can be determined with a high degree of accuracy (DENKENA & TÖNSHOFF 2011). However, the modeling effort and, depending on the modeling, the computational effort is considerable. Furthermore, a prerequisite for a reliable calculation is that the material behavior of the workpiece and the contact conditions between the workpiece and the tool are modeled with sufficient accuracy. Since the aim of this work is to simulate cutting forces as accurately as possible with low modeling effort, only empirical models will be considered further.

A commonly used empirical model is the cutting force model introduced by KIENZLE (1952). This model was originally established for turning only, but can be extended to other cutting processes, such as milling. The cutting forces are calculated by a power function based on the following equation:

$$F_i(t) = a_p \cdot K_{i1.1} \cdot h^{1-m_i}(t), \text{ with } i = t, r, f. \tag{2.18}$$

The indices t, r, f correspond to the tangential, radial, and feed directions, respectively. The specific cutting force coefficients and their so called main values $K_{i1.1}$ are dependent on the workpiece material, the cutting edge material, and most of the process parameters (KÖNIG ET AL. 1982). Hence, the cutting coefficients need to be identified separately for every new combination by cutting tests. The notation $K_{i1.1}$ corresponds to the K_i value for the tool-workpiece intersection quantities $a_p = 1$ mm and $h = 1$ mm. The $1 - m_i$ power value of the specific cutting force describes the slope of the cutting forces for a given workpiece-tool material combination. Identical to Eq. 2.1, a_p describes the DOC and $h(t)$ the dynamic chip thickness. An alternative approach for the simulation of dynamic cutting forces is described in WERNTZE (1973) with the identification of dynamic cutting force coefficients. Here, a machine tool is exposed to defined vibrations during the cutting force measurement. However, the identification of such frequency dependent and complex cutting force coefficients is very time-consuming and has therefore not become established. A disadvantage of the two cutting force models described above is that the edge forces, which cause cutting forces even for very small chip thicknesses ($h \approx 0$ mm), are neglected (WITT 2007). The linear mechanistic cutting force model described by ALTINTAS (2012) considers cutting edge coefficients and, due to the missing power coefficient, the cutting force coefficient identification requires fewer cutting tests. In addition, ALTINTAS (2012) also describes a more versatile linear oblique cutting force model, which transforms cutting force coefficients identified in orthogonal cutting tests to any cutting edge geometry. On the contrary, the great versatility of the oblique model is often accompanied by a loss of accuracy compared to the mechanistic model. Additionally, for both models described by ALTINTAS (2012), the range of validity

may be more limited since it is assumed that the cutting forces increase linearly with respect to chip thickness, while real-world cutting forces are best fit by a power function with a power lower than one. Due to the above mentioned advantages, the oblique and the mechanistic cutting force models were implemented for the work described in this dissertation. According to ALTINTAS (2012), the cutting forces for turning operations are

$$F_i(t) = K_{ic} a_p h(t) + K_{ie} a_p, \text{ with } i = t, r, f\,. \tag{2.19}$$

where K_{tc}, K_{rc}, and K_{fc} are the cutting and K_{te}, K_{re}, and K_{fe} the corresponding edge coefficients. The dynamic chip thickness $h(t)$ is affected by vibrations and, hence, the components of the force are coupled to the input side of the structural model of the machine.

2.4.5.3 Regenerative Cutting Process Model with Active Vibration Control

As shown in Fig. 2.1 and described in Eq. 2.1, vibrations between the tool and the workpiece lead to the dynamic chip thickness $h(t)$, which directly affects the output vector $\hat{\boldsymbol{y}}(t)$ from Eq. 2.13 through a transformation matrix. The resulting cutting forces need to be transformed into Cartesian coordinates in order to be linked to the input vector $\hat{\boldsymbol{u}}(t)$ from Eq. 2.17. The resulting *regenerative cutting process model* was already introduced for the most simple case in Sec. 2.1.2. In addition, the state space model from Eq. 2.17 must be extended by the AVC system. Since the controller and filter transfer functions are not known at this stage, only the actuator behavior is considered. Transforming the actuator transfer function G_A from Eq. 2.5 into state space form yields

$$\dot{\hat{\boldsymbol{x}}}_{\boldsymbol{A}}(t) = \begin{bmatrix} \dot{\hat{x}}_{A_1}(t) \\ \dot{\hat{x}}_{A_2}(t) \end{bmatrix} = \begin{bmatrix} \hat{x}_{A_2}(t) \\ F_A(t)/g_A \end{bmatrix} = \begin{bmatrix} 0 & 1 \\ -\omega_A^2 & -2\zeta_A\omega_A \end{bmatrix} \hat{\boldsymbol{x}}_{\boldsymbol{A}}(t) + \begin{bmatrix} 0 \\ 1 \end{bmatrix} \hat{u}_A(t)\,, \tag{2.20}$$

$$\hat{y}_A(t) = F_A(t) = \begin{bmatrix} -\omega_A^2 g_A & -2\zeta_A\omega_A g_A \end{bmatrix} \hat{\boldsymbol{x}}_{\boldsymbol{A}}(t) + g_A \hat{u}_A(t)\,, \tag{2.21}$$

with $\hat{x}_{A_1}$ and $\hat{x}_{A_2}$ representing the two states of the system. The input variable $\hat{u}_A(t)$ of the actuator is the voltage applied to the power amplifier and is identical to the control output $u(t)$. The output variable $\hat{y}_A(t)$ describes the actuator force $F_A(t)$ of the AVC system. Combining the two state space models from Eq. 2.21 and 2.17 yields

$$\dot{\hat{\boldsymbol{x}}} = \begin{bmatrix} \dot{\boldsymbol{q}}_{\boldsymbol{m}} \\ \ddot{\boldsymbol{q}}_{\boldsymbol{m}} \\ \dot{\hat{x}}_{A_1} \\ \dot{\hat{x}}_{A_2} \end{bmatrix} = \underbrace{\begin{bmatrix} \boldsymbol{0} & \boldsymbol{I} & \boldsymbol{0} & \boldsymbol{0} \\ -\boldsymbol{\Omega}^2 & -2\boldsymbol{Z}_{\boldsymbol{m}}\boldsymbol{\Omega} & -\boldsymbol{S}\omega_A^2 g_A & -\boldsymbol{S}2\zeta_A\omega_A g_A \\ \boldsymbol{0} & \boldsymbol{0} & 0 & 1 \\ \boldsymbol{0} & \boldsymbol{0} & -\omega_A^2 & -2\zeta_A\omega_A \end{bmatrix}}_{\hat{\boldsymbol{A}}} \hat{\boldsymbol{x}} + \underbrace{\begin{bmatrix} \boldsymbol{0} \\ \boldsymbol{S}g_A \\ 0 \\ 1 \end{bmatrix}}_{\hat{\boldsymbol{B}}} u, \tag{2.22}$$

with $\boldsymbol{S}$ substituting $\boldsymbol{B_m} \cdot \hat{\boldsymbol{f}}$. The actuator force $F_A(t) = \hat{y}_A(t)$ acts on the mechanical structure via the nodal degree of freedom described by the vector $\hat{\boldsymbol{f}}$. The output vector $\hat{\boldsymbol{y}}$ has only one entry: the output variable $y(t)$ of the controlled system, which is identical to the measured acceleration $\ddot{x}(t)$ at the actuator position because the sensor and the actuator are at the same location. From the modal transformation (Eq. 2.8) and the modal equation of motion (Eq. 2.10), the output variable can be expressed as

$$\begin{aligned}\hat{\boldsymbol{y}} = y &= \hat{\boldsymbol{f}}^T \ddot{\boldsymbol{x}} = \hat{\boldsymbol{f}}^T \boldsymbol{\Phi} \ddot{\boldsymbol{q}}_m \\ &= \underbrace{\hat{\boldsymbol{f}}^T \boldsymbol{\Phi} \begin{bmatrix} -\boldsymbol{\Omega}^2 & -2\boldsymbol{Z_m}\boldsymbol{\Omega} & -\boldsymbol{S}\omega_A^2 g_A & -\boldsymbol{S} 2\zeta_A \omega_A g_A \end{bmatrix}}_{\hat{\boldsymbol{C}}_G^T} \hat{\boldsymbol{x}} + \underbrace{\hat{\boldsymbol{f}}^T \boldsymbol{\Phi} \boldsymbol{S} g_A}_{\hat{\boldsymbol{D}}_G} u \,. \end{aligned} \tag{2.23}$$

The state space model of the controlled system (Eq. 2.22 and Eq. 2.23) is needed for the synthesis of a state controller (see Sec. 2.4.6.4). This model can be automatically identified, as will be explained in Sec. 2.4.7.1. For a model-based single-input-single-output (SISO) controller (see Sec. 2.4.6.5), the transfer function of the controlled system $G(s)$ is required, which can be derived from the system matrices as follows:

$$G(s) = \hat{\boldsymbol{C}}_G (s\boldsymbol{I} - \hat{\boldsymbol{A}})^{-1} \hat{\boldsymbol{B}} + \hat{\boldsymbol{D}}_G \,. \tag{2.24}$$

For the purpose of more realistic controller testing, stability and energy demand analysis, and actuator dimensioning, the state space model has to be further extended to be coupled with the cutting force model from Sec. 2.4.5.2. Therefore, three additional inputs for the cutting forces at the TCP and three additional outputs for the displacement at the TCP are added in the x, y, and z directions. The nodal degrees of freedom at the TCP are described by the three columns of the influence matrix $\boldsymbol{E}$. The additional cutting forces can then be expressed as

$$\boldsymbol{F_{TCP}(t)} = \underbrace{\begin{bmatrix} 1 & 0 & 0 \\ 0 & 1 & 0 \\ 0 & 0 & 1 \\ \vdots & \vdots & \vdots \\ 0 & 0 & 0 \end{bmatrix}}_{\boldsymbol{E}} \begin{bmatrix} f_{TCP_x}(t) \\ f_{TCP_y}(t) \\ f_{TCP_z}(t) \end{bmatrix}. \tag{2.25}$$

Analogously, the displacement at the TCP is derived as

$$\boldsymbol{x_{TCP}}(t) = \begin{bmatrix} x_{TCP_x}(t) \\ x_{TCP_y}(t) \\ x_{TCP_z}(t) \end{bmatrix} = \boldsymbol{E}^T \boldsymbol{\Phi} \boldsymbol{q_m(t)}. \tag{2.26}$$

In addition, the actuator force $F_A(t)$ is of great interest for controller tuning and actuator dimensioning. Hence, a further entry of the output vector $\hat{\boldsymbol{y}}(t)$ for the actuator force is defined based on Eq. 2.21. If the relationships in Eq. 2.25, Eq. 2.26, and Eq. 2.21 are considered for the additional inputs $\boldsymbol{F}_{TCP}(t)$ and the additional outputs $F_A(t)$ and $\boldsymbol{x}_{TCP}(t)$, the extended state space model is represented by:

$$\dot{\hat{\boldsymbol{x}}} = \begin{bmatrix} \dot{\boldsymbol{q}}_m \\ \ddot{\boldsymbol{q}}_m \\ \dot{x}_{A_1} \\ \dot{x}_{A_2} \end{bmatrix} = \hat{\boldsymbol{A}}\hat{\boldsymbol{x}} + \hat{\boldsymbol{B}}u + \begin{bmatrix} \boldsymbol{0} \\ \boldsymbol{B}_m \\ \boldsymbol{0} \\ \boldsymbol{0} \end{bmatrix} \boldsymbol{F}_{TCP} = \hat{\boldsymbol{A}}\hat{\boldsymbol{x}} + \begin{bmatrix} \boldsymbol{0} & \\ \boldsymbol{B}_m & \\ \boldsymbol{0} & \\ \boldsymbol{0} & \end{bmatrix} \begin{bmatrix} u \\ \boldsymbol{F}_{TCP} \end{bmatrix}, \tag{2.27}$$

$$\hat{\boldsymbol{y}} = \begin{bmatrix} y \\ F_A \\ \boldsymbol{x}_{TCP} \end{bmatrix} = \begin{bmatrix} & & \hat{\boldsymbol{C}}_G^T & \\ 0 & 0 & -\omega_A^2 g_A & -2\zeta_A \omega_A g_A \\ \boldsymbol{E}^T\boldsymbol{\Phi} & \boldsymbol{0} & \boldsymbol{0} & \boldsymbol{0} \end{bmatrix} \hat{\boldsymbol{x}} + \begin{bmatrix} \hat{\boldsymbol{D}}_G & \hat{\boldsymbol{f}}^T\boldsymbol{\Phi}\boldsymbol{B}_m \\ g_A & 0 \\ \boldsymbol{0} & \boldsymbol{0} \end{bmatrix} \begin{bmatrix} u \\ \boldsymbol{F}_{TCP} \end{bmatrix}. \tag{2.28}$$

Fig. 2.10 shows the block diagram representation of this *regenerative cutting process model with AVC*. The structural dynamics simulation is coupled with the cutting force model in the time domain (WITT 2007). One approach for this is the digital block simulation. This way, the structural model in state space representation can be connected to the cutting force model within a computer-aided control engineering program.

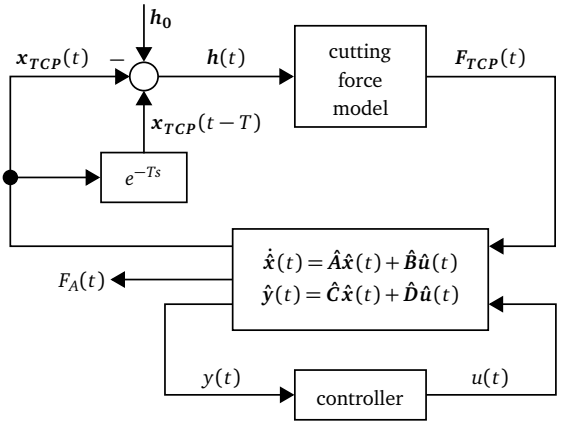

Fig. 2.10: Regenerative cutting process model with AVC

2.4.6 Control and Filter Strategies

Fig. 2.11 is a detail of Fig. 2.10 and shows the block diagram of the closed control loop for AVC. This essentially corresponds to a standard control loop according to LUNZE (2010). The measured controlled variable $y(t)$ is the acceleration at the actuator or sensor position. This acceleration should be controlled to zero according to the reference variable $r(t)$. The controller $C(s)$ generates the control output $u(t)$ from the error signal $e(t)$ in such a way that the generated actuator force $F_A(t)$, which acts on the machine tool structure $H(s)$, suppresses the vibrations in order to reach the control target. The variables $d_i(t)$ and $d_o(t)$ describe disturbances at the system input and output, respectively. However, the two variables are not shown in Fig. 2.10. In this example, the disturbance at the system input $d_i(t)$ may be described as control output noise, which is often negligible, while the disturbance at the system output $d_o(t)$ is commonly referred to as measurement noise.

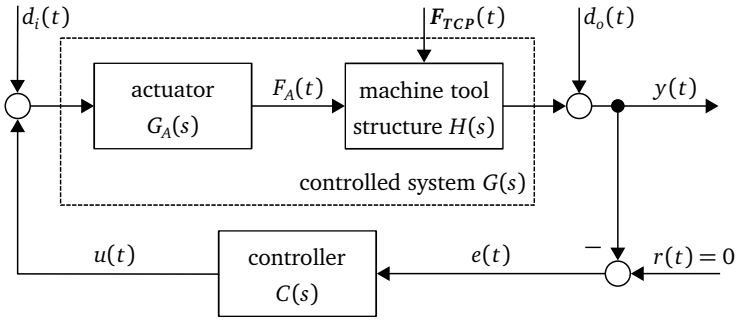

Fig. 2.11: Feedback loop of an active vibration controller

The basic idea of AVC is the generation of an actuator force in counterphase to the excitation force. Furthermore, some control strategies exist which shift the natural frequency of the controlled system (PREUMONT 2002) or disturb the regenerative effect by applying a delayed feedback (MANCISIDOR ET AL. 2019a) or an amplitude modulation (WEREMCZUK ET AL. 2015; SALLESE ET AL. 2017).

The choice of a suitable control algorithm plays a key role in AVC. As summarized in Sec. 2.3, the most commonly used control strategies for AVC in the literature are model-free control, model-based control synthesis, and adaptive control. All of these control strategies were also implemented in the context of this research work and are therefore briefly explained in the following sections. First, the stability criteria applied in this work are summarized and the filter strategies implemented for signal conditioning are presented. For more detailed information on the individual filter and controller architectures, please refer to the relevant technical literature (ZHOU ET AL. 1996; PREUMONT 2002; GAWRONSKI 2004; HANSEN 2012).

2.4.6.1 Stability Criteria

In control engineering, many different definitions of the stability of dynamic systems and many criteria for assessing it exist. This section is limited to the *Nyquist criterion* and the criterion of *asymptotic stability*, which were both used in the context of this dissertation.

According to the **Nyquist criterion**, a control loop is stable only when all solutions of the equation

$$F_o(s) + 1 = 0 \tag{2.29}$$

lie to the left of the imaginary axis and all possible pole-zero reductions within and between the transfer elements take place exclusively in the left complex half-plane (FÖLLINGER ET AL. 2013). Eq. 2.29 is called *characteristic equation*, with

$$F_o(s) = G(s)C(s) \tag{2.30}$$

representing the open-loop transfer function. If the open-loop transfer function is stable, closed-loop stability is fulfilled provided that the Nyquist plot of the open-loop frequency response must neither encircle nor include the critical point -1 in the complex plane. This is illustrated in Fig. 2.12. According to the Nyquist criterion, the system whose loop transfer function is shown on the left-hand side is unstable and the one on the right-hand side is stable. FÖLLINGER ET AL. (2013) recommend a gain margin of $A_m \approx 3$ together with a phase margin of $\phi_m \in [30°; 60°]$ in order to reach a good compromise between sufficient bandwidth and robust stability.

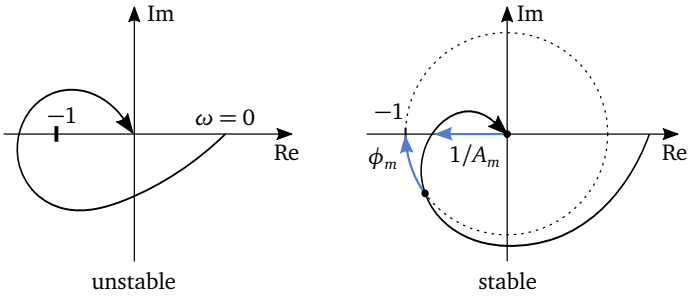

Fig. 2.12: Examples for unstable and stable systems with phase and gain margin

For the representation in the state space form, the term **asymptotic stability** is more suitable. A dynamic system as described by Eq. 2.12 and Eq. 2.13 is asymptotically stable, if the solution for $\hat{\boldsymbol{x}}(t)$ in the homogeneous differential equation

$$\dot{\hat{\boldsymbol{x}}}(t) = \hat{\boldsymbol{A}}\hat{\boldsymbol{x}}(t) \tag{2.31}$$

approaches $\mathbf{0}$ for $t \to +\infty$ (FÖLLINGER ET AL. 2013). This condition has to be fulfilled for every starting point $\hat{\boldsymbol{x}}(t=0) = \hat{\boldsymbol{x}}_{\mathbf{0}}$. This is equivalent to the dynamic system being asymptotically stable because all eigenvalues of $\hat{\boldsymbol{A}}$ lie in the left complex half-plane.

2.4.6.2 Filters

According to PREUMONT (2002), high-pass and low-pass filters are most commonly used in AVC for signal conditioning. While an analogue low-pass filter needs to be placed before the ADC to avoid aliasing (see Sec. 2.4.1), high-pass filters are often digitally implemented on the electronic control unit alternatively or in addition to an analogue high-pass filter. Furthermore, a compensation filter for the actuator transfer function is sometimes required (see Eq. 2.6). Notch filters can reduce signal noise at narrow frequency bands, but are also applied to suppress signal components caused by forced vibrations, such as vibrations from the run-out of the spindle-tool assembly or the tooth passing frequency and its harmonics in milling operations.

High-pass Filters
BAUR (2014) applied a first-order high-pass filter to prevent an undesired pre-magnetization of the AVC actuator coil as well as to eliminate static offsets in the measured acceleration signal, and selected the cut-off frequency ω_{hp} to be 4 % of the lowest critical chatter frequency ω_c. The filter's transfer function is defined as

$$G_{HP} = \frac{s}{s + \omega_{hp}} \, . \tag{2.32}$$

One of the main disadvantages of this filter strategy is the fact that inside the transition frequency band the magnitude and, even more importantly for AVC, the phase is changed. Therefore, the main target is to design filters with a narrow transition band. In general, a filter's roll-off becomes sharper with an increasing order, but at the same time the absolute phase delay increases. Hence, a trade-off between strong noise suppression and low phase delay (phase shift) has to be considered and a good compromise to be found.

Notch Filters
If signal noise occurs at a constant frequency, a notch filter, described by

$$G_{notch} = \frac{s^2 + \omega_{notch}^2}{s^2 + a_{notch} \cdot s + \omega_{notch}^2} \, , \tag{2.33}$$

can be tuned with ω_{notch} defining the frequency where the notch filter is located and a_{notch} setting its frequency band in rad/s.

Since the full actuator power is usually applied to increase chatter stability, it is useful to filter out the tooth passing frequency and its harmonics in machining processes with interrupted cut or with a multi-cutting-edge tool, such as milling (KERN 2009;

ROTH 2009; BAUR 2014). As explained in Sec. 2.1, these cause forced vibrations and are dominant in the operating vibration spectrum of a stable cutting process. Also for reasons of energy efficiency, the AVC system should not react to these signal components (BAUR 2014). The tooth passing frequency and its harmonics are directly proportional to the spindle speed. Since the spindle speed changes continuously under load, LTI notch filters, as described in Eq. 2.33, are unsuitable. KERN (2009), ROTH (2009), and BAUR (2014) implemented a recursive least-squares (RLS) adapted filter with a linear combination of orthogonal reference signals for this purpose. The mono-frequency harmonic signal component to be filtered is simulated by the weighted superposition of a sine and a cosine oscillation of the same frequency. The aim of the RLS algorithm is to adapt the filter in such a way that the estimated perturbation comes as close as possible to the harmonic component contained in the measurement signal at the same frequency. Subtracting the estimated perturbation from the measurement signal eliminates the unwanted tooth passing frequency component without adding any phase delay. Further information on this topic can be found in MOSCHYTZ & HOFBAUER (2000) or KERN (2009).

2.4.6.3 Model-free Control Strategies

In the literature, model-free LTI control strategies are most often used for AVC because of their simple tuning. The lack of the need for a model is especially advantageous if the controlled system changes, e.g. due to position-dependent dynamics (MANCISIDOR ET AL. 2014). However, sensor-actuator collocation is required in order to obtain a robust controller (PREUMONT 2002).

Collocation is achieved if a vibration generated by an actuator is measured with a sensor at the same location where the actuator force is applied to the structure. Collocated systems have special properties as, for example, possessing alternating poles and zeros along and always left the imaginary axis, which guarantee asymptotic stability of several control systems, e.g. DVF (PREUMONT 2002). On the contrary, non-collocated systems show pole-zero flipping above the gain margin and some of the poles can become unstable (PREUMONT 2002).

In the following, different existing model-free control strategies are presented. More information about these types of controllers can be found in PREUMONT (2002), except for *delayed position feedback*, which was introduced by MUNOA ET AL. (2013).

MUNOA ET AL. (2013) describe the working principle of the control strategies based on the DDE from Eq. 2.1, which is extended by the actuator force F_A:

$$\underbrace{m \cdot \ddot{x}(t)}_{\text{F1}} + \underbrace{d \cdot \dot{x}(t)}_{\text{F2}} + \underbrace{k \cdot x(t)}_{\text{F3}} = K_{fc} \cdot a_p \cdot [h_0 - x(t) + \underbrace{x(t-T)}_{\text{F4}}] + F_A \,. \tag{2.34}$$

Each of the following control strategies adapts one of the terms denoted by F1, F2, F3, and F4.

F1 - Direct Acceleration Feedback
Direct acceleration feedback (DAF) applies an actuator force proportional to the acceleration of the structure:

$$F_A = -g_C \cdot \ddot{x}(t) \,, \tag{2.35}$$

with g_C defining the gain. This control law affects the modal mass and, therefore, the natural frequency can be changed in either direction.

F2 - Direct Velocity Feedback
According to MUNOA ET AL. (2013), DVF is the most commonly used control strategy for AVC. The main idea here is to inject a viscous damping-like effect into the system by applying an actuator force proportional to the measured velocity signal:

$$F_A = -g_C \cdot \dot{x}(t) \,. \tag{2.36}$$

Another explanation of the effect of DVF can be given by analyzing the phase response of the SDOF system. At the natural frequency, the velocity signal of the moving mass is in phase with the excitation signal. Hence, applying a counterphase force proportional to the velocity signal yields a destructive interference (SCHULZ 2010; BAUR 2014).

Since accelerometers are mainly used as sensors (see Sec. 2.4.1), the measured signal must be integrated with respect to time. This integration causes that the controller's magnitude FRF tends towards infinity for low frequencies. Instead of a pure integrator, HOLTERMAN (2002) introduced a *leaking integrator*, which improves the low-frequency behavior. The overall transfer function of this controller is:

$$C_{DVF}(s) = \frac{g_C}{s + p_{leak}}, \quad p_{leak} \leq 0{,}2 \cdot \omega_c \,. \tag{2.37}$$

The cut-off frequency p_{leak} must be set to a value of less than 20 % of the lowest chatter frequency ω_c to be expected (HOLTERMAN 2002).

F3 - Direct Position Feedback
Similar to DAF, direct position feedback (DPF) also affects the natural frequency of the controlled system due to a modification of its stiffness. The control law is

$$F_A = -g_C \cdot x(t) \,. \tag{2.38}$$

F4 - Delayed Position Feedback
Delayed position feedback (DelPF) focuses on "reducing virtually the engagement [relative position] between the current and previous waves" (MUNOA ET AL. 2013, p. 409) in order to disturb the regenerative effect. This is achieved by the following control law:

$$F_A = -g_C \cdot x(t - T) \,. \tag{2.39}$$

If accelerometers are used for vibration measurement, it is beneficial to use *delayed acceleration feedback* (DelAF), because then the double integration block, which amplifies low frequency noise, can be avoided (MANCISIDOR ET AL. 2019a). DelAF leads to the same results as DPF, since, near a natural frequency, the acceleration and the position signal are in counterphase.

Fig. 2.13 shows the effect of the strategies F1 to F4 on the SLD for a SDOF system. While all strategies improve the chatter stability, the DVF controller shows the best performance, especially at the lower stability area. If the peaks in the SLD are to be improved, DelPF is the strategy of choice (MANCISIDOR ET AL. 2019a). However, for milling operations, precise tuning of DelPF requires a cutting process model, which increases the implementation effort (MANCISIDOR ET AL. 2019a).

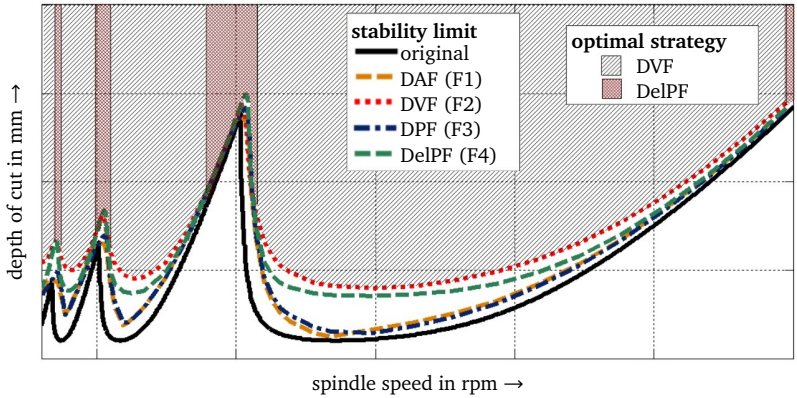

Fig. 2.13: Comparison of control strategies F1 to F4 over SDOF system stability lobes based on MUNOA ET AL. (2013).

Conclusion

Model-free controllers achieve a high robustness and are easy to tune if the sensor and actuator are collocated. However, collocation is an ideal state, which is never exactly fulfilled in reality (PREUMONT 2002). Furthermore, phase delays resulting from the sensor, the amplifier, the electronic control unit, and the actuator can affect the control performance and stability negatively (EHMANN 2004; PEREIRA ET AL. 2014). Therefore, a model of the controlled system is still required if the stability of the closed-loop system is intended to be evaluated analytically (EHMANN 2004). It should be mentioned that one advantage of DelPF and DelAF is to compensate phase delays already within the controller.

In addition, model-free control strategies make use of the behavior of mechanical structures when oscillating at their natural frequency, as described above for the DVF controller. If forced vibrations occur at frequencies much different than a natural

frequency, the vibration suppression performance decreases significantly, because the actuator force and the external excitation are not in perfect counter-phase anymore (WAIBEL 2012). However, chatter suppression performance is hardly affected, since the chatter frequency is always close to a machine tool's natural frequency (ALTINTAS 2012).

Further difficulties arise if a machine tool shows several dominant modes and the above mentioned control strategies are intended to be focused on damping only the most critical one. In this case, filters can be tuned accordingly (MANCISIDOR ET AL. 2015), but their tuning is a complex task and reduces the overall performance of the controller because of additional phase shifts (EHMANN 2004). By adding more poles and zeros to compensate for phase distortions (loop-shaping), control performance and stability can be improved, but this manual optimization requires in-depth expert knowledge (EHMANN 2004). A systematic way to design a powerful model-based controller that can be easily tuned to damp only certain eigenmodes is shown in the following section dealing with optimal control synthesis.

2.4.6.4 Optimal H_2 Control

Optimal H_2 control describes a synthesis method for LTI *state space controllers*. According to GAWRONSKI (2004), the term "optimal H_2" refers to the core of the control synthesis, i.e. a mathematical optimization based on the euclidean $\|\cdot\|_2$ norm. State controllers were originally developed for the control of MIMO systems, since "classical" controller tuning methods based on simple transfer functions, as described in the previous section, are difficult to apply in this case (PREUMONT 2002). However, state controllers in turn can easily be applied for SISO systems. Due to their strong performance in tracking and disturbance rejection applications, *Linear-Quadratic Regulators* (LQR) are often used for AVC of machine tools (e.g. SIMNOFSKE (2009), KERN (2009), BOLDERING (2015)). The LQR represents a special case of the H_2 design problem and minimizes the quadratic cost function of linear systems (WERNER 2017). Since it can be quite costly or even impossible to measure all the states of a controlled system, the states have to be estimated using, for example, a Luenberger observer or a Kalman filter as a state estimator (PREUMONT 2002). If a system is subject to both process noise and measurement noise, the Kalman filter is the better choice for estimating the states since it is also capable of filtering noisy signals (MÜLLER 1996). The combination of an LQR and a Kalman filter for the state estimation is called *Linear-Quadratic-Gaussian* (LQG) controller and will be described in the following section. First, the LQR is introduced, followed by the state estimation with a Kalman filter. Due to the separation theorem, both parts can be designed independently (PREUMONT 2002). Unless otherwise indicated, this section is based on FÖLLINGER ET AL. (2013).

Linear-Quadratic Regulator
As explained in Sec. 2.4.6.1, the dynamics and thus the stability of a controlled

system depend on the eigenvalues of the system matrix $\hat{\boldsymbol{A}}$. With state control it is possible to specify the eigenvalues of a dynamic closed-loop system arbitrarily as long as the open-loop system is fully controllable. The block diagram of a state controller including a state estimator is shown in Fig. 2.14. As the name "state control" already indicates, the constant feedback matrix $\boldsymbol{C}$ is used to feed back the estimated state vector $\hat{\boldsymbol{x}}(t)$. Hence, a state control law is defined as

$$\hat{\boldsymbol{u}}(t) = -\boldsymbol{C}\hat{\boldsymbol{x}}(t). \tag{2.40}$$

Inserting this control law into the first-order state space representation (Eq. 2.12) yields

$$\dot{\hat{\boldsymbol{x}}}(t) = (\hat{\boldsymbol{A}} - \hat{\boldsymbol{B}}\boldsymbol{C})\hat{\boldsymbol{x}}(t). \tag{2.41}$$

By selecting the eigenvalues of the closed-loop in the left complex half-plane, it is ensured that disturbances (e.g. cutting forces) are compensated. The further left the poles are, the more damped the system is (UNBEHAUEN 2009). Optimal control synthesis does not only focus on the resulting poles or on individual control loop parameters, but on the entire course of the controller outputs and error signals.

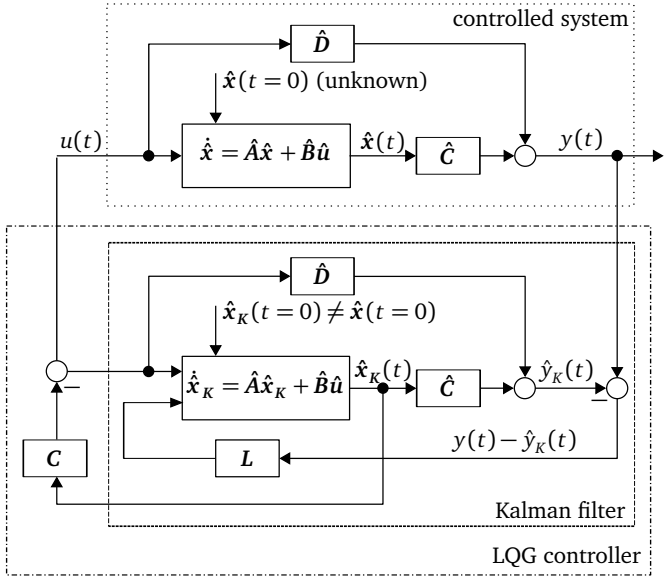

Fig. 2.14: Signal flow chart of a LQR with state estimation based on GAWRONSKI (2004)

Therefore, a control law in the form of Eq. 2.40 is sought, which minimizes the following cost function

$$J = \frac{1}{2}\int_0^\infty \hat{\boldsymbol{x}}^T(t)\boldsymbol{Q}\hat{\boldsymbol{x}}(t) + \hat{\boldsymbol{u}}^T(t)\boldsymbol{R}\hat{\boldsymbol{u}}(t)\,dt\ . \tag{2.42}$$

Here, $\boldsymbol{Q}$ and $\boldsymbol{R}$ are symmetrical and positive-definite[4] weighting matrices, which are usually selected to be diagonal because cross-diagonal elements only describe negligible coupling effects (If the state space matrices are expressed in modal coordinates, the states are already only coupled as pairs). The term $\hat{\boldsymbol{x}}^T\boldsymbol{Q}\hat{\boldsymbol{x}}$ ensures that the controlled state space vector entries approach zero after an initial displacement and a certain amount of time corresponding to their respective weight. The second term $\hat{\boldsymbol{u}}^T\boldsymbol{R}\hat{\boldsymbol{u}}$ is in a similar manner responsible for keeping the control effort as reasonably small as possible. In comparison to the model-free control strategies, LQR can be easily tuned to focus on damping only certain eigenmodes. Placing a high weight on the first state space vector entry, for example, yields a controller that leads to damping the corresponding first eigenmode. The larger a weight is selected in comparison to the others, the greater is the relative influence of the associated variable on the cost function J. Due to the objective of minimizing the cost function, the LQR will therefore ensure that this variable remains small compared to other variables that are less strongly weighted. The solution of this optimization problem can be derived using the *Hamilton method*, which yields the following control law:

$$\hat{\boldsymbol{u}}(t) = -\boldsymbol{C}\hat{\boldsymbol{x}}(t) = -\boldsymbol{R}^{-1}\hat{\boldsymbol{B}}^T\boldsymbol{P}\hat{\boldsymbol{x}}(t)\ , \tag{2.43}$$

with $\boldsymbol{P}$ describing the explicit and positive definite solution of the algebraic *Riccati equation*

$$\boldsymbol{P}\boldsymbol{C}^T\boldsymbol{R}^{-1}\boldsymbol{C}\boldsymbol{P} - \boldsymbol{P}\hat{\boldsymbol{A}}^T - \hat{\boldsymbol{A}}\boldsymbol{P} - \boldsymbol{Q} = \boldsymbol{0}\ , \tag{2.44}$$

which can be solved numerically using the software tool MATLAB®, for example.

Kalman Filter as a State Estimator

With the help of a Kalman filter, the states $\hat{\boldsymbol{x}}(t)$ can be estimated. Hence, the controller no longer needs to feed back the entire state vector $\hat{\boldsymbol{x}}(t)$, but only the output signal $y(t)$.

The state space model of the resulting SISO LQG controller is defined as

$$\dot{\hat{\boldsymbol{x}}}_K(t) = \left[\hat{\boldsymbol{A}} - \hat{\boldsymbol{B}}\boldsymbol{C} - \boldsymbol{L}\hat{\boldsymbol{C}} + \boldsymbol{L}\hat{\boldsymbol{D}}\boldsymbol{C}\right]\hat{\boldsymbol{x}}_K(t) + \boldsymbol{L}y(t), \tag{2.45}$$

$$u(t) = -\boldsymbol{C}\hat{\boldsymbol{x}}_K(t)\ . \tag{2.46}$$

In Fig. 2.14, it can be seen that the observer places a mathematical model of the state space system in parallel and calculates the estimated state vector $\hat{\boldsymbol{x}}_K(t)$ by

[4] A square symmetrical matrix $\boldsymbol{Q}$ is positive-definite exactly when all eigenvalues are greater than zero. Then $\hat{\boldsymbol{x}}^T\boldsymbol{Q}\hat{\boldsymbol{x}} > 0$ is valid for any vector $\hat{\boldsymbol{x}} \neq \boldsymbol{0}$.

feeding back the control variable $u(t)$ as well as the measured output signal $y(t)$. While $u(t)$ allows the course of the state vector $\hat{\boldsymbol{x}}_K(t) = \hat{\boldsymbol{x}}(t)$ to be calculated for the same initial state, the resulting difference between the measured output signal $y(t)$ and the reconstructed output signal $\hat{\boldsymbol{y}}_K(t)$ is weighted by the matrix $\boldsymbol{L}$ in order to consider unknown disturbances acting on the state vector $\hat{\boldsymbol{x}}(t)$ and noise acting on the estimated state vector $\hat{\boldsymbol{x}}_K(t)$. Thereby, differences between the system and the model are continuously reduced, too.

Conclusion
It has been shown that the characteristics of the LQR are set by means of the weighting matrices. These must be adjusted iteratively until the desired control performance is achieved. In contrast to the LQR with direct state feedback, no guaranteed general robustness properties can be expected for the LQR with a state estimator. Under certain circumstances, even the smallest deviations of the model from the real system can lead to instability. Therefore, the stability must be verified for each individual design on the real system (ZHOU ET AL. 1996). In contrast, *robust control synthesis*, which is described in the following section, offers a systematic methodology to identify a model-based controller with robust stability and performance without having to explicitly follow the step of designing a state observer.

2.4.6.5 Optimal H_∞ and µ Control

As already described in the previous section, often no exact model of the controlled system exists in reality. In addition, the dynamics of the mechanical structure can change due to various influences (e.g. TCP movement in the workspace or spindle speed changes) (WECK & BRECHER 2006c). In view of the nominal system, optimal H_2 control offers the best possible performance, but even small system deviations can strongly deteriorate its results. Optimal H_∞ and μ control refer to the field of LTI robust control synthesis and are approaches to ensure the stability and control performance of the closed-loop even if the system model $G(s)$ differs from the actual physical system. TØFFNER-CLAUSEN (1996) defines that *robust stability* is given if the stability of the closed-loop is guaranteed for all perturbations occurring in the system. *Robust performance* is more demanding and requires that the specified control performance of the closed-loop is achieved for all perturbations of the system with simultaneous stability. Since the synthesis of a robust controller is fundamentally based on the mathematical description of model uncertainties, these will be briefly discussed below. Unless otherwise indicated, this section is based on ZHOU ET AL. (1996).

Uncertainty Quantification
In addition to a linear representation of the nominal FRF of the controlled system, a model can contain information about uncertainties existing in the system. In uncertainty modeling, a distinction is made between *structured* and *unstructured* uncertainties.

Structured Uncertainties are recommended to describe variations of model parameters, such as the modal parameters. They are therefore also called parametric uncertainties and can model perturbations applicable to individual eigenmodes precisely. Further explanations can be found in ZHOU ET AL. (1996). Structured uncertainties can be considered in the μ synthesis only.

Unstructured Uncertainties represent the most general type of uncertainty description and thus enable a global consideration of the system's perturbations. However, in the case of the unstructured uncertainty description, its effect on the FRF is directly modeled instead of a parameter uncertainty. This results in a more conservative uncertainty description (overestimation), which in turn has a negative effect on the achievable performance. Unstructured uncertainties can be further separated into additive and multiplicative uncertainties. According to EHMANN (2004), additive uncertainties are suitable for mapping high-frequency eigenmodes that have not been taken into account in order to avoid spill-over effects. If the focus is on modeling variable dynamics of the nominal system, multiplicative uncertainties are more appropriate. The latter is therefore selected for the uncertainty description in this dissertation. Another advantage is the fact that multiplicative uncertainties usually have a lower order and the final order of the H_∞ controller correlates with the order of all weighting functions (EHMANN 2004). *Multiplicative uncertainties* can be specified according to

$$G(s) = G_n(s)(1 + \Delta_m(s)) \, . \tag{2.47}$$

The nominal transfer function G_n is overlaid by the frequency-dependent multiplicative uncertainty

$$\Delta_m(s) = W_m(s) \cdot \Delta(s) \, , \tag{2.48}$$

with $\Delta(s)$ describing an arbitrary, stable transfer function. The transfer function $W_m(s)$ contains the weighting information about the magnitude of the unstructured uncertainty as a function of frequency. By a multiplication with $\Delta(s)$, it is achieved that the unstructured multiplicative uncertainty $\Delta_m(s)$ spans over an uncertainty-range.

As shown in Fig. 2.15, the multiplicative uncertainty $\Delta_m(s)$ creates a circular uncertainty region around the Nyquist plot of the nominal transfer function $G_n(s)$ for each frequency ω. The respective radius $r(j\omega)$ is represented by $|W_m(j\omega)G_n(j\omega)|$. The hulls of the circles create the area in which the locus of the uncertain system can run.

Unlike the structured uncertainties, the unstructured uncertainties generate fully occupied, i.e. unstructured uncertainty matrices $\boldsymbol{\Delta_m}(s)$, which are also frequency dependent. The multiplicative uncertainties can be determined by subtracting the

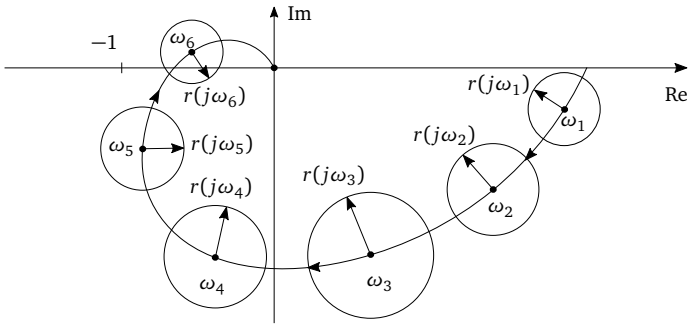

Fig. 2.15: Nyquist plot of a nominal system with multiplicative uncertainties based on HERZOG & KELLER (2011)

nominal model G_n from the measured perturbed transfer functions $\hat{G}$ and dividing by G_n (EHMANN 2004):

$$|W_m(j\omega)| > \left| \frac{\hat{G}(j\omega) - G_n(j\omega)}{G_n(j\omega)} \right|. \tag{2.49}$$

H_∞ Synthesis

The goal of H_∞ synthesis is to design a closed-loop control system that meets defined performance specifications. The evaluation of this control performance is done using the $\|\cdot\|_\infty$ norm, which, in SISO systems, corresponds to the largest magnitude of the transfer function, as can be viewed in a Bode diagram:

$$\|G\|_\infty = \max_\omega \|G(j\omega)\|. \tag{2.50}$$

An H_∞ controller meets the requirements for nominal stability and performance as well as for robust stability. It has been successfully tested for AVC of machine tools by several researchers (e.g. TEWANI ET AL. (1995), MONNIN ET AL. (2014a, b), BRECHER ET AL. (2016)). As illustrated in Fig. 2.16, the closed-loop system (i.e. controlled system $G(s)$ coupled with the controller dynamics $C(s)$) is extended into a MIMO transfer matrix (i.e. so-called Performance Channel) $\boldsymbol{T}_{zw}(s)$, inside of which the necessary performance requirements can be specified with adequate weighting functions (see Eq. 2.53). The weighted open-loop matrix transfer function $\boldsymbol{P}_r(s)$ contains the performance specifications. The aim of H_∞ synthesis is to find a controller $C(s)$ that stabilizes $\boldsymbol{P}_r(s)$ and minimizes the $\|\cdot\|_\infty$ norm of the performance channel $\boldsymbol{T}_{zw}(s)$. The challenge in H_∞ synthesis is to design the performance channel $\boldsymbol{T}_{zw}(s)$ by means of weighting function selection in such a way that a favorable control performance is achieved. The control performance is specified by so-called *boundaries* for the transfer functions of the closed-loop system. In the literature, this procedure is often referred to as *closed-loop shaping*.

In order to determine the boundaries for single-variable systems, the relationships between the relevant inputs and outputs of the control loop (see Fig. 2.11) must first be considered. The *sensitivity function*

$$S_c(s) = \frac{1}{1 + G(s)C(s)} \tag{2.51}$$

indicates the difference between the open-loop and the closed-loop disturbance response (LUNZE 2010). Because of the correlation

$$T_c(s) = 1 - S_c(s)\,, \tag{2.52}$$

the function $T_c(s)$ is called the *complementary sensitivity function* and describes the influence of the reference variable $r(t)$ on the controlled variable $y(t)$ (LUNZE 2010). In case of AVC, where $r(t) = 0$, $T_c(s)$ shows how the measurement noise $d_o(t)$ permeates the controlled variable $y(t)$. Of particular interest is the *process sensitivity function* $G(s)S_c(s)$, which represents in the SISO case the response of the sensor signal $y(t)$ to a disturbance at the system input $d_i(t)$ and is identical to the closed-loop system's response to disturbances acting at the controlled system's input level. Its boundary very significantly influences the damping performance and allows the controller to be focused on specific eigenmodes only. At the same time, the *control sensitivity function* $C(s)S_c(s)$ must be minimized in such a way that the actuator force required for active damping remains as low as possible. SCHÖNHOFF (2003) presents a method for the practical application of robust controllers for AVC, which simplifies the specification of the control-loop performance by means of a fixed weighting scheme. This method was also used in EHMANN (2004), KYTKA ET AL. (2007), and KERN (2009) for AVC of machine tools. The same weighting scheme was also used in the context of this dissertation and will therefore be presented in the following. As can be seen in Fig. 2.16, the open-loop transfer function is extended by the weighting functions (W_r, W_d, W_e, W_u), which help to shape the boundaries for the aforementioned sensitivity functions. According to SCHÖNHOFF (2003), the outer disturbance $d_o(t)$ can be included within the inner disturbance $d_i(t)$ in the SISO case.

If the control loop is closed with the controller $C(s)$, the transfer function of the performance channel $\boldsymbol{T_{zw}}(s)$ can be derived from the closed-loop transfer function matrix:

$$\underbrace{\begin{bmatrix} \tilde{e} \\ \tilde{u} \end{bmatrix}}_{\boldsymbol{z}(t)} = \underbrace{\begin{bmatrix} W_e S_c W_r & W_e G S_c W_d \\ -W_u C S_c W_r & -W_u T_c W_d \end{bmatrix}}_{\boldsymbol{T_{zw}}(s)} \cdot \underbrace{\begin{bmatrix} -\tilde{r} \\ \tilde{d}_i \end{bmatrix}}_{\boldsymbol{w}(t)}. \tag{2.53}$$

If a controller $C(s)$ can be found for which the inequality

$$\|\boldsymbol{T_{zw}}(s)\|_\infty \leq 1 \tag{2.54}$$

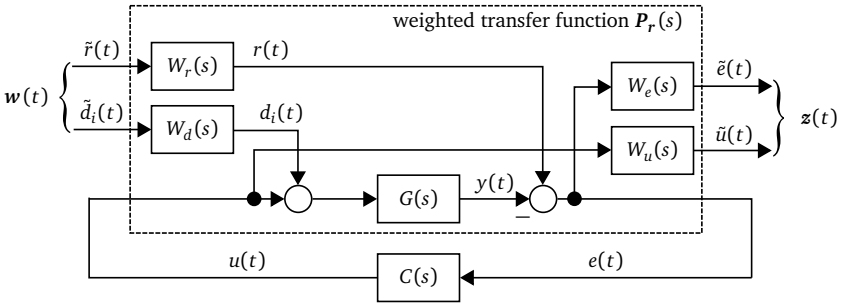

Fig. 2.16: Weighted transfer function matrix $\boldsymbol{P}_r(s)$ based on EHMANN (2004)

is true, the individual transfer functions of the closed-loop stay within their boundaries (ZHOU ET AL. 1996). It can be shown, that for multiplicative uncertainties, a system is robustly stable if

$$\left\| \Delta_m \cdot \frac{G_n C}{I + G_n C} \right\|_\infty = \|\Delta_m \cdot T_c\|_\infty \leq 1 \tag{2.55}$$

is fulfilled (ZHOU ET AL. 1996). Hence, multiplicative uncertainties can be considered within the weighting functions W_u and W_d and robust stability is met if $T_c(s)$ stays within the boundaries defined by W_u and W_d. The final calculation of an H_∞ controller is based on the γ *iteration* (MÜLLER 1996) and can be done in the software tool MATLAB®, for example. In this algorithm, each iteration step tries to calculate a controller $C(s)$ by solving two Riccati algebraic equations at a given value γ that stabilizes $\boldsymbol{P}_r(s)$ and satisfies $\|\boldsymbol{T}_{\boldsymbol{zw}}(s)\|_\infty \leq \gamma \leq 1$ (see Eq. 2.54). The larger the value γ, the better is the disturbance attenuation (HERZOG & KELLER 2011), because this way the controller is pushed towards its constraints and, hence, a more aggressive controller is synthesized. Therefore, a value close to one is usually targeted.

μ Synthesis

The μ synthesis is an extension of the H_∞ synthesis and can handle structured uncertainties. Several researchers have already successfully tested this control strategy for AVC of machine tools (e.g. EHMANN (2004), KERN (2009), JALIZI (2015)). The performance specification of the H_∞ synthesis can be adopted for the μ synthesis. In contrast to H_∞ synthesis, uncertainties in the μ synthesis are taken into account directly in the calculation of the controller by calculating the *structured singular value* μ. Therefore, no variation of the weighting schemes or boundaries, as described in the previous section, is necessary. Equal to the magnitude of a SISO system, μ is a scalar function which can be interpreted as a worst-case magnitude of the perturbed system. This way, not only robust stability but also robust performance is given if

$$\mu(\boldsymbol{T}_{\boldsymbol{zw}}, \Delta_m) \leq 1 \,. \tag{2.56}$$

The controller is synthesized by applying the so-called *D-K iteration*, which is a non-convex optimization problem (SCHÖNHOFF 2003). The D-K iteration is a complex non-convex mathematical operation (ZHOU ET AL. 1996) and is for that reason not explained here, but is commercially available for example in the *Robust Control Toolbox* of MATLAB®.

Conclusion
Robust control synthesis is complex and requires a high tuning effort. In turn, it offers the possibility of a systematic optimization under consideration of uncertainties of the controlled system. In the form of boundary conditions, the requirements on the controller can be sensibly incorporated into the design process. With the structured singular value, also a criterion exists for stability and control performance. These are decisive advantages of the robust control synthesis, especially with regard to an automated controller design, which will be further investigated in Sec. 2.4.7.2. However, the dynamics of a machine tool sometimes depend strongly on the machine position within the workspace (LAW & IHLENFELDT 2015). With increasing uncertainties, the achievable controller performance decreases (HERZOG & KELLER 2011). To overcome this drawback, approaches exist that identify separate LTI μ controllers with small uncertainties and switch between those depending on the current machine position or spindle speed (KERN 2009). However, such approaches lead to an increase in complexity for system identification, controller synthesis, and stability analysis. An alternative approach, where the effort needed does not increase with increasing uncertainty but still promises a high controller performance, is adaptive control, which is presented in the following.

2.4.6.6 Adaptive Control

Adaptive control is characterized by the fact that it can adapt its transmission behavior to variations within the open-loop system and to changing input signals. The adaptation algorithm continuously adjusts the controller transfer function, which can be represented by an adaptive filter. Adaptive control has found many applications within active noise cancellation (ANC). This section focuses on the *filtered-x least mean squares* (FxLMS) algorithm only, which is based on the LMS algorithm and is the most commonly used adaptive control strategy for AVC of machine tools (e.g. HAASE (2005), WAIBEL (2012), LOEIS (2013)). Since adaptability leads to time variant systems, the FxLMS algorithm is described best in the discrete z-domain (KUO ET AL. 1996). Unless otherwise indicated, this chapter is based on KUO ET AL. (1996) and HANSEN (2012).

Feed-forward Control with an LMS Algorithm
In the beginning of this section, it was explained that the basic principle of AVC often is to reduce vibrations by superimposing a 180° phase-shifted counter-signal. The LMS algorithm achieves this by a continuous adaptation of an FIR filter. As Fig. 2.17

shows, the signal $x(n)$, which corresponds to an excitation force F_{TCP} (see Fig. 2.11), causes a distortion $y_x(n)$.

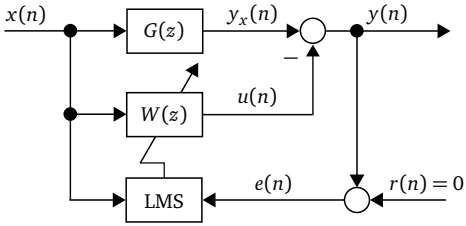

Fig. 2.17: Signal flow chart of the LMS algorithm

The FIR filter $W(z)$ generates a control output $u(n)$ based on the excitation signal $x(n)$ to suppress the vibration response. For this counter signal

$$u(n) \equiv y_x(n) \tag{2.57}$$

is targeted, which minimizes the error

$$e(n) = y_x(n) - u(n) \; . \tag{2.58}$$

The latter corresponds to the remaining oscillation $y(n)$ for a control reference of $r(n) = 0$. In order to modify the excitation signal $x(n)$ in such a way that the controller output results in the necessary counter signal, the FIR filter is continuously adapted by the LMS algorithm to match $G(z)$. Hence, the LMS algorithm adapts the filter with the aim of minimizing the error signal $e(n)$. This working principle can also be used for system identification (see Sec. 2.4.7.1). The transfer function of an FIR filter is defined as

$$W(z) = \frac{\sum_{i=0}^{l-1} w_i z^i}{z^l}, \tag{2.59}$$

with l specifying the number of filter coefficients w_i. Compared to other digital filters, the FIR filter is characterized by its guaranteed stability because following the stability criteria for time discrete systems all poles need to be inside the unit circle (FÖLLINGER ET AL. 2013). By convolution of the reference signal with the coefficient vector $\boldsymbol{w}(n)$, the counter signal $u(n)$ is generated. In vector form, this operation can be written as

$$u(n) = \boldsymbol{w}^T(n)\boldsymbol{x}(n) \; . \tag{2.60}$$

Consequently, the error signal is determined by

$$e(n) = y_x(n) - \boldsymbol{w}^T(n)\boldsymbol{x}(n) \; . \tag{2.61}$$

With the aim of minimizing the error signal, the gradient of the quadratic error with respect to the coefficient vector is established. Based on Eq. 2.61, this yields the expression

$$\frac{\partial e^2(n)}{\partial \boldsymbol{w}(n)} = 2e(n)\frac{\partial e(n)}{\partial \boldsymbol{w}(n)} = -2e(n)\boldsymbol{x}(n)\,, \tag{2.62}$$

which finally results in the adaptation formula of the LMS algorithm:

$$\boldsymbol{w}(n+1) = \boldsymbol{w}(n) + \mu e(n)\boldsymbol{x}(n)\,. \tag{2.63}$$

The algorithm continuously adjusts $\boldsymbol{w}(n)$ according to the method of steepest descent and thus minimizes the level of error $e(n)$. The step size parameter μ is a positive constant and defines the speed of the adaptation process.

Feedback Control with an FxLMS Algorithm

In the above presentation of the LMS algorithm, it was assumed that the control output $u(n)$ directly generates a counter signal. However, as explained in Sec. 2.4.6.3, the transfer function of the controlled system $G(z)$ must be taken into account. $G(z)$ generally delays and modifies the signal of the control output $u(n)$ in such a way that the resulting counter signal $y_u(n)$ cannot effectively attenuate the distortion $y_x(n)$. For this reason, the excitation signal $x(n)$ needs to be filtered by an estimation of the controlled system's transfer function $\hat{G}(z)$ before it is processed as $x_f(n)$ by the LMS algorithm. The resulting algorithm is therefore called *Filtered-x LMS* or *FxLMS* for short. However, the above FxLMS algorithm still requires the excitation signal $x(n)$ as an input. Since the cutting forces cannot be measured easily, the disturbance signal $y_x(n)$ is used as a new reference signal. Due to Eq. 2.58, $y_x(n)$ is estimated by $\hat{y}_x(n)$ based on the counter signal $y_u(n)$ and the error $e(n)$. The signal flow chart of the resulting feedback FxLMS controller is shown in Fig. 2.18. The error signal $e(n)$ is measured by a sensor. By filtering the control output with $\hat{G}(z)$,

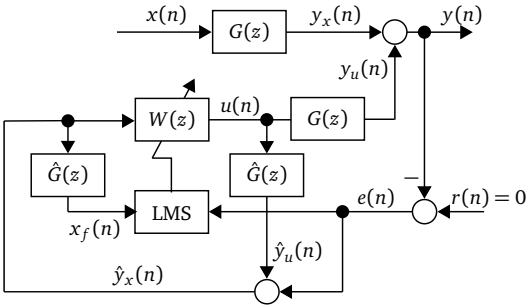

Fig. 2.18: Block diagram of the FxLMS feedback controller

an approximation $\hat{y}_u(n)$ can be obtained for the counter signal $y_u(n)$, which cannot be measured independently. An estimate of the disturbance signal is thus given by

$$\hat{y}_x(n) = e(n) + \hat{y}_u(n) \,. \tag{2.64}$$

Since no more feed-forward loop exists, the signal flow chart corresponds to a pure feedback control. Furthermore, it is obvious that the FIR filter $W(z)$ now adapts itself to the inverse of the controlled system's transfer function $G(z)$. For real applications, the FxLMS algorithm needs to be extended in order to eliminate the disturbing effect of coefficient drift, i.e., a steady increase of all filter coefficients. This drift is caused by rounding inaccuracies in the calculation of the coefficient vector and quantization errors in the analogue to digital conversion of the signals. It can result in a deterioration in control performance or even instability. To compensate for this phenomenon, a so-called *leakage factor* ν is applied to the coefficient vector, which reduces the values of all filter coefficients by a small amount at each time step. If a low leakage factor is selected, the algorithm no longer converges towards the optimum solution, but towards a shifted one. Hence, a value close to one is used for ν in order to compensate the drift effects without causing too much reduction of the vibration suppression. However, the selection of this parameter is often based on *trial and error* and may lead to controller instability.

Several publications in the field of signal processing describe further modifications of the LMS algorithm. Parameters such as the step size (KWONG & JOHNSTON 1992; ABOULNASR & MAYYAS 1997; SHENGKUI ET AL. 2007) or the leakage factor (KAMENETSKY & WIDROW 2004) can be modified by additional adaptive algorithms during controller operation. These approaches significantly improve the performance, but also increase the number of control parameters to be defined during commissioning from three (l, μ, ν) to ten. Due to their similarities, these algorithms can be transferred from LMS to FxLMS (GONTIJO ET AL. 2006). Furthermore, online system identification for the estimation of $\hat{G}(z)$ has to be implemented if strong changes in the controlled system's transfer function, e.g. position-dependent dynamics, occur (LOEIS 2013).

Conclusion
Numerous application examples from literature, also outside the machine tool research, have proven the potential of this control strategy. However, online system identification with an FIR filter, which is required for strongly changing dynamics, has not been investigated for metal cutting machine tools so far. Furthermore, the FxLMS controller has mainly been applied to AVC systems with piezoelectric stacks, which have much higher force loads compared to proof-mass actuators. In order to prevent saturation related damages, the control algorithm needs to be extended by a strategy that limits the controller output without causing strong stability-critical nonlinearities.

2.4.7 Commissioning of Active Vibration Control Systems

This section summarizes methodologies that reduce the effort needed for commissioning an AVC system. Most of the required steps have been presented above. The requirements to be met by the hardware components were named, and methodologies for the determination of an optimum actuator position were summarized. Thus, this section focuses on the tuning of the control strategy. Since model-based control synthesis techniques require a parametric model of the controlled system, different methods for a simplified identification are introduced first. Then, approaches for automatic controller tuning are summarized.

2.4.7.1 System Identification

System identification, which belongs to the field of experimental system analysis, deals with the determination of a model for a real existing system from the observation of the output variables for different input variables (NATKE 1983). In the case of this dissertation, a SISO system with input $u(t)$ and output $y(t)$ must be identified, as explained in Sec. 2.4.5.3 and illustrated in Fig. 2.11. The quality of the system identification can be influenced by the excitation signal and model parameterization algorithm used. According to ISERMANN (2008), existing techniques can be separated into *continuous-time* and *discrete-time system identification*. In the context of this dissertation, continuous-time system identification was used for the synthesis of LTI controllers, while the linear time variant (LTV) FxLMS control was extended by an online system identification based on a discrete-time method.

Continuous-time System Identification
First, the FRF has to be calculated based on the auto and cross power spectra of the discrete time signals $u(n)$ and $y(n)$ (EWINS 2000). This transformation from the time into the frequency domain can be performed by means of the commonly used discrete Fourier transform (DFT) or the periodogram method[5] introduced by WELCH (1967). Although the latter leads to less accurate results in theory, in practice it reduces disturbing influences, especially in terms of measurement noise. This is because it uses several overlapping signal sequences, each weighted individually with a window, which are transformed into the frequency range, and then averaged. The resulting FRF represents a non-parametric model (ISERMANN 2008) and needs to be curve-fitted using, for example, *modal analysis* or *subspace identification* in order to obtain a parametric model.

[5] In the literature the following terms are used synonymously: "The Welch method of averaged periodograms", "The weighted overlapped segment averaging method" and "The Bartlett Welch method" (JOKINEN ET AL. 2000).

Modal Analysis is an often-used curve-fitting technique for LTI systems, which can be classified into *local SDOF*, *local MDOF*, *global*, and *multi-reference* methods (SCHWARZ & RICHARDSON 1999). SDOF methods determine the modal parameters of each mode individually, whereas MDOF, global, and multi-reference methods calculate the modal parameters for two or more modes simultaneously. However, local methods are sufficient for this work because the parameters of a SISO system are to be determined based on a single measured FRF. SDOF methods can be applied for FRFs with no or light modal coupling, while MDOF methods must be used if strong modal coupling is present (SCHWARZ & RICHARDSON 1999). Commonly used and easy to implement is the SDOF *peak-amplitude method* (EWINS 2000), which first detects the magnitude and natural frequency of each eigenmode and then identifies the *half-power points* in order to calculate the modal damping value.

Subspace Identification is a MDOF method that directly yields a parametric LTI state space model from a single FRF (ISERMANN & MÜNCHHOF 2011). The state space model is required for the synthesis of a state controller as defined in Eq. 2.22 and Eq. 2.23. Since the states are not measured directly, but estimated with the help of a Kalman filter (see Sec. 2.4.6.4), it is not possible to apply a defined system structure. Therefore, the model is described by means of a similarity transformation. Since the model order is specified as the only parameter, the subspace identification technique can be automated with little effort.

Several examples for the above described methodologies can be found in the literature. As a first simplification, KERN (2009) measured the vibration response of the controlled system by using a magnetic actuator for excitation and calculated the FRF based on the periodogram method. Two restrictions concerning system identification using a built-in (AVC) actuator were identified. Firstly, eigenmodes can only be identified and modeled if they are within the bandwidth of the actuator and observable at the sensor position. Secondly, since the LTI model presumes a linear behavior of the identified system, the actuator has to show a linear behavior, too. KERN (2009) achieved good results with a sinusoidal sweep and a pseudo random binary signal (PRBS[6]) as excitation for system identification even during machining. Interference frequencies (e.g. imbalance or run-out) were filtered out from the measured vibration response by interpolating adjacent values. Based on the filtered FRF, KERN (2009) identified polynomial matrix fraction descriptions by minimizing the least squares error as presented by DE CALLAFON ET AL. (1996). Even though the excitation signal parameter selection and signal filtering were still performed manually, Kern mentioned the need for an automated system identification that robustly delivers sufficiently accurate models for the controller design without user

[6] PRBS is a binary signal of fixed amplitude with randomly varied pulse width and allows broadband excitation. Further advantages are a high amplitude density, an efficient implementation on DSP boards and its deterministic characteristics, which allow the exact calculation of the auto and cross power spectra. (ISERMANN 2008)

interaction. Similar approaches were performed by PARUS ET AL. (2013), who excited the controlled system with a PZT actuator also used for AVC and identified a state space model by applying the LMS algorithm. However, the type of excitation signal and a potential automation of the system identification were not named. BRECHER ET AL. (2016) measured the FRFs of a MIMO system by exciting the machine tool structure with hydraulic actuators also used for AVC. A stepped sinusoidal signal for excitation was applied and the modal parameters were manually selected based on the *polyreference least-squares complex frequency domain method*, also known as POLYMAX, which was introduced by PEETERS ET AL. (2004). The latter allows for an accurate estimation of stable structural poles of the measured MIMO system and can be automated (PEETERS ET AL. 2008). However, an application to a SISO system is not possible because this methodology requires eigenvectors.

The need for an automatic system identification for AVC was addressed by BOLDERING (2015), who implemented an automatic optimization of the excitation signal parameters as well as an automatic model parameterization. For band-limited noise and a PRBS, the effect of different excitation signal parameters on the FRF quality was evaluated by calculating the spectral power density and the coherence γ^2 based on the periodogram method. As a result, the signal amplitude and length showed the strongest effect and were automatically tuned based on an iterative evaluation of γ^2.

Furthermore, BOLDERING (2015) automated the model parameterization by implementing a subspace identification method. Applying the peak-amplitude method, the natural frequencies are identified first. Around each natural frequency, a frequency band that is used for the calculation of the model of the respective mode is defined. Using the subspace identification method, a second-order model is created for each mode and the natural frequency is determined. An iteration loop makes it possible to optimize the frequency band until the deviation between the measured and modeled natural frequency stops to improve. BOLDERING (2015) achieved good results with this methodology for an active grinding tool with two clearly separated modes.

Discrete-time System Identification
Several authors extended the LTV FxLMS controller by an online identification using an additional FIR filter, which is adapted by the LMS algorithm as already explained in Sec. 2.4.6.6. Most commonly, this is applied for active noise cancellation with a feedforward FxLMS controller. In order to minimize the mutual influence between sound attenuation and system identification, KUO & VIJAYAN (1997) introduced a third FIR filter in addition to the control and identification filter. Based on these results, ZHANG ET AL. (2001) changed the calculation formula for the third filter and thus achieved a further improvement in noise cancellation. AKHTAR ET AL. (2006) also used an additional filter, not for the online identification but to achieve a higher adaptation speed of the controller. The online identification was supplemented by a step size adaptation. A similar approach was used by CARINI & MALATINI (2008), who added analytical considerations to determine optimal parameters for the step

size adaptation and an algorithm for an automatic adjustment of the excitation signal. Simulations showed that both additions contribute to a faster convergence and a higher attenuation of the interfering signal. For the feedback FxLMS controller, GAN ET AL. (2005) implemented an online identification for an ANC headphone, which is shown in Fig. 2.19. The modeling signal $v(n)$ is superimposed to the controller output $u(n)$, which results in the following modified control signal:

$$u_v(n) = u(n) + v(n) \,. \tag{2.65}$$

Due to superposition, the modified control output filtered by the controlled system $y_{u,v}(n)$ can be expressed by

$$y_{u,v}(n) = y_u(n) + y_v(n) \,. \tag{2.66}$$

Here, $y_u(n)$ describes the theoretical signal that is created if the control output is filtered by the controlled system, while $y_v(n)$ is the counterpart for the modeling signal filtered by the controlled system. Therefore, the error signal $e(n)$, which is used to adapt both the control and the modeling FIR filter, is

$$e(n) = y_x(n) - y_{u,v}(n) + \hat{y}_v(n) = (y_x(n) - y_u(n)) + (\hat{y}_v(n) - y_v(n)) \,. \tag{2.67}$$

By feeding $e(n)$ through the control and the modeling filter, two mathematical terms are minimized simultaneously: firstly, the difference between the physical representation of the filter output $y_u(n)$ and the disturbance signal $y_x(n)$ and, secondly, the difference between the system response to the identification signal $y_v(n)$ and the modeling filter's response $\hat{y}_v(n)$. Thus, the FxLMS controller with online identification still works in the same way as without online identification, while the modeling filter $\hat{G}(z)$ is adapted to emulate the dynamic behavior of the controlled system $G(z)$. The filter coefficients are continuously copied to both modeling filters used in the original FxLMS algorithm.

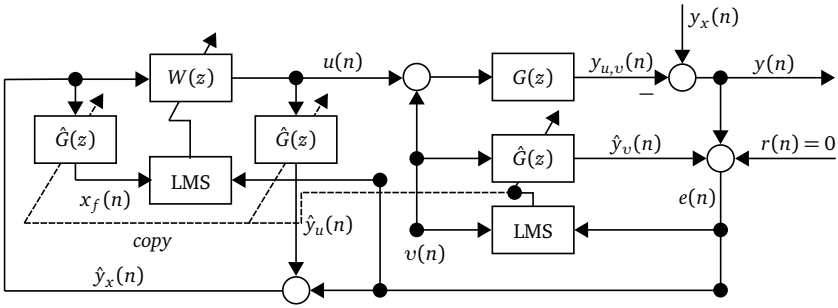

Fig. 2.19: Feedback FxLMS controller with online identification based on GAN ET AL. (2005)

MOKHTARPOUR & HASSANPOUR (2012) extended the online identification of the feedback FxLMS by an algorithm for a step size adaptation which adapts both the speed of the controller adaptation and the speed of the system identification depending on the current level of the measured sound signal.

An application regarding AVC was investigated by PU ET AL. (2014). The algorithm presented is based on the results of CARINI & MALATINI (2008) and is characterized by modified calculation formulas for the step size and noise level adaptation algorithms. Tests were performed both in simulation as well as on a test carrier and proved that the convergence speed and the controller performance increase compared to previous algorithms.

For AVC of wood machining centers, LOEIS (2013) implemented a feedforward FxLMS controller with online identification using a FIR filter which was adapted by a recursive least square (RLS) or an LMS algorithm. Compared to LMS, the RLS algorithm showed a slower adaptation, but achieved a higher precision (LOEIS 2013). The FxLMS-RLS controller was applied to an active workpiece holder as well as a counter-pressure shoe. Both systems were actuated by piezoelectric stacks. However, the above presented further developments of the basic LMS algorithm for system identification were not considered in the comparison of the LMS and the RLS algorithms.

Model Evaluation Criteria

Different analytical criteria exist for the comparison of a measured FRF G_{ref} and a curve fitted system FRF G_{sys} (ALLEMANG 2003). Most popular is the *frequency response assurance criterion* (FRAC), which was introduced by HEYLEN & LAMMENS (1996). Its definition in vector notation is

$$FRAC = \frac{\left|\sum_{\omega_1}^{\omega_2} G_{ref}^*(\omega) G_{sys}(\omega)\right|^2}{\left(\sum_{\omega_1}^{\omega_2} G_{ref}^*(\omega) G_{ref}(\omega)\right)\left(\sum_{\omega_1}^{\omega_2} G_{sys}^*(\omega) G_{sys}(\omega)\right)}\,, \tag{2.68}$$

with ω_1 and ω_2 defining the considered frequency bandwidth. The result of this criterion is a real-valued scalar between zero and one. A value close to one corresponds to a high correlation of the two FRFs. Unfortunately, the FRAC is sensitive to small deviations of the natural frequencies, which can lead to low FRAC values although the overall behavior of the two systems is similar (REBELEIN 2019). POLICARPO ET AL. (2013) stated that the FRAC is well suited to compare the shape of two frequency responses, i.e., at which frequencies the eigenmodes are located. However, no information about the absolute amplitude of the FRF is provided.

Since a constant offset often occurs during system identification using the LMS algorithm, a further criterion is applied in the context of this work that takes absolute

amplitude differences into account. The so-called *frequency amplitude assurance criterion* (FAAC) is defined by ALLEMANG (2003) as follows:

$$FAAC = \frac{2\left|\sum_{\omega_1}^{\omega_2} G^*_{ref}(\omega) G_{sys}(\omega)\right|}{\left(\sum_{\omega_1}^{\omega_2} G^*_{ref}(\omega) G_{ref}(\omega)\right) + \left(\sum_{\omega_1}^{\omega_2} G^*_{sys}(\omega) G_{sys}(\omega)\right)} . \tag{2.69}$$

Again, the FAAC ranges between zero and one with high values indicating a high correspondence.

2.4.7.2 Controller Tuning

In the literature, the tuning of **model-free controllers** is often based on a time consuming manual adjustment of the filter and gain parameters (i.e. trial and error). A first simplification for the tuning of a DVF controller for AVC was presented by BAUR (2014), who introduced a structured manual procedure. Based on a measured acceleration signal of an unstable machining process, the filter parameters are selected in relation to the identified chatter frequency. Then, a time domain simulation of the actuator and controller transfer function is performed for feeding the controller input with the measured acceleration signal and tuning the controller gain in such a way that the actuator does not saturate. Additionally, notch filters are manually tuned to suppress signal noise or eigenmodes that are not intended to be damped. The fine-tuning of the controller is performed during machining. MANCISIDOR ET AL. (2015) applied a similar approach in combination with the coupled model presented in Sec. 2.4.5.3. This way, the optimum gains for different spindle speeds can be determined within simulation. For the more complex case of a cascaded machine tool feed drive controller, KETTERER (1995) introduced an automatic tuning methodology for electromechanical, elastically coupled feed drive systems. Based on this work, BRETSCHNEIDER (2000) optimized the solution space of the P controller of the position loop and the PI controller of the velocity loop by a genetic algorithm.

Automatic tuning of a model-based **LQG controller** for an active grinding tool was presented by BOLDERING (2015), who conducted a full factorial parameter variation of the $\boldsymbol{Q}$ and $\boldsymbol{R}$ matrices within simulation and finally selected the parameter set with the best damping performance. For the resulting controller, the output $u(t)$, which results from a band-limited noise excitation, is checked to stay below a defined maximum. However, the machining process is not considered even though it directly affects the controller output and might cause actuator saturation. Furthermore, the approach's ability and robustness in stabilizing chatter were not tested.

The definition of the weighting functions for the $\boldsymbol{H_\infty}$ **synthesis** is a comprehensive task and requires in-depth expert knowledge. This is especially due to the fact that the transfer function matrix $\boldsymbol{T_{zw}}(s)$ of the extended system is influenced by the weighting functions in all entries. Hence, specific limits for a single variable of the

extended system cannot be defined independently of the other control variables. Approaches for an automated H_∞ synthesis for AVC cannot be found in the literature. However, automated approaches of performance specification exist with regard to other control engineering problems. Due to the non-convex nature of the γ iteration, deterministic optimization approaches such as gradient methods cannot be used (SCHUMACHER 2013). In the literature, stochastic optimization approaches such as genetic or swarm-based algorithms have been proven successful. LEE ET AL. (1998) used a genetic algorithm for the determination of optimal weighting functions for an H_∞ control in a reactor system application. DO ET AL. (2010) also used a genetic algorithm for the best possible parameterization of the weighting functions for the robust control of a semi-active suspension system. ALI ET AL. (2011) implemented a particle swarm optimization (PSO) for the optimal choice of the weighting parameters. The goal was to minimize the maximum gain of the transfer function of a controlled pneumatic actuator by an H_∞ controller. For the control of a flexible beam, EINI (2014) implemented an H_∞ controller and compared a genetic and a particle swam optimization. The PSO showed an improved efficiency compared to genetic procedures in terms of computing time.

Adaptive controllers do not require an automatic tuning, since the adaptation algorithm implies already that the controller is tuned continuously. However, the selection of the optimum adaptation parameters is also part of this dissertation and is presented in Sec. 4.6.

2.5 Summary and Need for Actions

The productivity of machine tools is often limited by the appearance of chatter vibrations, which lead to significantly increased tool wear, high noise pollution, and even damage of the workpiece as well as the machine components. The adaptation of process parameters or the disturbance of the regenerative effect by means of special tool geometries and continuous spindle speed variation are powerful measures, but show a limited application range within the stability lobe diagram and sometimes lead to productivity losses as the installed drive power cannot be fully exploited. For new machine designs, simulations are used to identify and eliminate local structural weaknesses. Due to uncertainties in the modeling, however, an accurate prediction of the dynamic behavior is still challenging and conceptually inevitable weak spots can sometimes not be avoided constructively and economically at all. Especially in these cases, passive and semi-active systems for vibration mitigation can lead to a significant improvement in the damping behavior. Unfortunately, both are often associated with a comparatively high increase in weight, which has a negative effect on the system's feed drive dynamics. AVC systems overcome these drawbacks, since they generate large damping forces over a wide bandwidth with comparably low masses and sizes.

Despite promising results from several researchers, almost none of the prototype AVC systems have been industrialized. So far only one machine tool builder offers a manually tunable AVC system to customers (DANOBATGROUP 2017). Commercial retrofit solutions for AVC of machine tools do not exist. Even though cost-efficient hardware components are commercially available, the multidisciplinary expert knowledge required to set the dimensions and to commission an AVC system is an entry barrier for industrial use. Industry needs efficient and reliable solutions as well as methodologies for the design of an optimum and robust AVC system (MUNOA ET AL. 2016a). However, often specific individual system solutions were presented so far, which are only transferable to a limited extent. Furthermore, the performance of AVC systems has often been tested for one controller only and mostly on a test bench with laboratory AVC hardware. In most cases, only a single machining process was considered for validation. So far, there is only limited scientific work available on the industrial use of AVC systems for machining applications and the challenges involved.

Especially for retrofit solutions, AVC systems with a proof-mass actuator are most suitable, since they are easy to integrate and achieve a high damping performance. However, to set the dimensions of the actuator properly is still a challenge. Existing approaches are limited to the available installation space or suffer from insufficient estimates of the required actuator force and bandwidth. Even though holistic simulation approaches are able to accurately predict the behavior of an AVC system, the detection of worst case scenarios for the actuator dimensioning is missing.

While simulation-based approaches for the integration of AVC systems in new machines already exist, retrofitting of machines is insufficiently addressed. BAUR (2014) provides a first draft to simplify the integration and commissioning by a structured approach that does not require complex machine simulation models. However, multidisciplinary expert knowledge and equipment is still required for the controller design, which are rarely found in manufacturing companies. In addition, the procedure disregards the machining process, which has a significant influence on the dimensioning and commissioning.

Even though several approaches exist for virtual commissioning, a lot of trial and error is still necessary for the controller tuning, because there are always deviations between the simulated and the real machine behavior. Furthermore, disturbing influences acting on the sensor signal cannot be simulated. An automated identification of the machine's dynamic behavior and a subsequent automated controller tuning would ensure a simple transferability and realize an implementation without requiring too much expert knowledge. In addition, changes within the controlled system due to wear or maintenance actions could be tracked and the system would be able to adapt automatically. For LTV FxLMS feedback controllers, several authors have proven that the extension by an additional FIR filter for online identification is a feasible approach to compensate for strong changes within the controlled system. However, the manual optimization of the adaptation parameters still requires expert

knowledge and is a time consuming task. For LTI controllers, the approach presented by BOLDERING (2015) for automatic system identification shows promising results. Several publications exist showing how the subsequent controller tuning can be automated.

Therefore, the above identified entry barriers for industrial use of AVC systems unveil the following need for actions: in order to reduce the dimensioning effort needed, already existing simulation approaches should be used to determine the required actuator force and bandwidth in an automated way. Since the controller is the most important part of an optimum and robust AVC system, different control strategies existing in the literature need to be compared, both in simulation and, especially, experimentally in extensive machining tests. In addition, challenges resulting from an industrial application, such as the occurrence of high accelerations during multi-axis machining, must be taken into account in the controller evaluation. A methodology for an automatic commissioning of AVC systems with proof-mass actuators would yield a great simplification and, hence, a highly transferable solution. Therefore, the system identification and subsequent controller synthesis need to be automated. The performance and robustness of such a *plug and play* system has to be tested under industrial operating conditions. Furthermore, the use of AVC hardware suitable for industrial application must be evaluated, especially the substitution of expensive DSP boards with cost-efficient PLCs.

In the following chapter, research targets are defined based on the above identified needs for action.

3 Objective and Methodology

3.1 Objective

The objective of this dissertation is to enable the industrial use of AVC systems for machine tools by means of reducing the integration and commissioning effort to a minimum. This is achieved by two independent strategies which are merged to an overall methodology. The overall methodology must be applicable to both newly developed machine tools and already-in-use machine tools. Since proof-mass actuators are the easiest to integrate as a retrofit solution, this dissertation focuses on such AVC systems. Industrial use requires, among other things, that the integration of an AVC system must not affect the process capability index negatively, but increase the machine's performance, production quality, and availability, leading to an improved overall equipment effectiveness. Consequently, no workspace restrictions should be caused by mounting the actuator. Based on the need for actions identified in Sec. 2.5, the following research targets **RT1** to **RT4** must be achieved to enable the industrial use of AVC for machine tools:

RT1 **Hardware Dimensioning:** A strategy for hardware dimensioning needs to be developed in order to reduce the integration effort. Dimensioning of the actuator should not only focus on the available assembly space, but consider the maximum actuator force and bandwidth required to achieve the desired chatter stability. Therefore, existing simulation approaches must be merged and extended in order to estimate the expected maximum forced and self-excited vibration amplitudes, which must be known to accurately dimension the actuator.

RT2 **Comparison of Control Strategies:** The AVC system has to be robust against changes within the controlled system and varying excitations from different machining processes. Promising control strategies, which were identified from literature, must be implemented and tested in machining experiments in order to be compared against each other. A focus on multi-axis machining is necessary because potential challenges that may be caused by high accelerations originating from the motion of the feed drives need to be investigated.

RT3 **Automatic Commissioning:** The commissioning effort for an AVC system has to be reduced in order to enable implementation by non-experts. Hence, a strategy for automatic system identification and subsequent controller tuning must be developed and implemented for the most performant control strategies from **RT2** for testing and demonstration purposes. Besides automated commissioning, the strategy has to successfully perform in the presence of changes originating from the machine tool dynamics. It is also important to take the machining process into account for an automatic tuning,

because it has a great influence on the vibration amplitudes that occur, and these in turn have a great influence on the controller output signal. The latter must not lead to saturation of the actuator, as otherwise the actuator may be damaged or controller instability could also occur.

RT4 **Evaluation of Industrial Suitability:** The strategy for automatic commissioning from **RT3** must be tested under industrial operating conditions in order to evaluate its performance and robustness. For the final solution, only hardware suitable for industrial application should be selected and evaluated. Very challenging in this context is substituting high-performance DSP boards with cost-efficient PLCs without sacrificing usability. Furthermore, the durability of the actuator, which is the only mechanical component subject to wear, has to be analyzed.

When all these research targets are achieved, the overall methodology developed in the context of this dissertation will be suitable for a low-effort dimensioning and commissioning of AVC systems with proof-mass actuators, resulting in a highly transferable solution.

3.2 Methodology

For enabling the industrial use of AVC systems with proof-mass actuators, this dissertation follows the approach depicted in Fig. 3.1. Each step required to integrate and commission an AVC system is simplified by different strategies. In this way, the requirements previously defined will all be satisfied. The result is an overall methodology that helps the end user to select the actuator dimension properly, choose the right control strategy depending on the application, and commission the system automatically.

This dissertation is publication-based and consists of seven publications: KLEINWORT ET AL. (2014), KLEINWORT ET AL. (2015), KLEINWORT ET AL. (2016), ZAEH ET AL. (2017), KLEINWORT ET AL. (2018a), KLEINWORT ET AL. (2018b), and KLEINWORT ET AL. (2021). In Chapter 4, each publication is summarized, and the contribution of the author is explained. The full publications can be found in the respective journals with the following bibliographical information[7]:

① Kleinwort, R.; Altintas, Y.; Zaeh, M. F.: Active Damping of Heavy Duty Milling Operations. In: Akkok, M.; Erden, A.; Kilic, S. E.; Konukseven, E. I.; Budak, E.; Lazoglu, I. (Editor): 16th International Conference on Machine Design and Production. Ankara, Turkey: METU-Ankara 2014. pp. 443–458.

[7] Wherever the number is not indicated, the respective journal does not use an issue number.

② Kleinwort, R.; Popp, R. S.; Cavalié, B.; Zaeh, M. F.: Energy Demand Simulation of Machine Tools with Improved Chatter Stability Achieved by Active Damping. Applied Mechanics and Materials 805 (2015), pp. 187–195.

③ Kleinwort, R.; Weishaupt, P.; Zaeh, M. F.: Simulation-Based Dimensioning of the Required Actuator Force for Active Vibration Control. International Journal of Automation Technology 12 (2018) 5, pp. 658–668.

④ Kleinwort, R.; Schweizer, M.; Zaeh, M. F.: Comparison of Different Control Strategies for Active Damping of Heavy Duty Milling Operations. Procedia CIRP 46 (2016), pp. 396–399.

⑤ Zaeh, M. F.; Kleinwort, R.; Fagerer, P.; Altintas, Y.: Automatic tuning of active vibration control systems using inertial actuators. CIRP Annals 66 (2017) 1, pp. 365–368.

⑥ Kleinwort, R.; Platz, J.; Zaeh, M. F.: Adaptive Active Vibration Control for Machine Tools with Highly Position-Dependent Dynamics. International Journal of Automation Technology 12 (2018) 5, pp. 631–641.

⑦ Kleinwort, R.; Herb, J.; Kapfinger, P.; Sellemond, M.; Weiss, C.; Buschka,M.; Zaeh, M. F.: Experimental comparison of different automatically tuned control strategies for active vibration control. CIRP Journal of Manufacturing Science and Technology 35 (2021), pp. 281–297.

Publication ① lays the foundation for a simulation model in which the machine dynamics are represented by a state space model, and the behavior of the AVC system is described by a second-order differential equation. The model is used to compare two different controllers in both the time domain and the frequency domain. An AVC system was commissioned according to the state of the art. Finally, the increase in chatter stability was validated with cutting tests on a Mori Seiki NMV5000 5-axis machining center. The same model was used in publication ②, where the model was parameterized for a SPINNER U5-620 5-axis machining center and extended with a cutting force model to evaluate the stability behavior of machining processes with and without AVC in simulation. The focus of this publication, however, is on the simulation-based evaluation of the energy efficiency increase achieved by AVC. Publication ③ is dedicated to the challenge of selecting the correct actuator force and bandwidth needed for a specific machine tool to be equipped with an AVC system. First of all, critical process parameters have to be identified in order to estimate the maximum forced and self-excited vibration amplitudes that can be expected. Then, the required actuator force and bandwidth for damping such vibration amplitudes can be determined with the extended simulation model from publication ②.

The fact that different control strategies have different advantages and disadvantages has already been outlined in publication ①. Publications ④, ⑤, ⑥, and ⑦ therefore deal intensively with the evaluation of different control strategies. Publication ④ describes a first investigation on the performance of the DVF, LQG, H_∞, and μ controllers using the simulation model from publication ②, and validates

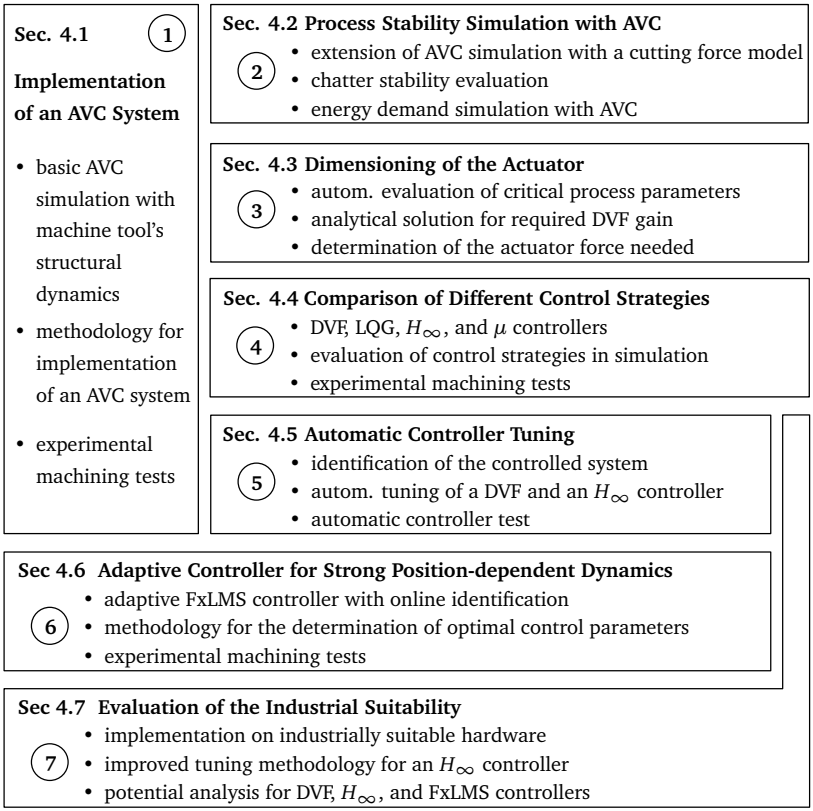

Fig. 3.1: Methodology of this publication-based dissertation

the results with machining tests on the SPINNER U5-620 5-axis milling center. The investigation showed that the LQG controller was unsuitable for AVC of machine tools, and that no μ controller could be practically found that satisfied the desired robust performance specification. Subsequently, publication ⑤ shows a methodology for automatic tuning of the two remaining control strategies, DVF and H_∞, which significantly simplifies the commissioning of AVC systems. In experimental investigations, the H_∞ controller showed better performance on both the SPINNER U5-620 5-axis machining center and a PITTLER PV630 vertical lathe. However, the experiments also revealed that the performance of the robust controller decreases with the increase in model uncertainties, which usually result from the machine tool's position-dependent dynamics. In order to take advantage of the performance benefits of a model-based controller, even on machine tools with strong position-dependent dynamics, publication ⑥ is dedicated to an adaptive control strategy. The imple-

mented feedback FxLMS controller is easily tuned with the help of an integrated online identification algorithm and an automatic parameter tuning. Demonstrated through extensive experiments on the SPINNER U5-620 5-axis machining center, a strong performance is observed even with a significant change of the controlled system's transfer function.

Publication ⑦ provides a final comparison of the three control strategies, DVF, H_∞, and FxLMS. A fundamental improvement is presented for the automatic tuning of the H_∞ controller introduced in publication ⑤. The solution space is widened and the optimal parameter set is reached by applying a PSO algorithm. To investigate the robustness of the automatic commissioning of the DVF, H_∞, and FxLMS controllers, extensive machining tests with different process parameters and tool positions were carried out on the SPINNER U5-620 5-axis machining center and the PITTLER PV630 vertical lathe. Lastly, the resulting vibration amplitudes and surface qualities were analyzed for a final evaluation of the different controllers and the developed automatic commissioning methodology.

Fig. 3.2 illustrates how the publications ① to ⑦ address the research targets **RT1** to **RT4** defined in Sec. 3.1. A detailed description of the publications can be found in the following Chapter 4.

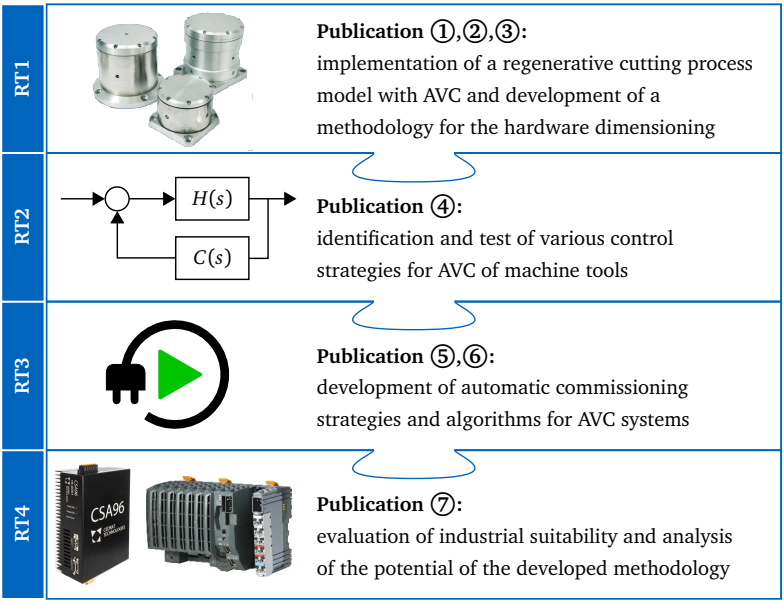

Fig. 3.2: Relation between the publications and the research targets (image sources: METRA MESS- UND FREQUENZTECHNIK IN RADEBEUL E.K. (2020); B&R AUTOMATION (2020a); CEDRAT TECHNOLOGIES (2020); CSA ENGINEERING (2020))

4 Dimensioning and Automatic Commissioning of Active Vibration Control Systems

4.1 Publication 1: Active Damping of Heavy Duty Milling Operations

For publication ①, a commercial MORI SEIKI NMV5000 5-axis machining center was equipped with an AVC system. A methodology based on the work of EHMANN (2004) was applied in order to select a suitable location for the actuator. In a first step, the compliance FRFs in three spatial directions at the TCP were measured. These were used, together with the tool and material parameters, as input variables for an analytical SLD calculation. The machine tool showed a critical natural frequency at 75 Hz. An experimental modal analysis subsequently indicated that this frequency belongs to the first bending mode of the machine's z-slide. The optimum actuator placement, in terms of maximum damping performance, is therefore as close as possible to the tool, since this is the location where the highest vibration amplitudes occur. The accelerometer and actuator (Micromega Dynamics ADD45) were then attached to the machine tool structure by magnets.

A DVF as well as a model-based velocity feedback (MbVF) controller were implemented and tested. The latter represents a manual loop-shaping of the DVF controller, which allows the damping of selected natural frequencies only (see Fig. 4.1). Since the loop-shaping was conducted based on measured FRFs, the control strategy suffers from a lack of robustness against non-modeled effects of the controlled system transfer function. For the purpose of performance investigations, an AVC simulation model was implemented in the software tool MATLAB/SIMULINK®. While the structural dynamics of the machine tool were described by a state space model, the behavior of the AVC system was modeled by a double differentiated PT2 element. The AVC system exclusively represents the proof-mass actuator because the sensor and power amplifier transfer functions were assumed to be constant due to their

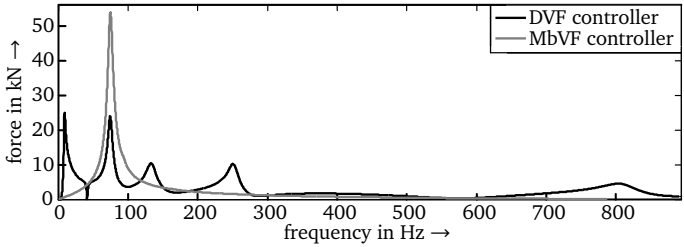

Fig. 4.1: FFT of the simulated actuator force – DVF controller & MbVF controller based on KLEINWORT ET AL. (2014)

comparably high bandwidth. Simulated impulse hammer tests showed a reduction of the dynamic compliance at the TCP by 6.5 % (DVF) and 26 % (MbVF). Experimental impulse hammer tests on the real machine structure led to comparable results for the DVF controller, but could not confirm the high values for the MbVF controller, which achieved a reduction of only 12 %. This is on account of a poor signal-to-noise ratio, which was neglected in the simulation, and modeling inaccuracies, which were not considered during loop-shaping. In cutting tests, the analytical SLD was validated, and it was shown that the chatter-free DOC increases by 33 %, from 3 mm to 4 mm, when using the MbVF controller.

In summary, this publication shows the possibility of increasing the chatter stability limit on a commercial machining center by installing an AVC system. Even with simple control strategies, a significant increase in productivity is achievable. Focusing the controller on the most critical natural frequency improves the performance. However, a high effort remains needed to tune the AVC system. Therefore, this publication advocated a further comparison of different control strategies and the development of an automatic tuning methodology for AVC systems. The AVC simulation model presented here is the basis for publications ② and ③.

The individual contributions of the author of this dissertation to this publication are depicted in Fig. 4.2.

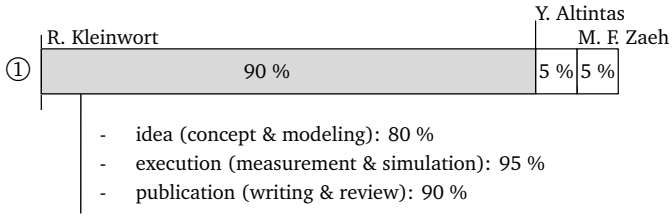

Fig. 4.2: Individual contributions of the author to publication ①[8]

The following three achievements were obtained through publication ①:

- A simulation model of the machine tool's structural dynamics including an AVC system was verified to be used for controller performance evaluation.
- A model-based loop-shaping controller was introduced, which showed a higher damping performance compared to a model-free DVF controller.
- The analytical determination of the SLD with the simulation model for a machine tool with and without AVC was validated by machining tests.

[8] The average estimate was agreed upon by all authors. A detailed listing of the contributions of the author of this dissertation (R. Kleinwort) regarding *idea*, *execution*, and *publication* is also given in the figure. The overall contribution of the author is an averaged result of these specific contributions.

4.2 Publication 2: Energy Demand Simulation of Machine Tools with Improved Chatter Stability Achieved by Active Damping

The base load of machine tools accounts for a high proportion of the total energy consumption. A reduction in net machining time, for example through higher material removal rates, therefore often leads to a reduction in energy consumption per workpiece produced. In publication ②, the energy consumption of a SPINNER U5-620 5-axis milling center was modeled to evaluate the increase in energy efficiency that can be achieved by installing an AVC system. The energy demand model considers the energy consumption of the main spindle, the feed drives, and the auxiliary units, as well as the remaining base load. In addition, the simulation model includes a regenerative cutting process model, which makes it possible to predict the increased chatter-free DOC through AVC. The input parameters of the energy demand model are the NC program and the workpiece blank geometry, as illustrated in Fig. 4.3. An interpreter module reads the NC program and transmits the program sequence to the energy consumption module and the regenerative cutting process model. The latter first determines the intersection of the tool and the workpiece for each calculation step based on the tool path and the tool geometry. Then, the cutting process simulation is executed. A mechanistic cutting force model based on BUDAK & ALTINTAS (1998) calculates the cutting forces which are sent to the state space model introduced in publication ①. The vibration response affects the dynamic chip thickness, and thereby the cutting force simulation. The coupled model allows

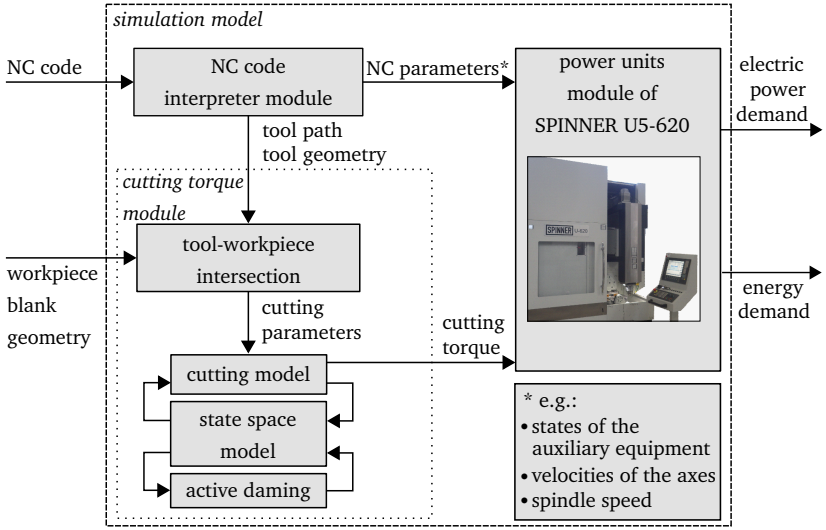

Fig. 4.3: Modules of the energy demand simulation model based on KLEINWORT ET AL. (2015)

the chatter stability to be evaluated. The calculated cutting torques of the main spindle are transferred to the energy consumption module. The influence of the cutting forces on the energy consumption of the feed drives, however, is negligible. Machining tests showed deviations between simulation and measurement of less than 1.3 % in terms of energy consumption, and less than 5 % in terms of electrical power. The most significant source of error was identified to be the differences in tool change times, which depend on the current tool changer position and cause time deviations between the simulated and the real process.

The simulated stable DOC was increased by 100 % when using the AVC system. The resulting energy savings are strongly dependent on the respective NC program. In a very favorable scenario, doubling the limiting DOC reduces the net machining time by 50 % and the total cycle time by 38 %. Despite a significantly increased power consumption of up to 43 % due to the increased DOC, this resulted in energy savings of about 34 %.

The individual contributions of the author of this dissertation to this publication are shown in Fig. 4.4.

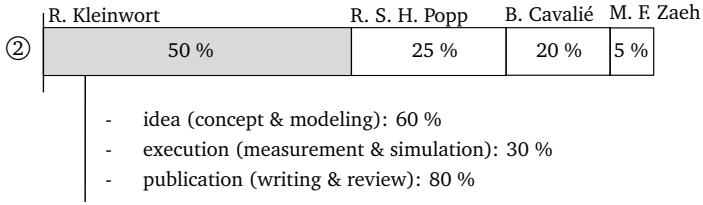

Fig. 4.4: Individual contributions of the author to publication ②

To sum up, this publication presents the transferability of the simulation model introduced in publication ① to other machine tools, as well as its extension for the purpose of energy demand simulation and controller performance testing. Furthermore, the increase in energy efficiency through AVC was evaluated for a sample workpiece.

Publication ② led to the achievement of the following four goals:

- The simulation model introduced in publication ① was extended by a cutting force model to become a regenerative cutting process model with AVC.
- It was verified that the regenerative cutting process model is capable of simulating the increase in chatter stability through AVC.
- An energy demand simulation, which calculates the energy consumption for an arbitrary NC program, was developed and validated.
- Simulation and experimental results proved a significant increase in energy efficiency through AVC.

4.3 Publication 3: Simulation-based Dimensioning of the Required Actuator Force for Active Vibration Control

The research target **RT1** from Sec. 3.1 addresses the dimensioning of an AVC system. The biggest challenge is to determine the correct performance class for the actuator. Publication ③ presents a simulation model that allows the required actuator force and the bandwidth to be calculated. The objective is to increase the chatter stability of a specific machine tool such that the full power capacity of the drives can be utilized. The basic idea is to identify critical process parameters in terms of maximum vibration amplitudes, and then determine the required dimensions of the AVC system for these cutting conditions. The critical process parameters are determined based on the compliance FRF at the TCP, the technical data of the main spindle, the maximum allowable tool diameter, and the hardest material to be machined, as illustrated in Fig. 4.5. Then, it is required to find the machining process conditions that result in the highest forced and highest self-excited vibration amplitudes. A genetic algorithm is used to identify the most critical cutting conditions in terms of forced vibrations. For the most critical self-excited vibrations, the solution space was first reduced based on a literature review. This allowed for the formulation of a directly solvable algebraic equation. The result serves as a reference process in order to tune the DVF controller of the AVC system. The analytically determined stability limit is set in relation to the maximum DOC possible with the installed spindle power. Then, the controller gain required to increase the stable DOC is calculated accordingly. At the same time, the Nyquist closed-loop stability criterion is checked. Finally, the regenerative cutting process model introduced in publication ② calculates the actuator forces in the time domain. The simulation is performed for both the process that results

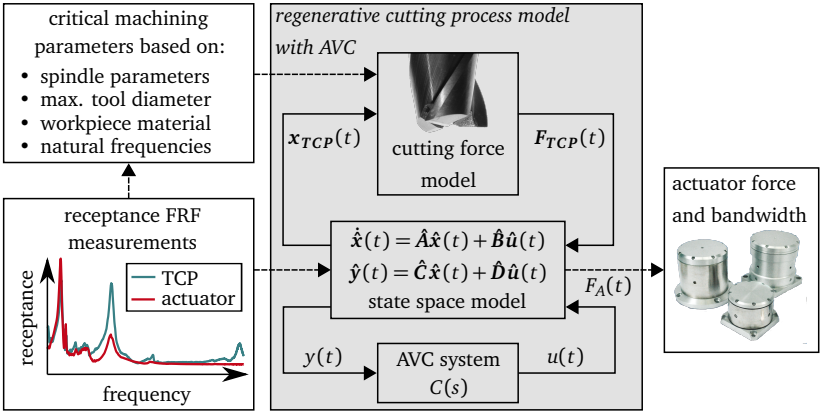

Fig. 4.5: Overview of the simulation-based actuator dimensioning approach based on KLEINWORT ET AL. (2018b)(image source: CSA ENGINEERING (2020))

in the maximum forced vibration amplitudes and the process that results in the maximum self-excited vibration amplitudes. This way, the required actuator force and bandwidth are determined by selecting the maximum values obtained. The methodology was successfully verified by applying it to the SPINNER U5-620 5-axis machining center.

The individual contributions of the author of this dissertation to this publication are represented in Fig. 4.6.

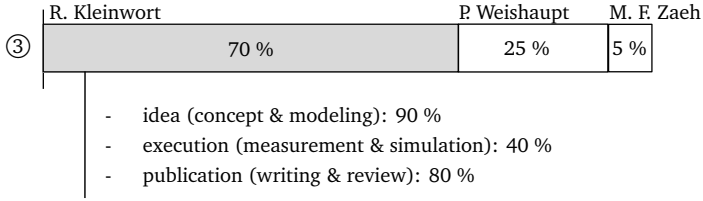

Fig. 4.6: Individual contributions of the author to publication ③

In summary, this publication addresses **RT1** from Sec. 3.1: the dimensioning of an AVC actuator for a specific machine tool. A genetic algorithm identifies the most critical machining process in terms of forced vibration amplitudes at the TCP. Based on an algebraic equation, the most unstable process is found and analytical calculations yield the controller gain that stabilizes this most critical machining process. Using the regenerative cutting process model with AVC from publication ②, the process stability is finally examined in the time domain and the required actuator force and bandwidth are simulated.

The following four major achievements were outlined through publication ③:

- The most critical process parameters in terms of forced vibration amplitudes were identified by a genetic algorithm.
- The cutting conditions that lead to the highest self-excited vibration amplitudes were determined by an algebraic equation.
- The DVF controller gain needed to stabilize the most critical process can be easily obtained through an analytical solution.
- The required actuator force and bandwidth can be determined by the regenerative cutting process model from publication ② taking into account the machine tool's structural dynamics, the installed spindle power, and the most critical cutting conditions to be expected.

4.4 Publication 4: Comparison of Different Control Strategies for Active Damping of Heavy Duty Milling Operations

Publication ④ compares four control strategies for AVC that have been often implemented in the literature. The SPINNER 5-axis machining center served as a test system, and was equipped with a MOOG SA10-V30 actuator. For the simulative evaluation of the control strategies' performance, the same state space model of the machine structure that had been used for publication ② was employed. The control strategies investigated were a model-free DVF, a model-based LQG, a robust H_∞, and a robust μ controller. According to MUNOA ET AL. (2013), the DVF controller shows the best performance among the model-free control strategies. Compared to the DVF controller, the LQG controller is capable of weighting the individual states. These correlate with the eigenmodes enabling the LQG controller to focus on damping the most critical natural frequencies only. This can also be achieved by robust controllers through their weighting functions. Furthermore, modeled uncertainties are considered within the synthesis. This allows, for example, considering changes within the structural behavior due to position-dependent dynamics. The model-based controllers were synthesized based on the experimentally identified state space model and tuned manually. Global convergence is not guaranteed for the synthesis of a μ controller, which is why the resulting controller can depend on the selected initial design value. In this case, no μ controller could be found that satisfied the desired robust performance specification for the structured uncertainties modeled. However, the μ synthesis showed that the previously calculated H_∞ controller yields a local minimum.

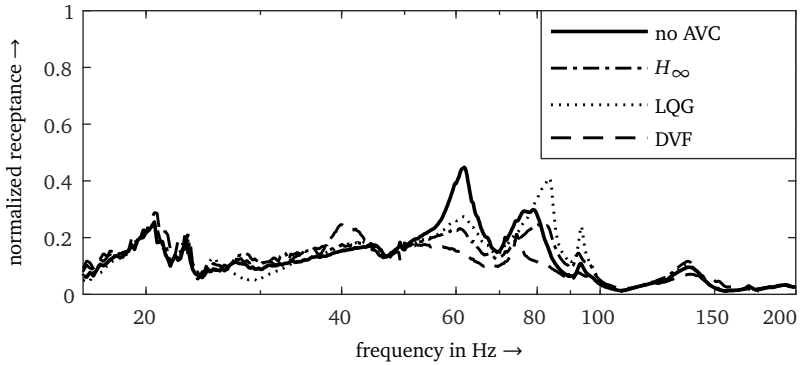

Fig. 4.7: Comparison of the different control strategies determined with tap testing at a position different from the model reference position based on KLEINWORT ET AL. (2016)

In both the simulated and experimentally measured FRF, the DVF controller showed the best damping effect, followed by the H_∞ controller, and, last of all, the LQG controller. When the TCP is moved, the structural dynamics of the machine change. In this case, the LQG controller increases the magnitudes of some modes compared to the original FRF, as shown in Fig. 4.7. In machining experiments, the chatter-free DOC increased from 1.5 mm to 2.9 mm, which corresponds to the spindle power limit, with both the DVF and H_∞ controllers. The LQG controller achieved a maximum DOC of 2.4 mm. Due to the significantly poorer damping performance and the lack of robustness against changes of the controlled system's transfer function, the LQG controller cannot be recommended for the AVC of machine tools. In the course of the experiments, the sensitivity of the DVF controller to low-frequency vibrations was noticeable, especially during high accelerations originating from the motion of the feed drives. These can lead to controller instabilities. Hence, a special filter strategy is introduced for the DVF controller in publication ⑤.

Fig. 4.8 indicates the individual contributions of the author of this dissertation to this publication.

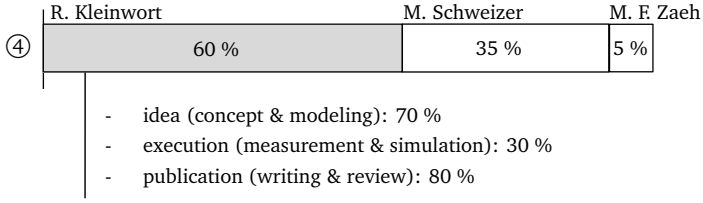

Fig. 4.8: Individual contributions of the author to publication ④

In summary, the comparison of different control strategies in simulation and cutting tests presented in this publication closes one further gap identified in Sec. 2.5 by addressing **RT2**.

The following two goals were achieved through publication ④:

- Based on a literature review, three commonly used control strategies for AVC were selected and implemented on a commercial machining center.
- In both the simulation and the experiments the DVF and the H_∞ controllers were identified to be the most promising control strategies for AVC of machine tools.

4.5 Publication 5: Automatic Tuning of Active Vibration Control Systems using Inertial Actuators

This publication addresses **RT3** and presents a methodology that reduces the high commissioning effort of AVC systems. Since the DVF and H_∞ controllers showed the best performance according to publication ④, a three-step method for their automatic commissioning is introduced: *system identification*, *controller synthesis*, and *controller test*. First, the actuator excites the machine structure by a PRBS, causing it to vibrate. The measured FRF of the controlled system is then processed by a subspace identification method, which parameterizes a state space model. The *controller synthesis* of the DVF controller uses the previously identified state space model to determine the lowest natural frequency to be damped. Depending on this frequency, the filters' cut-off frequencies are determined. Compared to publication ④, the pure integrator of the DVF controller is replaced by a weak integrator in combination with a second-order high-pass filter and an actuator compensation filter. These changes lead to reduced sensitivity to low-frequency noise and an extended working bandwidth, at the cost of reduced robustness against changes within the controlled system. An operational vibration measurement during a lightly unstable machining process serves as a reference signal for determining the controller gain. Iteratively, the controller gain is adapted in such a way that the actuator force is pushed to its limits without saturating. Furthermore, the controller behavior is evaluated within a simulation by analyzing whether the damped vibration amplitudes continue to decrease while ensuring that the Nyquist stability criterion is not violated. The same procedure is applied for tuning the H_∞ controller. The sensitivity function S_c and the controller sensitivity function CS_c are defined as a constant value and a fixed low-pass filter, respectively. Only the passband amplitude of the process sensitivity function

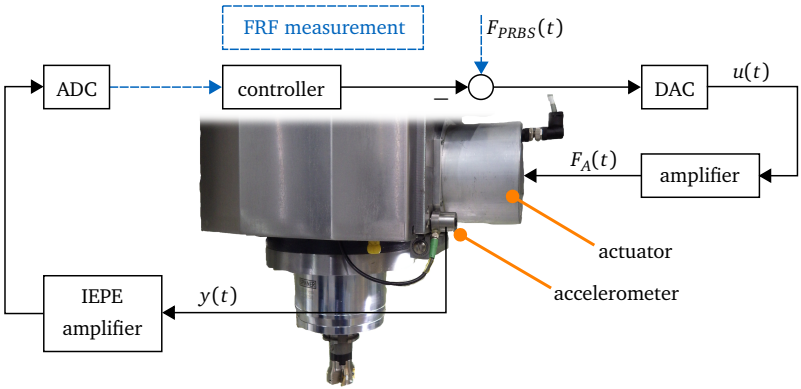

Fig. 4.9: SPINNER U5-620 equipped with an AVC system based on ZAEH ET AL. (2017)

GS_c, which is also designed as a low-pass filter, is adjusted iteratively, since it has the strongest impact on the damping performance. For the *controller test*, the system identification cycle is carried out again, but this time with the controller switched on, as illustrated in Fig. 4.9. The measured closed-loop transfer function is analyzed to ensure that the desired damping performance is achieved. The experiments were carried out on a PITTLER PV630 lathe and the SPINNER 5-axis machining center. Both were equipped with a MOOG SA10-V30 actuator. The experiments proved that the extended DVF controller is robust against low-frequency signal components due to the additional filters, but that this robustness is accompanied by a lower damping performance. The H_∞ controller showed a significantly higher damping performance in both tests. In machining experiments, both control strategies increased the chatter-free DOC by 100 %, which corresponds to the spindle power limit.

This publication was led by M. F. Zaeh as a member of the International Academy for Production Engineering (French: College International pour la Recherche en Productique - CIRP). However, the author of this dissertation (R. Kleinwort) contributed the largest portion of the publication, as depicted in Fig. 4.10.

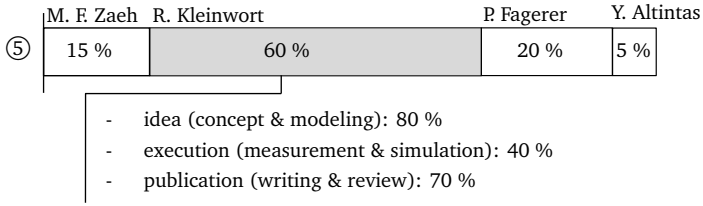

Fig. 4.10: Individual contributions of the author to publication ⑤

To sum up, this publication introduced a methodology for the automatic commissioning of the DVF and H_∞ controllers. By using the AVC system for the identification of the controlled system, followed by an automatic controller tuning and test, the effort needed for commissioning an AVC system is reduced to that of a *plug and play* solution. A further development of the automatic tuning methodology for the H_∞ controller is presented in publication ⑦.

The following three achievements were obtained through publication ⑤:

- An automatic commissioning methodology for the DVF and H_∞ controllers was derived.
- The DVF controller's working bandwidth and sensitivity to low frequency noise was reduced.
- The high transferability and performance of the presented methodology was validated by cutting tests on two different machine tools.

4.6 Publication 6: Adaptive Active Vibration Control for Machine Tools with Highly Position-dependent Dynamics

The control approaches evaluated in publication ⑤ become significantly less efficient if the machine structure to be damped shows strong position-dependent dynamics. To overcome this drawback, a position-dependent adaptation of the controller transfer function would be necessary, but this contradicts the objective of this dissertation being a low commissioning effort. In publication ⑥, an adaptive control strategy, previously implemented for AVC of machine tools at the *Institute for Machine Tools and Industrial Management* of the Technical University of Munich (WAIBEL 2012), was therefore employed and further developed. The FxLMS algorithm is extended by a *variable step size*, a *variable leakage*, and a *re-scaling* algorithm. While the first two extensions continuously adapt the step size and the leakage factor in order to achieve an optimum damping performance in each situation, the latter automatically attenuates the controller in the case of actuator saturation. However, the extended FxLMS algorithm still has a variety of setting parameters that influence the controller stability and the damping performance. Thus, the aim of this publication is to introduce a way to automatically determine the optimum setting parameters in order to simplify the commissioning.

Since the FxLMS algorithm needs a model of the controlled system, an offline or online system identification is required. The latter is preferred if the controlled system's transfer function changes due to strong position-dependent dynamics. For both procedures, the optimal parameters were determined within the scope of an extensive series of simulations. As an example, the optimization of the adaptation step size α is presented in Fig. 4.11. Analyzing the FAAC value shows that α has a

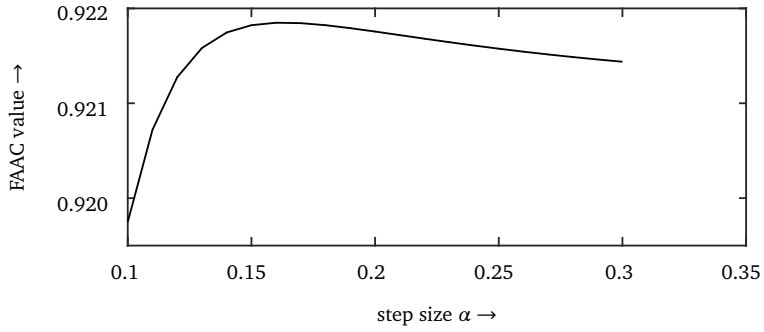

Fig. 4.11: FAAC value depending on the adaptation step size α based on KLEINWORT ET AL. (2018a)

significant influence on the accuracy of the system identification. For the experimental validation, the proof-mass actuator excited the machine structure at a fixed frequency, while the TCP was moved in order to force a change in dynamics. During this test, online system identification achieved a significantly higher vibration suppression in the new machine position compared to offline system identification because for the latter the controlled system transfer function was not adapted to the changing dynamics but fixed. In contrast to the previous publications, the controller was implemented on a cost-efficient B&R X20CP1586 PLC control system. Final cutting tests confirmed the performance of the setup and the methodology. The chatter-free DOC was increased by a significant amount of 160 % from 1.0 mm to 2.6 mm.

Fig. 4.12 depicts the individual contributions of the author of this dissertation to this publication.

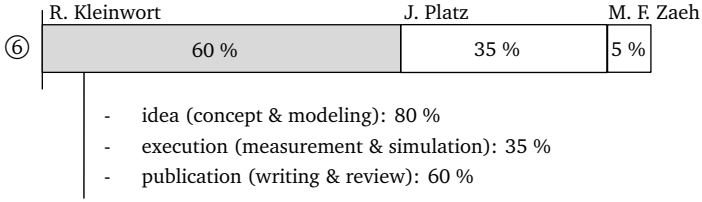

Fig. 4.12: Individual contributions of the author to publication ⑥

In summary, this publication introduced an adaptive control strategy for AVC that is advantageous if the machine tool shows strong position-dependent dynamics. The presented online identification and methodology for control parameter selection enables a commissioning of the controller with minimum effort, as demanded by **RT3**. The included attenuation of the controller in the case of actuator saturation ensures long service life. However, there are caveats concerning the industrial use of this control strategy because the classical stability criteria from control engineering (see Sec. 2.4.6.1) are not applicable.

This publication won the Best Paper Award 2018 from the International Journal of Automation Technology (IJAT).

Publication ⑥ presents the following three achievements:

- An adaptive FxLMS controller with online system identification was implemented, which proved to yield high damping performance even if the machine tool exhibits strong position-dependent dynamics.
- A simulation-based methodology was derived that allows for an optimization of the control parameters.
- The controller was successfully implemented on a cost-efficient industrial PLC and tested in machining experiments.

4.7 Publication 7: Evaluation of Different Automatically Tuned Control Strategies for Active Vibration Control

Since the DVF, H_∞, and FxLMS controllers all showed a reasonable performance according to publications ① to ⑥, publication ⑦ presents a final evaluation of these control strategies with extensive cutting tests under industrial operation conditions. Not only are the controllers' performance assessed, but also the transferability and the robustness of the automatic tuning methodologies, as mandated by **RT4**. In addition to machining tests on the SPINNER U5-620, the H_∞ controller was also tested on the turning lathe PITTLER PV 630. Since the lathe did not show strong position-dependent dynamics, the FxLMS controller was only tested on the 5-axis milling machine. All controllers were implemented on the B&R X20CP1586 PLC. For this publication, a more powerful CEDRAT MICA 300M actuator was attached to the lathe, as illustrated in Fig. 4.13, while the milling machine was still equipped with the MOOG SA10-V30 actuator. Compared to publication ⑤, measures for increasing

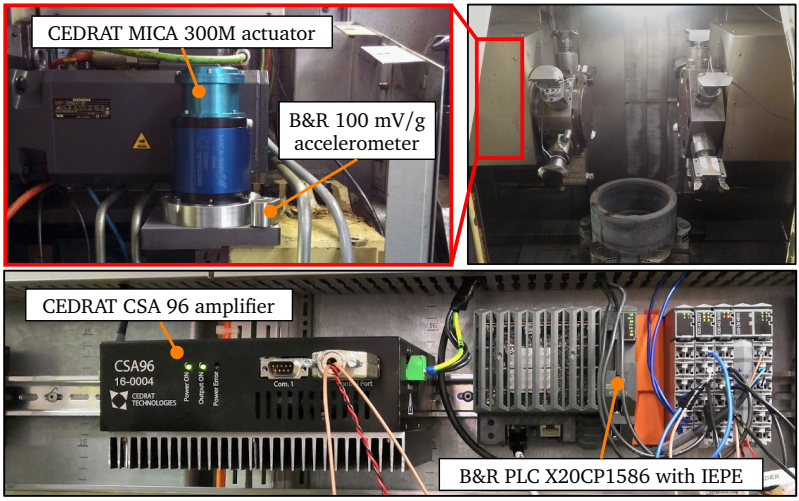

Fig. 4.13: AVC hardware integrated on the PITTLER PV630 based on KLEINWORT ET AL. (2021)

the robustness of a DVF controller were investigated in more detail. In addition, the automatic tuning methodology for the H_∞ controller was further developed. The new methodology allows all three closed-loop transfer functions $(S(s), CS(s), GS(s))$ to be considered instead of only one. The increased complexity in loop-shaping is handled by a PSO. The optimization searches for the global minimum of the cost function $||GS||_\infty$ and aborts if the swarm has converged. This leads to a much higher calculation effort because for each particle of the swarm the H_∞ synthesis needs to be performed. To reduce the computational time, the actuator saturation

is tested in the frequency domain instead of the time domain, which was the case in publication ⑤. The maximum actuator force is considered within the boundary function of the control sensitivity function $CS(s)$, which prevents the actuator from saturating.

Extensive cutting tests for different TCP positions and process parameters were successfully performed, which proves the robustness of the automatic commissioning methodologies of the DVF, H_∞, and FxLMS controllers. The resulting vibration amplitudes and surface roughness were examined, along with the durability of the proof-mass actuator. After having put the AVC system on the PITTLER PV630 successfully into operation, it has been in use in series production ever since. The publication concludes with a list of advantages and disadvantages of the individual controllers and provides the end user with recommendations on how to select the most suitable control strategy for an application.

Fig. 4.14 shows the individual contributions of the author of this dissertation to this publication.

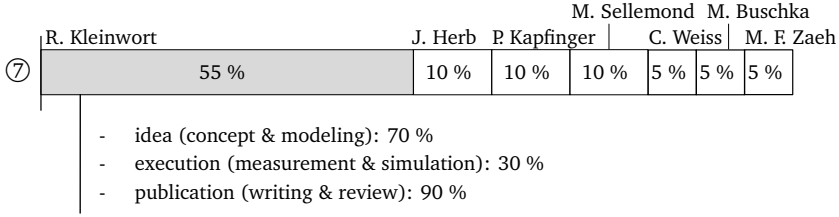

Fig. 4.14: Individual contributions of the author to publication ⑦

In summary, publication ⑦ presents an improved automatic tuning methodology for the H_∞ controller and proves the performance and robustness of all developed automatic commissioning methodologies during extensive machining tests under varying conditions. Furthermore, the hardware components of an AVC system are evaluated in terms of their industrial suitability.

The work leading to publication ⑦ achieved the following five goals:

- The automatic commissioning for the H_∞ controller was improved.
- The DVF, H_∞, and FxLMS controllers were evaluated by comparing the resulting vibration amplitudes and surface roughness values for different TCP positions and process parameters.
- All controllers were successfully implemented on a cost-efficient PLC.
- Extensive machining experiments proved the robustness and performance of the automatic commissioning methodologies under industrial operation conditions.
- The AVC system on the PITTLER PV630 has been tested in serial production.

4.8 Discussion

This section discusses the main contributions of all publications compared to the state of the art, as illustrated in Fig. 4.15.

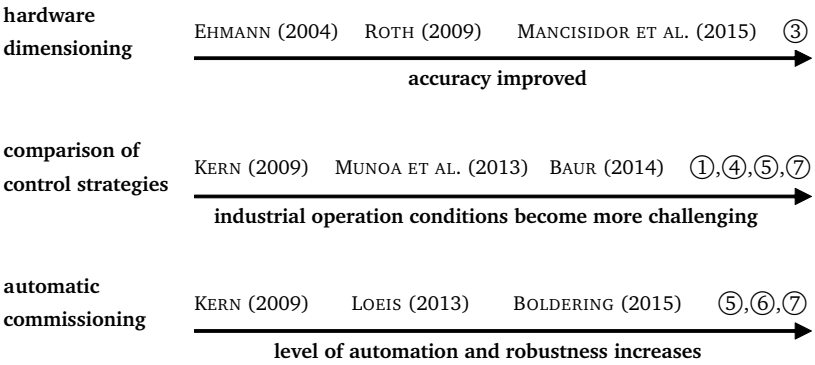

Fig. 4.15: Classification of the publications in comparison to exemplary works in the literature

While EHMANN (2004) presented fundamental calculations for the required actuator force and identified the high influence of the cutting forces, ROTH (2009) and ABELE ET AL. (2016) stated that the actuator must be able to provide the same force magnitude as the cutting forces. The simulation approach presented by MANCISIDOR ET AL. (2015) identifies the resulting actuator forces for a certain process at different actuator locations. A similar simulation model was implemented in the context of publications ① and ② of this dissertation. In publication ③, the simulation model is combined with a methodology for determining the maximum forced and self-excited vibrations to be expected for a certain machine tool. This novelty allows for the first time to precisely obtain the actuator force required in order to improve the chatter stability in such a way that the full spindle power can be exploited.

A theoretical comparison of different control strategies for the AVC of machine tools was first presented by EHMANN (2004), who, in the end, implemented a μ controller. However, no cutting tests were performed. Several publications presented the performance of a single control strategy in simple cutting tests, including WAIBEL (2012), who implemented an adaptive FxLMS controller. KERN (2009) compared a LQG and a μ controller for an AMB spindle. The LQG controller showed a lack of robustness against the spindle speed-dependent dynamics, and was not able to increase the chatter stability in contrast to the robust μ controller. MUNOA ET AL. (2013) evaluated different model-free control strategies in simulations and performed cutting tests with a DVF controller on a commercial ram-type milling machine.

Extensive machining tests were performed by BAUR (2014) for a DVF and a model-based loop shaping controller with manually selected poles. A similar comparison is shown in publication ①, but, in contrast to the results of BAUR (2014), stronger controller performance is achieved with the model-based loop shaping controller. The reason is that the model-based loop shaping controller can be focused on damping only the most critical eigenmode. For the first time, publication ④ shows a direct comparison of the DVF, LQG, H_∞, and μ controllers. However, since the non-convex μ synthesis has yielded no solution that satisfied the desired robust performance specification, the increase in chatter stability was experimentally evaluated only for the remaining three controllers. The results for the LQG controller agree with Kern's findings: due to changes in the transfer function of the controlled system as well as modeling errors, the controller performance decreases significantly. Furthermore, a comparison of the DVF and H_∞ controllers with automatic commissioning is shown in publication ⑤, and machining tests with the two controllers under industrial operation conditions are presented in publication ⑦.

A first simplification of the commissioning of AVC systems with LTI controllers was introduced by KERN (2009), PARUS ET AL. (2013), and BRECHER ET AL. (2016). All of them used the AVC actuator to excite the mechanical structure, thereby directly determining the FRF of the controlled system. BOLDERING (2015) automated the system identification and the subsequent synthesis of an LQG controller for an active grinding tool holder. However, no machining tests for validation were performed. Publication ⑤ uses a similar approach for automatic system identification and introduces an automatic tuning methodology for a DVF and an H_∞ controller. In contrast to the procedure presented by Boldering, the machining process is considered. The process forces directly affect the controller output and, thus, must be taken into account to avoid damaging the actuator due to saturation. Additional machining tests and further improvements to the automatic commissioning of the H_∞ controller are presented in publication ⑦. At the same time of publication ⑤, UHLMANN ET AL. (2017) also presented a methodology for automatic tuning of an H_∞ controller for the AVC of a portal machine tool structure test bed. Three lead zirconate titanate piezoelectric actuators were integrated serially within the force flux. However, no machining process was considered for the tuning methodology and, due to only using an individual laboratory setup, no cutting tests were performed.

For LTV controllers, LOEIS (2013) implemented an online identification for an adaptive feedforward FxLMS controller. Since the focus was on noise suppression, the increase of chatter stability during wood machining was not investigated. In publication ⑥, a feedback FxLMS controller with online identification is introduced. In contrast to the work of LOEIS (2013), several modifications found in the literature for improving the LMS algorithm were implemented and evaluated with respect to chatter stability improvements. The remaining parameters of the adaptive controller to be selected during commissioning are optimized by a simulation-based approach, leading to a methodology for automatic commissioning of the FxLMS controller.

Additional extensive machining tests under industrial operation conditions were conducted and described in publication ⑦.

Several publications show that the methods developed within this dissertation have a high degree of transferability, and that the automated commissioning lowers the barriers to market entry, especially for retrofit solutions. Inspired by publication ⑤, MANCISIDOR ET AL. (2018) implemented an automatic system identification using the proof-mass actuator of the AVC system in order to obtain the position-dependent dynamics of a ram-type milling machine, thereby simplifying the controller tuning. The high transferability of the methodology developed is proven by BEUDAERT ET AL. (2019), who implemented a similar approach as presented in publication ⑤ for the automatic tuning of a DVF controller for a portable proof-mass actuator. The latter was used for chatter suppression on flexible workpieces. Instead of modeling the controlled system, only the FRF was determined and used for controller tuning. In addition to the controller gain, the parameters of the filters were tuned, too. In addition to a stability analysis in simulation, an online gain margin verification approach was introduced that progressively increases the controller gain in order to obtain the real stability limit. However, no machining process is considered during the controller tuning in order to prevent the actuator from saturating as a result of too high sensor amplitudes. The portable damping system is called DYNAMIC WORKPIECE STABILIZER, and is available as a commercial product (DANOBATGROUP 2019). A further evaluation of the achievements is presented in the next chapter.

5 Evaluation

For the industrial use of AVC systems on machine tools, its technology maturity as well as its economic and ecological impacts are most important. The latter was already evaluated by BAUR (2014), who determined the energy demand per material removal in J/mm^3. Machining tests showed that the *specific energy demand* can be reduced by 15 % if the stability limit is improved by 45 %. In publication ②, simulations obtained comparable results with energy savings of 34 % for an increase in chatter stability of 100 %. However, these results reflect best-case scenarios, since the net machining time is significantly reduced. General statements about the increase in energy efficiency through AVC cannot be made. However, the simulation approach presented in publication ② allows for an easy assessment of individual processes.

In addition to the above mentioned ecological evaluation, the following sections contain an assessment of the AVC system derived in this dissertation in terms of technology maturity and possible return on investment.

5.1 Technology Maturity Assessment

The evaluation of technologies goes back to the concept of the technology readiness level (TRL) developed by the *National Aeronautics and Space Administration* (NASA) (MANKINS 1995). Since the nine TRLs focus on components for aerospace and astronautic systems, they cannot easily be transferred to manufacturing technologies. BROUSSEAU ET AL. (2010) introduced a technology maturity assessment to define the maturity of micro and nano production processes by seven different maturity stages. REINHART & SCHINDLER (2012) adapted Brousseau's approach in order to consider common manufacturing technologies. The seven resulting maturity stages are shown in Fig. 5.1. Within the *basic technology research* stage, working principles and hypothetical theories are observed, documented and comprehended. In the second stage, formulated theories allow for simulations. In addition, first experiments for the proof of concept are performed. The *technology development* stage includes the evaluation of alternative technologies. Furthermore, all relevant process parameters are identified and estimated using simulations. In the fourth stage, a functional hardware prototype is built in order to show the functionality of the technology in a laboratory environment. The next stage is called *resource integration* and requires the integration of the technology into a real production resource. Extensive experiments are conducted in order to validate the results of lower maturity stages and contemplate the process window under realistic conditions. At this stage, technological and economic indicators are also assessed, such as process times, machine availability, or resource efficiency. The *production environment integration* focuses on the interfaces to other production technologies as well as upstream and downstream processes.

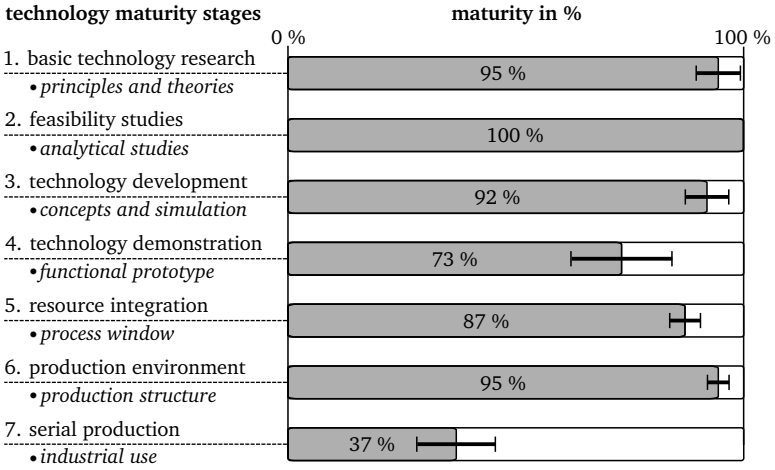

Fig. 5.1: Evaluation of the technology maturity stages for the AVC system derived within this dissertation using the criteria of REINHART & SCHINDLER (2012)

Extensive experiments are conducted to show all influences on the process window. The last stage indicates that the technology can now be used within *serial production*. Here, standardized procedure documents exist and regular maintenance actions are established in the company. (REINHART & SCHINDLER 2012)

Five technicians and engineers from the companies *SPINNER Werkzeugmaschinenfabrik* and *Schaeffler Group*, who were involved in the research work described in this dissertation, assessed the maturity of the developed AVC system based on a standardized survey presented in SCHINDLER (2015). For each maturity stage, these experts evaluated several criteria, which were weighted equally. In Fig. 5.1, the resulting mean value for the maturity of each stage is shown, together with its standard deviation. The maturity stages one to six received a high evaluation. In contrast to that, the comparably low value of stage four is caused by a lack of long term experience with the system and the wish for additional extensive machining tests. Similar points were criticized at stage five. Additionally, the investment costs were perceived as too high. In order to reach a higher evaluation at stage seven, more experience has to be gained with the system inside the companies, especially with respect to maintenance services and hardware installation.

BAUR (2014) applied the TRLs presented by MANKINS (1995) in order to evaluate the maturity of the AVC system that he developed. Since a prototype was built and tested on two different machine tools, TRL 5 was reached. According to REINHART & SCHINDLER (2012), this level corresponds to a technology maturity between stage four and five. The survey shown in Fig. 5.1 indicates that with the methodologies developed within this dissertation, the AVC system has reached the highest technology

maturity stage. In order to complete this stage, more experience with the system installed in serial production has to be gained by the companies.

5.2 Economic Assessment

A generally valid economic assessment of an investment such as an AVC system is not possible within academia, since comprehensive cost and revenue information is not available at universities. Thus, this has to be done individually for each machine tool, which is intended to be equipped with such a system. Furthermore, the revenue depends strongly on the achievable increase in chatter stability as well as the product range. The targeted increase in chatter stability defines the actuator dimension required and hence affects the investment costs significantly. Based on the product range, the reduction in machining time due to the increased chatter stability must be analyzed. Most likely, an improvement in net machining time can only be achieved for heavy duty milling operations.

As an example, the economic assessment is performed below for the sample workpiece presented in publication ②, which was machined on a SPINNER U5-620 milling machine. Only those costs that change significantly as a result of the use of AVC are taken into account. The calculated investment costs are then compared with the potential cost reduction through net machining time reduction. Tab. 5.1 summarizes the assumed cost rates.

Tab. 5.1: Assumed cost rates

name	**unit**	**value**
engineer personnel costs	€/h	80
technician personnel costs	€/h	55
machine hour rate	€/h	30

The methodology developed within this dissertation significantly reduces the time required to commission an AVC system. For industrial applications, it is possible that the system identification and controller tuning has to be repeated at regular intervals due to changes within the controlled system (e.g wear effects, structural changes during maintenance). It is assumed, that an experienced engineer needs 8 h for the manual setup. Using the automatic approach, a technician can commission the system in less than 1 h. This yields the following cost savings for each setup:

$$\Delta C_{setup} = 8\ \text{h} \cdot 80\ €/\text{h} - 1\ \text{h} \cdot 55\ €/\text{h} = 585\ €. \tag{5.1}$$

Besides the costs for commissioning, the investment costs for an AVC system have to be taken into account. Based on quotations available to the author of this dissertation,

the total costs including software licenses are broken down in Tab. 5.2. The actuator

Tab. 5.2: Investment costs based on quotations

name	**price in €**
MMF KS80D acceleration sensor including cable	270
B&R X20CP1586 PLC incl. D/A and A/D with IEPE amplifier	2600
BEAK BAA 120 power amplifier	2000
MOOG SA10-V30 actuator	2500
total costs	**7370**

and power amplifier are comparably expensive and account for over 60 % of the costs, as they are only produced in very small quantities. Furthermore, the dimensions for these components have to be selected specifically for the respective machine tool. In total, the commissioning and investment costs for the above mentioned hardware configuration sum up to

$$C_{AVC} = 1\ \text{h} \cdot 55\ €/\text{h} + 7370\ € = 7425\ €. \tag{5.2}$$

For the sample workpiece in publication ②, the increase in chatter stability of 100 % leads to a reduction of the total cycle time from $t_{tct} = 209$ s to $t_{tct,AVC} = 130$ s. Hence, the direct production cost per workpiece is reduced by

$$\Delta C_{total} = (209\ \text{s} - 130\ \text{s}) \cdot (55\ €/\text{h} + 30\ €/\text{h}) = 1.865\ €. \tag{5.3}$$

Assuming a change-over time between two workpieces of $t_{cot} = 30$ s, the breakeven point is reached after

$$t_{be} = \frac{C_{AVC}}{\Delta C_{total}} \cdot (130\ \text{s} + 30\ \text{s}) = 177\ \text{h}\ . \tag{5.4}$$

Hence, for a production in two shifts with a working time of 40 h/week, the breakeven point is reached in under three weeks. In the above calculations, energy costs were neglected. However, as shown by BAUR (2014) and publication ②, energy efficiency is increased through AVC which would further reduce the required time t_{be} until breakeven. It should be noted that the above example is close to a best-case scenario. To calculate the breakeven for arbitrary processes, Eq. 5.4 can be generalized to

$$t_{be} = \frac{C_{AVC}}{(t_{tct} - t_{tct,AVC}) \cdot 85\ €/\text{h}} \cdot (t_{tct,AVC} + t_{cot})\ . \tag{5.5}$$

6 Summary and Outlook

6.1 Summary

Increasing scarcity of resources as well as the current climate change create a demand for more sustainable and energy efficient production technologies. In the case of machine tools, this calls for retrofit solutions that are able to lift an existing machine to an even more favorable economical and competitive level. Since the installed drive power of such machines often cannot be fully exploited due to the dynamic compliance of the basic structure that result in chatter, the integration of an active vibration control system can lead to a significant increase in productivity. For new machine designs, desires for reduced energy demand call for lower accelerated masses. However, lightweight design yields worse compliance in terms of damping behavior and is thus in conflict with the targeted chatter stability. With the help of active vibration control systems, low dynamic compliance (high dynamic stiffness) over a high bandwidth can be achieved. Nevertheless, the use of such systems has so far been very limited in industry. The reasons for this are a lack of knowledge about the dimensioning of an active vibration control system, the high effort and expertise needed for commissioning such a system, and a lack of experience about their robustness in industrial use which directly brings about reliability and safety implications. The objective of this dissertation was to overcome these challenges by presenting a methodology consisting of a user-friendly simulation-based approach to accurately select the actuator dimensions and specifications, and a robust and industrially-suitable automatic commissioning strategy for corresponding active vibration control systems.

First, a simple modeling approach was implemented for simulating the performance of an active vibration control system. By using the model, the actuator force required for damping the expected maximum vibration amplitudes on a specific machine tool can be determined, thus utilizing the full power of the spindle without inducing chatter. In this context, an analytical solution calculates worst case process parameters that lead to a high instability, and a genetic optimization algorithm determines the process parameters with maximum cutting forces.

Based on a literature review, the most promising LTI control strategies were selected and compared during machining tests. For the model-free direct velocity feedback and the model-based H_∞ controller, which showed the highest increase in chatter stability, an automatic commissioning was introduced. The actuator excites the machine tool structure, and a subspace identification technique automatically identifies a model of the controlled system. Then, taking into account the process to be stabilized and the maximum actuator force, a controller is tuned in such a way that optimal damping performance is achieved. However, the direct velocity feedback controller,

when used alone, has a high sensitivity at low frequencies. This behavior can lead to instabilities and actuator saturation if, for example, high feed drive accelerations occur. Additional high-pass filters, which are required to ensure industrial suitability, reduce the damping performance. H_∞ synthesis overcomes these drawbacks since the resulting controller shows a low sensitivity to low-frequency noise, and allows the controller design to be focused on damping only the most critical modes. However, the damping performance decreases with increasing uncertainties. Hence, for machine tools with strong position-dependent dynamics, the implementation of an LTV adaptive FxLMS controller is preferable. Equipped with online identification and a largely automated adaptation of the controller parameters, this control strategy also allows for easy commissioning. For the remaining parameters, a simulation-based approach determines the optimal settings. On the contrary, the stability proof and guarantee in the case of FxLMS is not as straightforward.

Extensive machining tests with varying process parameters and conditions were conducted and have proven the robustness and performance of the control strategies as well as the automatic commissioning. Since the machining tests were performed on two different machine tools – a 5-axis milling machine and a vertical lathe – with different hardware components, the transferability of the automatic commissioning was also demonstrated with evidence. A final evaluation of the resulting active vibration control system confirmed a high technology readiness level. The use of cost-efficient and commercially available components ensures industrial suitability.

By comparing the methodology developed to the state of the art, the potentials and benefits were pointed out: the actuator can be dimensioned more accurately, end-users are now able to select the optimum control strategy for their application, and the commissioning effort needed is reduced to a minimum. Finally, an economic assessment showed that for machine tools with low dynamic stiffness and a significant share of heavy duty machining operations, an active vibration control system offers a high return on investment if the methodology developed within this dissertation is applied.

6.2 Outlook

BEUDAERT ET AL. (2019) adapted the presented solutions for automatic commissioning to a portable active vibration control system for flexible workpieces, which has also been commercialized (DANOBATGROUP 2019). Several approaches exist showing how the automatic system identification can be used for other objectives as well. As already mentioned by JALIZI (2015) and MANCISIDOR ET AL. (2018), it can be applied to detect wear-related changes in the dynamic behavior of a machine. Together with statistical approaches, this leads to a predictive maintenance approach that is capable of predicting the failure of machine components. First studies of this topic have already been performed by ELLINGER ET AL. (2019), who used the automatic

system identification approach of this dissertation. Hence, besides performance and production quality enhancements, the machine's availability is also improved. Altogether, this leads to a significantly improved overall equipment effectiveness.

Furthermore, the works of KOSUB ET AL. (2012) and BRECHER ET AL. (2015) advocate a simple determination of a machine tool's position-dependent dynamics. Especially in combination with the results of a finite element model, automatic system identification allows for accurate parameterization of a digital twin, which considers the current loads and the wear status of the machine components. As a result, more accurate stability lobe diagram calculations and, subsequently, an appropriate selection of process parameters ensure high chatter stability and low surface roughness.

The research project *Identification and Modeling of Process-induced Damping in Machine Tools*, which is currently being worked on at the *Institute for Machine Tools and Industrial Management* of the Technical University of Munich, investigates the use of automatic system identification during machining for the analysis of process damping. The expected results will further improve the stability lobe diagram prediction. However, system identification during machining is still a challenge because of the process induced measurement noise. First investigations have already been conducted by KERN (2009), but further development is necessary. This would also improve the active vibration control system and its condition monitoring capability, since an online monitoring of the controlled system replaces the time required for offline identification and ensures optimum controller tuning at any time.

In addition, the automatic tuning of LTI controllers can be further improved by considering the critical cutting conditions from publication ③ instead of the measured vibration amplitudes of an arbitrary unstable process. This will result in a conservative, but more robust controller tuning that will reduce the risk of a need for re-commissioning due to actuator saturation.

Bibliography

The references are sorted alphabetically according to the names of the first authors. Where year or number are not indicated, they do not exist or are not available to the author of this dissertation. The numbers ① to ⑦ indicate the publications belonging to this publication-based dissertation.

ABELE ET AL. 2008

Abele, E.; Hanselka, H.; Haase, F.; Schlote, D.; Schiffler, A.: Development and design of an active work piece holder driven by piezo actuators. Production Engineering 2 (2008) 4, pp. 437–442.

ABELE ET AL. 2016

Abele, E.; Pfeiffer, G.; Jalizi, B.; Bretz, A.: Simulation and development of an active damper with robust μ-control for a machine tool with a gantry portal. Production Engineering 10 (2016) 4-5, pp. 519–528.

ABOULNASR & MAYYAS 1997

Aboulnasr, T.; Mayyas, K.: A robust variable step-size LMS-type algorithm: analysis and simulations. IEEE Transactions on signal processing 45 (1997) 3, pp. 631–639.

ÅKESSON ET AL. 2007

Åkesson, H.; Smirnova, T.; Claesson, I.; Håkansson, L.: On the development of a simple and robust active control system for boring bar vibration in industry. International Journal of Acoustics and Vibration 12 (2007) 4, pp. 139–152.

AKHTAR ET AL. 2006

Akhtar, M. T.; Abe, M.; Kawamata, M.: A new variable step size LMS algorithm-based method for improved online secondary path modeling in active noise control systems. IEEE Transactions on Audio, Speech, and Language Processing 14 (2006) 2, pp. 720–726.

AL-REGIB ET AL. 2003

Al-Regib, E.; Ni, J.; Lee, S.-H.: Programming spindle speed variation for machine tool chatter suppression. International Journal of Machine Tools and Manufacture 43 (2003) 12, pp. 1229–1240.

ALBIZURI ET AL. 2007

Albizuri, J.; Fernandes, M. H.; Garitaonandia, I.; Sabalza, X.; Uribe-Etxeberria, R.; Hernández, J. M.: An active system of reduction of vibrations in a centerless grinding machine using piezoelectric actuators. International Journal of Machine Tools and Manufacture 47 (2007) 10, pp. 1607–1614.

ALI ET AL. 2011

Ali, H.; Noor, S.; Marhaban, M.; Bashi, S.: Design of H_∞ controller with tuning of weights using particle swarm optimization method. IAENG International Journal of Computer Science 38 (2011) 2, pp. 103–112.

ALIZADEH ET AL. 2003

Alizadeh, A.; Ehmann, C.; Schönhoff, U.; Nordmann, R.: Active Bearing of Rotors Utilizing Robust Controlled Piezo Actuators. In: Shabana, A. A. (Editor): Proceedings of the 2003 ASME Design Engineering Technical Conferences and Computers and Information in Engineering Conference. New York, NY: American Society of Mechanical Engineers 2003. pp. 2669–2677.

ALLEMANG 2003

Allemang, R. J.: The Modal Assurance Criterion – Twenty Years of Use and Abuse. Journal of Sound and Vibration 37 (2003) 8, pp. 14–21.

ALTINTAS 2012

Altintas, Y.: Manufacturing Automation: Metal Cutting Mechanics, Machine Tool Vibrations, and CNC Design. 2nd edition. Cambridge: Cambridge University Press 2012. ISBN: 978-0-521-17247-9.

ALTINTAS & CHAN 1992

Altintas, Y.; Chan, P. K.: In-process detection and suppression of chatter in milling. International Journal of Machine Tools and Manufacture 32 (1992) 3, pp. 329–347.

ALTINTAS & KO 2006

Altintas, Y.; Ko, J. H.: Chatter Stability of Plunge Milling. CIRP Annals 55 (2006) 1, pp. 361–364.

ALTINTAS ET AL. 1999

Altintas, Y.; Engin, S.; Budak, E.: Analytical Stability Prediction and Design of Variable Pitch Cutters. Journal of Manufacturing Science and Engineering 121 (1999) 2, pp. 173–178.

ALTINTAS ET AL. 2005

Altintas, Y.; Brecher, C.; Weck, M.; Witt, S.: Virtual Machine Tool. CIRP Annals 54 (2005) 2, pp. 115–138.

ALTINTAS ET AL. 2011

Altintas, Y.; Verl, A.; Brecher, C.; Uriarte, L.; Pritschow, G.: Machine tool feed drives. CIRP Annals 60 (2011) 2, pp. 779–796.

Barrenetxea et al. 2018

Barrenetxea, D.; Mancisidor, I.; Beudaert, X.; Munoa, J.: Increased productivity in centerless grinding using inertial active dampers. CIRP Annals 67 (2018) 1, pp. 337–340.

Baur 2014

Baur, M.: Aktives Dämpfungssystem zur Ratterunterdrückung an spanenden Werkzeugmaschinen. PhD Thesis. Technische Universität München (2014). Munich, Germany: Herbert Utz 2014. ISBN: 978-3-83164-408-7. (290).

Bediaga et al. 2011

Bediaga, I.; Zatarain, M.; Muñoa, J.; Lizarralde, R.: Application of continuous spindle speed variation for chatter avoidance in roughing milling. Proceedings of the Institution of Mechanical Engineers, Part B: Journal of Engineering Manufacture 225 (2011) 5, pp. 631–640.

Beudaert et al. 2017

Beudaert, X.; Barrios, A.; Erkorkmaz, K.; Munoa, J.: Limiting Factors for Active Suppression of Structural Chatter Vibrations Using Machine's Drives. Transactions of Nanjing University of Aeronautics and Astronautics 34 (2017) 4, pp. 341–348.

Beudaert et al. 2019

Beudaert, X.; Erkorkmaz, K.; Munoa, J.: Portable damping system for chatter suppression on flexible workpieces. CIRP Annals 68 (2019) 1, pp. 423–426.

Bickel et al. 2014

Bickel, W.; Litwinski, K.; Denkena, B.: Increase of Process Stability with Innovative Spindle Drives. In: Denkena, B. (Editor): New Production Technologies in Aerospace Industry. Cham and s.l.: Springer International 2014. Lecture Notes in Production Engineering. pp. 145–151.

Bilbao-Guillerna et al. 2012

Bilbao-Guillerna, A.; Azpeitia, I.; Luyckx, S.; Loix, N.; Munoa, J.: Low Frequency Chatter Suppression using an Inertial Actuator. In: 9th International Conference on High Speed Machining. Bilbao, Spain 2012. pp. 1–6.

Boldering 2015

Boldering, A. L.: Automatisierte Identifikation zur aktiven Reduzierung von Maschinenschwingungen. PhD Thesis. Technische Universität Braunschweig (2015). Essen, Germany: Vulkan 2015. ISBN: 978-3-8027-8339-5.

B&R Automation 2020a

B&R Automation: X20CP1586. https://www.br-automation.com/fileadmin/1313696279380-de-bigicon-1.2.jpg - 20.03.2020.

B&R Automation 2020b

B&R Automation: X20CP1586. https://www.br-automation.com/en/products/software/modeling-and-simulation/automation-studio-target-for-simulink/ - 22.04.2020.

B&R Automation 2020c

B&R Automation: Condition Monitoring Modul. https://www.br-automation.com/de/produkte/steuerungssysteme/x20-system/sonstige-funktionen/x20cm4810/ - 02.03.2020.

Brecher et al. 2008

Brecher, C.; Manohran, D.; Stephan Witt, E. W. E.: Structure integrated adaptronical systems for machine tools. Production Engineering 2 (2008) 2, pp. 219–223.

Brecher et al. 2010

Brecher, C.; Manoharan, D.; Ladra, U.; Köpken, H.-G.: Chatter suppression with an active workpiece holder. Production Engineering 4 (2010) 2-3, pp. 239–245.

Brecher et al. 2013

Brecher, C.; Baumler, S.; Brockmann, B.: Avoiding Chatter by means of Active Damping System for Machine Tools. Journal of Machine Engineering 13 (2013) 3, pp. 117–128.

Brecher et al. 2015

Brecher, C.; Altstädter, H.; Daniels, M.: Axis Position Dependent Dynamics of Multi-axis Milling Machines. Procedia CIRP 31 (2015), pp. 508–514.

Brecher et al. 2016

Brecher, C.; Fey, M.; Brockmann, B.; Chavan, P.: Multivariable control of active vibration compensation modules of a portal milling machine. Journal of Vibration and Control 24 (2016) 1, pp. 3–17.

Bretschneider 2000

Bretschneider, J.: Reglerselbsteinstellung für digital geregelte, elektromechanische Antriebssysteme an Werkzeugmaschinen. PhD Thesis. Universität Stuttgart (2000). Stuttgart, Germany: Jost-Jetter 2000. (ISW-Forschung und -Praxis 134).

BROCK 1946

Brock, J. E.: A note on the damped vibration absorber. Journal of Applied Mechanics 13 (1946) 4, pp. A–284.

BROUSSEAU ET AL. 2010

Brousseau, E.; Barton, R.; Dimov, S.; Bigot, S.: A methodology for evaluating the technological maturity of micro and nano fabrication processes. In: International Precision Assembly Seminar. Chamonix, France 2010. pp. 329–336.

BUDAK & ALTINTAS 1998

Budak, E.; Altintas, Y.: Analytical Prediction of Chatter Stability in Milling–Part I: General Formulation. Journal of Dynamic Systems, Measurement, and Control 120 (1998) 1, pp. 22–30.

CALLOYTOOL 2020

CalloyTool: roughing end mill DLTUPR650-4F-060. https://www.calloytool.com/Roughing/0117125.html - 31.3.2020.

CARINI & MALATINI 2008

Carini, A.; Malatini, S.: Optimal variable step-size NLMS algorithms with auxiliary noise power scheduling for feedforward active noise control. IEEE transactions on audio, speech, and language processing 16 (2008) 8, pp. 1383–1395.

CEDRAT TECHNOLOGIES 2020

Cedrat Technologies: CSA96. https://www.cedrat-technologies.com/en/products/magnetic-controllers/oem-amplifiers.html - 20.03.2020.

CHENG 2009

Cheng, K. (Editor): Machining Dynamics: Fundamentals, Applications and Practices. London: Springer 2009. ISBN: 978-1-84628-368-0. Springer Series in Advanced Manufacturing.

CHUNG ET AL. 1997

Chung, B.; Smith, S.; Tlusty, J.: Active Damping of Structural Modes in High-Speed Machine Tools. Journal of Vibration and Control 3 (1997) 3, pp. 279–295.

CLAESSON & HÅKANSSON 1998

Claesson, I.; Håkansson, L.: adaptive active control of machine-tool vibration in a lathe. International Journal of Acoustics and Vibration 3 (1998) 4, pp. 155–162.

CSA ENGINEERING 2020

CSA Engineering: Actuators. https://www.csaengineering.com/products-services/sa-series-actuators/standard-actuators.html - 20.03.2020.

DANOBATGROUP 2017

DANOBATGROUP: SORALUCE creates system capable of increasing productivity by up to 300 %. https://www.danobatgroup.com/en/press-releases/soraluce-creates-system-capable-of-increasing-productivity-by-up-to-300 - 20.03.2020.

DANOBATGROUP 2019

DANOBATGROUP: DWS - Dynamic Workpiece Stabilizer. https://www.soraluce.com/en/dws - 20.03.2020.

DE CALLAFON ET AL. 1996

de Callafon, R. A.; de Roover, D.; Van den Hof, P. M.: Multivariable least squares frequency domain identification using polynomial matrix fraction descriptions. In: Proceedings of 35th IEEE Conference on Decision and Control. Kobe, Japan 1996. pp. 2030–2035.

DEN HARTOG 1947

Den Hartog, J. P.: Mechanical Vibrations. New York, NY: McGraw-Hill 1947.

DENKENA & GÜMMER 2012

Denkena, B.; Gümmer, O.: Process stabilization with an adaptronic spindle system. Production Engineering 6 (2012) 4, pp. 485–492.

DENKENA & TÖNSHOFF 2011

Denkena, B.; Tönshoff, H. K.: Spanen - Grundlagen. Berlin, Heidelberg: Springer 2011. ISBN: 978-3-642-19771-0.

DENKENA ET AL. 2004

Denkena, B.; Kallage, F.; Ruskowski, M.; Popp, K.; Tönshoff, H. K.: Machine Tool with Active Magnetic Guides. CIRP Annals 53 (2004) 1, pp. 333–336.

DIN 60529 2000

DIN 60529: DIN EN 60529/Schutzarten durch Gehäuse (IP-Code). Berlin: Beuth 2000.

DO ET AL. 2010

Do, A. L.; Soualmi, B.; de Jesus Lozoya-Santos, J.; Sename, O.; Dugard, L.; Ramirez-Mendoza, R.: Optimization of weighting function selection for H_∞ control of semi-active suspensions. In: 12th mini conference on vehicle system dynamics, identification and anomalies (VSDIA 2010). Budapest, Hungary. 2010. pp. 12–25.

DOHNER ET AL. 2004

Dohner, J. L.; Lauffer, J. P.; Hinnerichs, T. D.; Shankar, N.; Regelbrugge, M.; Kwan, C.-M.; Xu, R.; Winterbauer, B.; Bridger, K.: Mitigation of chatter instabilities in milling by active structural control. Journal of Sound and Vibration 269 (2004) 1, pp. 197–211.

DOMBOVARI & STEPAN 2012

Dombovari, Z.; Stepan, G.: The Effect of Helix Angle Variation on Milling Stability. Journal of Manufacturing Science and Engineering 134 (2012) 5, p. 739.

DONG & ZHANG 2019

Dong, X.; Zhang, W.: Chatter suppression analysis in milling process with variable spindle speed based on the reconstructed semi-discretization method. The International Journal of Advanced Manufacturing Technology 105 (2019) 5-6, pp. 2021–2037.

EHMANN 2004

Ehmann, C.: Methoden und Komponenten für die Realisierung aktiver Schwingungsdämpfung. PhD Thesis. Technische Universität Darmstadt (2004). Darmstadt, Germany: Shaker 2004.

EHMANN & NORDMANN 2002

Ehmann, C.; Nordmann, R.: Low Cost Actuator for Active Damping of Large Machines. IFAC Proceedings Volumes 35 (2002) 2, pp. 179–184.

EHMANN ET AL. 2001

Ehmann, C.; Schonhoff, U.; Nordmann, R.: Aktive Schwingungsdampfung bei Portalfrasmaschinen. VDI Berichte 1606 (2001), pp. 163–182.

EINI 2014

Eini, R.: Flexible beam robust H_∞ loop shaping controller design using particle swarm optimization. Journal of Advances in Computer Research 5 (2014) 3, pp. 55–67.

EISELE & SADOWY 1955

Eisele, F.; Sadowy, M.: Rattern und dynamische Steifigkeit von Werkzeugmaschinen. In: Werkzeugmaschinen-Praxis, Sonderheft 2. FoKoMa (Forschungs- und Konstruktionskolloquium Werkzeugmaschinen). Munich, Germany 1955.

ELLINGER ET AL. 2019

Ellinger, J.; Semm, T.; Benker, M.; Kapfinger, P.; Kleinwort, R.; Zah, M. F.: Feed Drive Condition Monitoring using Modal Parameters. MM Science Journal 2019 (2019) 4, pp. 3206–3213.

EUROPEAN COMMISSION 2019

European Commission: Communication from the Commission to the European Parliament, the European Council, the Council, the European Economic and Social Committee and the Committee of the Regions - The European Green Deal. https://ec.europa.eu/info/sites/info/files/european-green-deal-communication_en.pdf - 22.03.2020.

EUROPEAN COMMISSION 2020

European Commission: Circular Economy Action Plan: The European Green Deal. https://ec.europa.eu/commission/presscorner/detail/en/fs_20_437 - 22.03.2020.

EWINS 2000

Ewins, D. J.: Modal Testing: Theory, Practice and Application. 2nd edition. Baldock: Research Studies Press 2000. ISBN: 978-0-863-80218-8.

EYNIAN 2014

Eynian, M.: Vibration frequencies in stable and unstable milling. International Journal of Machine Tools and Manufacture 90 (2014), pp. 44–49.

FAASEN 2007

Faasen, R.: Chatter Prediction and Control for High-Speed Milling: Modelling and Experiments. PhD Thesis. TU Eindhoven (2007). Eindhoven, Netherlands 2007.

FERNANDES ET AL. 2009

Fernandes, M. H.; Garitaonandia, I.; Albizuri, J.; Hernández, J. M.; Barrenetxea, D.: Simulation of an active vibration control system in a centerless grinding machine using a reduced updated FE model. International Journal of Machine Tools and Manufacture 49 (2009) 3, pp. 239–245.

FLADERER 2007

Fladerer, F.: Schwingungsdämpfung für Werkzeugmaschinen. Maschinenmarkt (2007). https://www.maschinenmarkt.vogel.de/schwingungsdaempfung-fuer-werkzeugmaschinen-a-92396/ - 23.3.2020.

FÖLLINGER ET AL. 2013

Föllinger, O.; Konigorski, U.; Lohmann, B.; Roppenecker, G.; Trächtler, A.: Regelungstechnik: Einführung in die Methoden und ihre Anwendung. 11th edition. Berlin: VDE 2013. ISBN: 978-3-8007-3231-9.

FORD ET AL. 2013

Ford, D. G.; Myers, A.; Haase, F.; Lockwood, S.; Longstaff, A.: Active vibration control for a CNC milling machine. Proceedings of the Institution of Mechanical Engineers, Part C: Journal of Mechanical Engineering Science 228 (2013) 2, pp. 230–245.

GAN ET AL. 2005

Gan, W. S.; Mitra, S.; Kuo, S. M.: Adaptive feedback active noise control headset: Implementation, evaluation and its extensions. IEEE Transactions on Consumer Electronics 51 (2005) 3, pp. 975–982.

GANGULI 2005

Ganguli, A.: Chatter reduction through active vibration damping. PhD Thesis. Université Libre de Bruxelles (2005). Brussels, Belgium 2005.

GARITAONANDIA ET AL. 2013

Garitaonandia, I.; Albizuri, J.; Hernandez-Vazquez, J. M.; Fernandes, M. H.; Olabarrieta, I.; Barrenetxea, D.: Redesign of an active system of vibration control in a centerless grinding machine: Numerical simulation and practical implementation. Precision Engineering 37 (2013) 3, pp. 562–571.

GAWRONSKI 2004

Gawronski, W. K.: Advanced Structural Dynamics and Active Control of Structures. New York, NY: Springer 2004. ISBN: 978-0-387-72133-0.

GMN 2020

GMN: HCS series. https://www.tuhh.de/t3resources/ics/PDFs/Opt_Robust_Ctrl/orc.pdf - 31.3.2020.

GONTIJO ET AL. 2006

Gontijo, W. A.; Tobias, O. J.; Seara, R.; Lopes, E. M.: FxLMS algorithm with variable step size and variable leakage factor for active vibration control. In: IEEE International Telecommunications Symposium. Chengdu, China 2006. pp. 572–575.

GRAB 1973

Grab, H.: Periodische Drehzahländerungen beim Ausdrehen mit Bohrstangen. Industrie Anzeiger 95 (1973), p. 1524.

HAASE 2005

Haase, F.: The investigation and design of a piezoelectric active vibration control system for vertical machining centres. PhD Thesis. University of Huddersfield (2005). Huddersfield, UK 2005.

HANSEN 2012

Hansen, C. H.: Active control of noise and vibration. 2nd edition. Boca Raton, FL: CRC Press Taylor & Francis Group 2012. ISBN: 978-1-4822-3400-8.

HANSEN 2001

Hansen, R. C.: Overall equipment effectiveness: A powerful production/maintenance tool for increased profits. 1st edition. New York, NY: Industrial Press 2001. ISBN: 0831131381.

HARMS ET AL. 2004

Harms, A.; Denkena, B.; Lhermet, N.: Tool adaptor for active vibration control in turning operations. In: 9th International Conference on New Actuators. Bremen 2004. pp. 694–697.

HASHEMI & OHADIR 2007

Hashemi, O.; Ohadir, A.: Active Control of Chatter Vibrations in a Turning Process using an Adaptive FxLMS Algorithm. In: 14th International Congress on Sound & Vibration (ICSV). Cairns, Australia 2007.

HEIDENHAIN 2013

Heidenhain: Dynamic Efficiency – Working Efficiently and with Process Reliability. Traunreut: Dr. Johannes Heidenhain GmbH 2013. https://www.heidenhain.de/fileadmin/pdb/media/img/1081192-20_Dynamic_Efficiency_en.pdf - 02.04.2020.

HEISEL & KANG 2012

Heisel, U.; Kang, C.: Aktiver Werkzeughalter zur Formfehlerkompensation. wt Werkstatttechnik online 102 (2012) 1–2.

HERZOG & KELLER 2011

Herzog, R.; Keller, J.: An Overview on Robust Control. http://www.sga-asspa.ch/cms/images/PDF/2011-01%20an%20overview%20on%20robust%20control.pdf - 31.3.2020.

HESSELBACH 2011

Hesselbach, J. (Editor): Adaptronik für Werkzeugmaschinen: Forschung in Deutschland. Aachen: Shaker 2011. ISBN: 978-3-8322-9809-8. Berichte aus dem Maschinenbau.

HESSELBACH ET AL. 2010

Hesselbach, J.; Hoffmeister, H.-W.; Schuller, B.-C.; Loeis, K.: Development of an active clamping system for noise and vibration reduction. CIRP Annals 59 (2010) 1, pp. 395–398.

HEYLEN & LAMMENS 1996

Heylen, W.; Lammens, S.: FRAC: a Consistent Way of Comparing Frequency Response Functions. In: Friswell, M. I.; Mottershead, J. E. (Editor): Identification in Engineering Systems. Swansea: University of Wales 1996. pp. 48–57.

HOLTERMAN 2002

Holterman, J.: Vibration control of high-precision machines with active structural elements. PhD Thesis. University of Twente (2002). Enschede, Netherlands 2002.

HUANG ET AL. 2015

Huang, T.; Chen, Z.; Zhang, H.-T.; Ding, H.: Active Control of an Active Magnetic Bearings Supported Spindle for Chatter Suppression in Milling Process. Journal of Dynamic Systems, Measurement, and Control 137 (2015) 11, pp. 111003–1–11.

HUBER ET AL. 1997

Huber, J. E.; Fleck, N. A.; Ashby, M. F.: The selection of mechanical actuators based on performance indices. Proceedings of the Royal Society of London. Series A: Mathematical, Physical and Engineering Sciences 453 (1997) 1965, pp. 2185–2205.

INASAKI ET AL. 2001

Inasaki, I.; Karpuschewski, B. a.; Lee, H.-S.: Grinding chatter–origin and suppression. CIRP Annals 50 (2001) 2, pp. 515–534.

ISERMANN 2008

Isermann, R.: Mechatronische Systeme: Grundlagen. 2nd edition. Berlin: Springer 2008. ISBN: 978-3-5403-2336-5.

ISERMANN & MÜNCHHOF 2011

Isermann, R.; Münchhof, M.: Identification of Dynamic Systems: An Introduction with Applications. Berlin, Heidelberg: Springer 2011. ISBN: 978-3-5407-8878-2.

JALIZI 2015

Jalizi, B.: Kompensation quasi-statischer und dynamischer Verlagerungen bei kompakten Portalfräsmaschinen. PhD Thesis. Technische Universität Darmstadt (2015). Aachen, Germany: Shaker 2015. ISBN: 978-3-8440-4237-5.

JANOCHA 1992

Janocha, H.: Aktoren: Grundlagen und Anwendungen. Berlin, Heidelberg: Springer 1992. ISBN: 978-3-662-00418-0.

JANOCHA 2007

Janocha, H.: Adaptronics and Smart Structures. Berlin, Heidelberg: Springer Berlin Heidelberg 2007. ISBN: 978-3-540-71965-6.

JOKINEN ET AL. 2000

Jokinen, H.; Ollila, J.; Aumala, O.: On windowing effects in estimating averaged periodograms of noisy signals. Measurement 28 (2000) 3, pp. 197–207.

KAMENETSKY & WIDROW 2004

Kamenetsky, M.; Widrow, B.: A variable leaky LMS adaptive algorithm. In: Conference Record of the 38th IEEE Asilomar Conference on Signals, Systems and Computers. Pacific Grove, CA 2004. pp. 125–128.

KAYHAN & BUDAK 2016

Kayhan, M.; Budak, E.: An experimental investigation of chatter effects on tool life. Proceedings of the Institution of Mechanical Engineers, Part B: Journal of Engineering Manufacture 223 (2016) 11, pp. 1455–1463.

KEMMERLING-LAMPARSKY 1987

Kemmerling-Lamparsky, M.: Dynamische Stabilisierung spanender Fertigungsprozesse mit aktiven Zusatzsystemen. Düsseldorf: VDI 1987. VDI-Fortschrittberichte Reihe 11 Nr. 94.

KERN 2009

Kern, S.: Erhöhung der Prozessstabilität durch aktive Dämpfung von Frässpindeln mittels elektromagnetischer Aktoren. PhD Thesis. Technische Universität Darmstadt (2009). Aachen, Germany 2009. ISBN: 978-3-8322-8132-8.

KERSTING 2009

Kersting, M.: Entwicklung und Anwendung eines adaptiven Schwingungsdämpfers für das Einlippentiefbohren. PhD Thesis. Technische Universität Dortmund (2009). Essen, Germany: Vulkan 2009. (Schriftenreihe des ISF 47).

KETTERER 1995

Ketterer, G.: Automatisierte Inbetriebnahme elektromechanischer, elastisch gekoppelter Bewegungsachsen. PhD Thesis. Universität Stuttgart (1995). Berlin, Germany: Springer 1995. ISBN: 3-5405-9031-5. (ISW-Forschung und Praxis 108).

KIENZLE 1952

Kienzle, O.: Die Bestimmung von Kräften und Leistungen an spanenden Werkzeugen und Werkzeugmaschinen. VDI Z 94 (1952) 11/12, pp. 299–305.

KIM ET AL. 2006

Kim, N. H.; Won, D.; Ziegert, J. C.: Numerical analysis and parameter study of a mechanical damper for use in long slender endmills. International Journal of Machine Tools and Manufacture 46 (2006) 5, pp. 500–507.

KLEINWORT ET AL. 2014, publication ①

Kleinwort, R.; Altintas, Y.; Zaeh, M. F.: Active Damping of Heavy Duty Milling Operations. In: Akkok, M.; Erden, A.; Kilic, S. E.; Konukseven, E. I.; Budak, E.; Lazoglu, I. (Editor): 16th International Conference on Machine Design and Production. Ankara, Turkey: METU-Ankara 2014. Machining Day. pp. 443–458.

KLEINWORT ET AL. 2015, publication ②

Kleinwort, R.; Popp, R. S.; Cavalié, B.; Zaeh, M. F.: Energy Demand Simulation of Machine Tools with Improved Chatter Stability Achieved by Active Damping. Applied Mechanics and Materials 805 (2015), pp. 187–195.

KLEINWORT ET AL. 2016, publication ④

Kleinwort, R.; Schweizer, M.; Zaeh, M. F.: Comparison of Different Control Strategies for Active Damping of Heavy Duty Milling Operations. Procedia CIRP 46 (2016), pp. 396–399.

KLEINWORT ET AL. 2018a, publication ⑥

Kleinwort, R.; Platz, J.; Zaeh, M. F.: Adaptive Active Vibration Control for Machine Tools with Highly Position-Dependent Dynamics. International Journal of Automation Technology 12 (2018) 5, pp. 631–641.

KLEINWORT ET AL. 2018b, publication ③

Kleinwort, R.; Weishaupt, P.; Zaeh, M. F.: Simulation-Based Dimensioning of the Required Actuator Force for Active Vibration Control. International Journal of Automation Technology 12 (2018) 5, pp. 658–668.

KLEINWORT ET AL. 2021, publication ⑦

Kleinwort, R.; Herb, J.; Kapfinger, P.; Sellemond, M.; Weiss, C.; Buschka, M.; Zaeh, M. F.: Experimental comparison of different automatically tuned control strategies for active vibration control. CIRP Journal of Manufacturing Science and Technology 35 (2021), pp. 281–297.

KNOSPE 2007

Knospe, C.: Active magnetic bearings for machining applications. Control Engineering Practice 15 (2007) 3, pp. 307–313.

KÖNIG ET AL. 1982

König, W.; Essel, K.; Witte, L.: Spezifische Schnittkraftwerte für die Zerspanung metallischer Werkstoffe. Düsseldorf: Stahleisen 1982. ISBN: 3-514-00129-4.

KÖNIGSBERG ET AL. 2018

Königsberg, J.; Reiners, J.; Ponick, B.; Denkena, B.; Bergmann, B.: Highly Dynamic Spindle Integrated Magnet Actuators for Chatter Reduction. International Journal of Automation Technology 12 (2018) 5, pp. 669–677.

KOSUB ET AL. 2012

Kosub, T.; Hannig, S.; Brecher, C.; Bäumler, S.; M., D.: Adaptive measurement solution for the dynamic flexibility of machine tools. In: Proceedings. Leuven: Department Werktuigkunde 2012. pp. 3215–3224.

KUO & VIJAYAN 1997

Kuo, S. M.; Vijayan, D.: A secondary path modeling technique for active noise control systems. IEEE Transactions on Speech and Audio Processing 5 (1997) 4, pp. 374–377.

KUO ET AL. 1996

Kuo, S. M.; Kuo, M. S.; Morgan, D. R.: Active noise control systems: Algorithms and DSP implementations. Hoboken, NJ: Wiley-Blackwell 1996. ISBN: 978-0-4711-3424-4.

KUTTNER 2015

Kuttner, T.: Praxiswissen Schwingungsmesstechnik. Wiesbaden: Springer Vieweg 2015. ISBN: 978-3-6580-4637-8.

KWAN ET AL. 1997

Kwan, C. M.; Xu, H.; Lin, C.; Haynes, L.; Dohner, J.; Regelbrugge, M.; Shankar, N.: H_∞ control of chatter in octahedral hexapod machine. In: Proceedings of the 1997 American Control Conference (Cat. No.97CH36041). Albuquerque, NM 1997. pp. 1015–1016.

KWONG & JOHNSTON 1992

Kwong, R. H.; Johnston, E. W.: A variable step size LMS algorithm. IEEE Transactions on signal processing 40 (1992) 7, pp. 1633–1642.

KYTKA ET AL. 2007

Kytka, P.; Ehmann, C.; Nordmann, R.: Active vibration μ-synthesis-control of a hydrostatically supported flexible beam. Journal of Mechanical Science and Technology 21 (2007) 6, pp. 924–929.

LAW & IHLENFELDT 2015

Law, M.; Ihlenfeldt, S.: A Frequency-based Substructuring Approach to Efficiently Model Position-dependent Dynamics in Machine Tools. Proceedings of the Institution of Mechanical Engineers, Part K: Journal of Multi-body Dynamics 229 (2015) 3, pp. 304–317.

LEE ET AL. 1998

Lee, Y.-J.; Cho, K.-H.; Kim, S.: Robust design of reactor power control system with genetric algorithm-applied weighting functions. Journal of the Koream Nuclear Society 30 (1998) 4, pp. 353–363.

LINK 2020

Link: End mills in solid carbide with variable pitch. https://www.linkindustrialtools.com/en/end-mills-in-solid-carbide-with\-variable-pitch-universal-kerfolg-vari-z4.html - 31.3.2020.

LOEIS 2013

Loeis, K.: Entwicklung und Implementierung eines adaptiven Filters zur aktiven Schwingungsreduzierung in Holzbearbeitungsmaschinen. PhD Thesis. Technische Universität Braunschweig (2013). Essen, Germany: Vulkan 2013. ISBN: 978-3-8027-8331-9.

LOIX & VERSCHUEREN 2004

Loix, N.; Verschueren, J. P.: Stand Alone Active Damping Device. In: Proceedings of the 9th International Conference on New Actuators. Bremen, Germany 2004. pp. 14–16.

LUNZE 2010

Lunze, J.: Regelungstechnik 1 – Systemtheoretische Grundlagen, Analyse und Entwurf einschleifiger Regelungen. 8. Berlin: Springer 2010. ISBN: 978-3-6421-3808-9.

LYSEN 1955

Lysen, H. W.: Statische und dynamische Stabilität der Werkstoff-Formung. In: Werkzeugmaschinen-Praxis, Sonderheft 2. FoKoMa (Forschungs- und Konstruktionskolloquium Werkzeugmaschinen). Munich, Germany 1955.

MADOLIAT ET AL. 2011

Madoliat, R.; Hayati, S.; Ghalebahman, A. G.: Modeling and Analysis of Frictional Damper Effect on Chatter Suppression in a Slender Endmill Tool. Journal of Advanced Mechanical Design, Systems, and Manufacturing 5 (2011) 2, pp. 115–128.

MANCISIDOR ET AL. 2014

Mancisidor, I.; Munoa, J.; Barcena, R.: Optimal control laws for chatter suppression using inertial actuator in milling processes. In: 11th International Conference on High Speed Machining (HSM). Prague, Czech Republic 2014.

MANCISIDOR ET AL. 2015

Mancisidor, I.; Munoa, J.; Barcena, R.; Beudaert, X.; Zatarain, M.: Coupled model for simulating active inertial actuators in milling processes. The International Journal of Advanced Manufacturing Technology 77 (2015) 1-4, pp. 581–595.

MANCISIDOR ET AL. 2018

Mancisidor, I.; Beudaert, X.; Aguirre, G.; Barcena, R.; Munoa, J.: Development of an Active Damping System for Structural Chatter Suppression in Machining Centers. International Journal of Automation Technology 12 (2018) 5, pp. 642–649.

MANCISIDOR ET AL. 2019a

Mancisidor, I.; Pena-Sevillano, A.; Dombovari, Z.; Barcena, R.; Munoa, J.: Delayed feedback control for chatter suppression in turning machines. Mechatronics 63 (2019), p. 102276.

MANCISIDOR ET AL. 2019b

Mancisidor, I.; Sevillano, A. P.; Barcena, R.; Franco, O.; Munoa, J.; Lacalle, L. N. L. D.: Comparison of model free control strategies for chatter suppression by an inertial actuator. International Journal of Mechatronics and Manufacturing Systems 12 (2019) 3/4, p. 164.

MANKINS 1995

Mankins, J.: Technology Readiness Level – A White Paper. Advanced Concepts Office, Office of Space Access and Technology (1995).

MANOHARAN 2012

Manoharan, D.: Aktive Systeme zur Leistungssteigerung von Fräsprozessen. PhD Thesis. RWTH Aachen (2012). Aachen, Germany: Apprimus 2012. ISBN: 978-3-8635-9063-5. (Ergebnisse aus der Produktionstechnik 9/2012).

MAPAL 2018

MAPAL: IMPULSE: Zerspanung auf dem Weg zur Elektromobilität. https://www.mapal.com/fileadmin/mapal_ftp/Blaetterkataloge/catalogs/MAPAL-IMPULSE-66/pdf/MAPAL-IMPULSE-66.pdf - 23.03.2020.

MENEROUD ET AL. 2016

Meneroud, P.; Bouchet, C.; Pages, A.: Compact, Efficient and Controllable Moving Iron Actuation Chain for Industrial Application. In: Borgmann, H. (Editor): ACTUATOR 2016. Bremen, Germany: Messe Bremen WFB Wirtschaftsförderung Bremen GmbH 2016. pp. 143–147.

MERDOL & ALTINTAS 2004

Merdol, S. D.; Altintas, Y.: Mechanics and Dynamics of Serrated Cylindrical and Tapered End Mills. Journal of Manufacturing Science and Engineering 126 (2004) 2, pp. 317–326.

MERINO ET AL. 2019

Merino, R.; Bediaga, I.; Iglesias, A.; Munoa, J.: Hybrid Edge–Cloud-Based Smart System for Chatter Suppression in Train Wheel Repair. Applied Sciences 9 (2019) 20, p. 4283.

MERRIT 1965

Merrit, H. E.: Theory of self-excited machine-tool chatter-contribution to machine tool chatter. ASME Journal of Engineering for Industry 87 (1965) 4, pp. 447–454.

MESCHKE 1995

Meschke, J.: Verbesserung des dynamischen Verhaltens von Werkzeugmaschinen durch Erhöhung der Systemdämpfung. PhD Thesis. Technische Universität Braunschweig (1995). Essen, Germany: Vulkan 1995.

METRA MESS- UND FREQUENZTECHNIK 2017

Metra Mess- und Frequenztechnik: IEPE-Standard. https://www.mmf.de/iepe-standard.htm - 16.09.2017.

METRA MESS- UND FREQUENZTECHNIK IN RADEBEUL E.K. 2020

Metra Mess- und Frequenztechnik in Radebeul e.K.: KS80D. https://www.mmf.de/images/large/ks80D.jpg - 20.03.2020.

MICHELS 1999

Michels, F.: Stabilisierung des Schleifprozesses mit aktiven Systemen. PhD Thesis. RWTH Aachen (1999). Aachen, Germany: Shaker 1999. (Berichte aus der Produktionstechnik 9/1999).

MICROMEGA DYNAMICS 2020

Micromega Dynamics: Active Dampers. https://micromega-dynamics.com/products/building_blocks/active-damper/ - 23.3.2020.

MÖHRING ET AL. 2015

Möhring, H.-C.; Brecher, C.; Abele, E.; Fleischer, J.; Bleicher, F.: Materials in machine tool structures. CIRP Annals 64 (2015) 2, pp. 725–748.

MOKHTARPOUR & HASSANPOUR 2012

Mokhtarpour, L.; Hassanpour, H.: A self-tuning hybrid active noise control system. Journal of the Franklin Institute 349 (2012) 5, pp. 1904–1914.

MONNIN ET AL. 2014a

Monnin, J.; Kuster, F.; Wegener, K.: Optimal control for chatter mitigation in milling–Part 1: Modeling and control design. Control Engineering Practice 24 (2014), pp. 156–166.

MONNIN ET AL. 2014b

Monnin, J.; Kuster, F.; Wegener, K.: Optimal control for chatter mitigation in milling–Part 2: Experimental validation. Control Engineering Practice 24 (2014), pp. 167–175.

MOSCHYTZ & HOFBAUER 2000

Moschytz, G. S.; Hofbauer, M.: Adaptive Filter: Eine Einführung in die Theorie mit Aufgaben und MATLAB-Simulationen auf CD-ROM. Berlin, Heidelberg: Springer 2000. ISBN: 978-3-642-18250-1.

MÜLLER 1996

Müller, K.: Entwurf robuster Regelungen. Wiesbaden and s.l.: Vieweg+Teubner 1996. ISBN: 3-519-06173-2.

MUNOA ET AL. 2013

Munoa, J.; Mancisidor, I.; Loix, N.; Uriarte, L. G.; Barcena, R.; Zatarain, M.: Chatter suppression in ram type travelling column milling machines using a biaxial inertial actuator. CIRP Annals 62 (2013) 1, pp. 407–410.

MUNOA ET AL. 2015

Munoa, J.; Beudaert, X.; Erkorkmaz, K.; Iglesias, A.; Barrios, A.; Zatarain, M.: Active suppression of structural chatter vibrations using machine drives and accelerometers. CIRP Annals 64 (2015) 1, pp. 385–388.

MUNOA ET AL. 2016a

Munoa, J.; Beudaert, X.; Dombovari, Z.; Altintas, Y.; Budak, E.; Brecher, C.; Stepan, G.: Chatter suppression techniques in metal cutting. CIRP Annals 65 (2016) 2, pp. 785–808.

MUNOA ET AL. 2016b

Munoa, J.; Iglesias, A.; Olarra, A.; Dombovari, Z.; Zatarain, M.; Stepan, G.: Design of self-tuneable mass damper for modular fixturing systems. CIRP Annals 65 (2016) 1, pp. 389–392.

NATKE 1983

Natke, H. G.: Einführung in Theorie und Praxis der Zeitreihen- und Modalanalyse: Identifikation schwingungsfähiger elastomechanischer Systeme. Wiesbaden: Springer 1983. ISBN: 978-3-528-08145-4.

NEUGEBAUER ET AL. 2007

Neugebauer, R.; Denkena, B.; Wegener, K.: Mechatronic Systems for Machine Tools. CIRP Annals 56 (2007) 2, pp. 657–686.

NEUGEBAUER ET AL. 2010

Neugebauer, R.; Pagel, K.; Bucht, A.; Wittstock, V.; Pappe, A.: Control concept for piezo-based actuator-sensor-units for uniaxial vibration damping in machine tools. Production Engineering 4 (2010) 4, pp. 413–419.

NIEHUES 2016

Niehues, K.: Identifikation linearer Dämpfungsmodelle für Werkzeugmaschinenstrukturen. PhD Thesis. Technische Universität München (2016). Munich, Germany: Herbert Utz 2016. ISBN: 978-3-8316-4568-8. (Forschungsberichte IWB 318).

ORMONDROYD & DEN HARTOG 1928

Ormondroyd, J.; Den Hartog, J. P.: The theory of the dynamic vibration absorber. Journal of Applied Mechanics 49-50 (1928), pp. 9–22.

PAHL ET AL. 2007

Pahl, G.; Beitz, W.; Feldhusen, J.; Grote, K.-H.: Konstruktionslehre: Grundlagen erfolgreicher Produktentwicklung; Methoden und Anwendung. 7th edition. Berlin and Heidelberg: Springer 2007. ISBN: 978-3-5403-4060-7.

PARK ET AL. 2007

Park, G.; Bement, M. T.; Hartman, D. A.; Smith, R. E.; Farrar, C. R.: The use of active materials for machining processes: A review. International Journal of Machine Tools and Manufacture 47 (2007) 15, pp. 2189–2206.

PARUS ET AL. 2013

Parus, A.; Powałka, B.; Marchelek, K.; Domek, S.; Hoffmann, M.: Active vibration control in milling flexible workpieces. Journal of Vibration and Control 19 (2013) 7, pp. 1103–1120.

PEETERS ET AL. 2004

Peeters, B.; van der Auweraer, H.; Leuridan, J.; Vasel, T.: PolyMAX Modal Parameter Estimation: Challenging Automotive and Aerospace Applications. In: VDI-Schwingungstagung. Düsseldorf: VDI 2004. VDI-Berichte. pp. 1–13.

PEETERS ET AL. 2008

Peeters, B.; Lau, J.; Lanslot, J.; Van der Auweraer, H.: Automatic modal analysis-Myth or reality? Sound and Vibration 42 (2008) 3, pp. 17–21.

PEREIRA ET AL. 2014

Pereira, E.; Díaz, I. M.; Hudson, E. J.; Reynolds, P.: Optimal control-based methodology for active vibration control of pedestrian structures. Engineering Structures 80 (2014), pp. 153–162.

POLICARPO ET AL. 2013

Policarpo, H.; Neves, M.; Maia, N.: A simple method for the determination of the complex modulus of resilient materials using a longitudinally vibrating three-layer specimen. Journal of sound and vibration 332 (2013) 2, pp. 246–263.

PREUMONT 2002

Preumont, A.: Vibration Control of Active Structures: An Introduction. 2nd edition. Dordrecht: Kluwer Academic Publishers 2002. ISBN: 1-4020-0496-6. (Solid Mechanics and Its Applications 96).

PRITSCHOW & CROON 2013

Pritschow, G.; Croon, N.: Ball screw drives with enhanced bandwidth by modification of the axial bearing. CIRP Annals 62 (2013) 1, pp. 383–386.

PRITSCHOW ET AL. 2003

Pritschow, G.; Eppler, C.; Lehner, W.-D.: Ferraris Sensor – The Key for Advanced Dynamic Drives. CIRP Annals 52 (2003) 1, pp. 289–292.

PU ET AL. 2014

Pu, Y.; Zhang, F.; Jiang, J.: A new online secondary path modeling method for adaptive active structure vibration control. Smart Materials and Structures 23 (2014) 065015.

QUINTANA & CIURANA 2011

Quintana, G.; Ciurana, J.: Chatter in machining processes: A review. International Journal of Machine Tools and Manufacture 51 (2011) 5, pp. 363–376.

RASHID & MIHAI NICOLESCU 2006

Rashid, A.; Mihai Nicolescu, C.: Active vibration control in palletised workholding system for milling. International Journal of Machine Tools and Manufacture 46 (2006) 12-13, pp. 1626–1636.

RAYLEIGH 1877

Rayleigh, J.: The Theory of Sound. 1st edition. London: Macmillan and co. 1877.

REBELEIN 2019

Rebelein, C.: Prognosefähige Simulation von Dämpfungseffekten in mechatronischen Werkzeugmaschinenstrukturen. PhD Thesis. Technische Universität München (2019). Munich, Germany: Herbert Utz 2019. ISBN: 978-3-8316-4790-3. (Forschungsberichte IWB 346).

REINHART & SCHINDLER 2012

Reinhart, G.; Schindler, S.: Strategic Evaluation of Technology Chains for Producing Companies. In: ElMaraghy, H. A. (Editor): Enabling Manufacturing Competitiveness and Economic Sustainability. Berlin, Heidelberg: Springer 2012. pp. 391–396.

REITHOFER 2010

Reithofer, N.: Mobilität neu gedacht. In: Hoffmann, H.; Reinhart, G.; Zäh, M. (Editor): Münchener Kolloquium: Innovationen für die Produktion (Produktionskongress 2010). Munich: Utz 2010. pp. 19–30.

RIES ET AL. 2006

Ries, M.; Pankoke, S.; Gebert, K.: Increase of Material Removal Rate with an Active HSC Milling Spindle. In: Proceedings of the Adaptronic Congress 2006. Göttingen, Germany 2006.

ROTH 2009

Roth, M.: Einsatz und Beurteilung eines aktiven Strukturdämpfers in einem Bearbeitungszentrum. PhD Thesis. Technische Universität Darmstadt (2009). Aachen, Germany: Shaker 2009. ISBN: 978-3-8322-8256-1.

SALLESE ET AL. 2017

Sallese, L.; Innocenti, G.; Grossi, N.; Scippa, A.; Flores, R.; Basso, M.; Campatelli, G.: Mitigation of chatter instabilities in milling using an active fixture with a novel control strategy. The International Journal of Advanced Manufacturing Technology 89 (2017) 9, pp. 2771–2787.

SANDVIK COROMANT 2020

Sandvik Coromant: Silent Tools Damped machining tools. https://www.sandvik.coromant.com/en-gb/products/silent_tools/pages/default.aspx - 23.3.2020.

SCHINDLER 2015

Schindler, S.: Strategische Planung von Technologieketten für die Produktion. PhD Thesis. Technische Universität München (2015). Munich, Germany: Herbert Utz 2015. ISBN: 978-3-8316-4434-6. (Forschungsberichte IWB 294).

SCHÖNHOFF 2003

Schönhoff, U.: Practical Robust Control of Mechatronical Systems with Structural Flexibilities. PhD Thesis. Technische Universität Darmstadt (2003). Darmstadt, Germany: Shaker 2003. Forschungsberichte Mechatronik & Maschinenakustik.

SCHULZ 2010

Schulz, A.: Elektrohydraulisches aktives Dämpfungssystem für Werkzeugmaschinenstrukturen. PhD Thesis. RWTH Aachen (2010). Aachen, Germany: Apprimus-Verlag 2010. ISBN: 978-3-9405-6546-4. (Ergebnisse aus der Produktionstechnik Werkzeugmaschinen 3/2010).

SCHUMACHER 2013

Schumacher, A.: Optimierung mechanischer Strukturen: Grundlagen und industrielle Anwendungen. 2nd edition. Berlin and Heidelberg: Springer 2013. ISBN: 978-3-642-34699-6.

SCHWARZ & RICHARDSON 1999

Schwarz, B. J.; Richardson, M. H.: Experimental modal analysis. CSI Reliability week 35 (1999) 1, pp. 1–12.

SCHWARZ 2015

Schwarz, S.: Prognosefähigkeit dynamischer Simulationen von Werkzeugmaschinenstrukturen. PhD Thesis. Technische Universität München (2015). Munich, Germany: Herbert Utz 2015. ISBN: 978-3-8316-4542-8. (Forschungsberichte IWB 313).

SEMM ET AL. 2020

Semm, T.; Spescha, D.; Ceresa, N.; Wegener, K.; Zaeh, M. F.: Efficient Dynamic Machine Tool Simulation with Included Damping and Linearized Friction Effect. In: Proceedings of the 53rd CIRP Conference on Manufacturing Systems (CMS). Chicago, IL 2020.

SHENGKUI ET AL. 2007

Shengkui, Z.; Zhihong, M.; Suiyang, K.: A fast variable step-size LMS algorithm with system identification. In: 2nd IEEE Conference on Industrial Electronics and Applications. Harbin, China 2007. pp. 2340–2345.

SHIRAISHI ET AL. 1991

Shiraishi, M.; Yamanaka, K.; Fujita, H.: Optimal control of chatter in turning. International Journal of Machine Tools and Manufacture 31 (1991) 1, pp. 31–43.

SIMNOFSKE 2009

Simnofske, M.: Adaptronische Versteifung von Werkzeugmaschinen durch strukturintegrierte aktive Module. PhD Thesis. Technische Universität Braunschweig (2009). Braunschweig, Germany: Vulkan 2009. ISBN: 978-3-8027-8306-7.

SIMS 2007

Sims, N. D.: Vibration absorbers for chatter suppression: A new analytical tuning methodology. Journal of Sound and Vibration 301 (2007) 3-5, pp. 592–607.

SKF 2020

SKF: Magnetic Bearings. https://www.skf.com/uk/products/magnetic-bearings-systems/systems-and-support - 03.04.2020.

SMITH & TLUSTY 1992

Smith, S.; Tlusty, J.: Stabilizing chatter by automatic spindle speed regulation. CIRP Annals 41 (1992) 1, pp. 433–436.

SORALUCE 2020

SORALUCE: Fahrständer Fräs-, Dreh- und Bohrcenter. https://www.bimatec-soraluce.de/maschine/fahrstaender-fraes-dreh-und-bohrcenter-fp/ - 21.05.2020.

STEPHENS 1996

Stephens, C. R., L. und Knospe: μ-Synthesis based, robust conroller design for AMB machining spindles. In: 5th International Symposium on Magnetic Bearings. Kanazawa, Japan 1996. pp. 153–158.

TAYLOR 1907

Taylor, F. W.: On the Art of Cutting Metals. Transactions of the American Society of Mechanical Engineers (1907).

TELLBÜSCHER 1986

Tellbüscher, E.: Konstruktion von Dämpfern und deren Einsaz an Rundschleifmaschinen. PhD Thesis. Universität Hannover (1986). Hannover, Germany: VDI 1986.

TEWANI ET AL. 1995

Tewani, S. G.; Rouch, K. E.; Walcott, B. L.: A study of cutting process stability of a boring bar with active dynamic absorber. International Journal of Machine Tools and Manufacture 35 (1995) 1, pp. 91–108.

TLUSTY & POLACEK 1963

Tlusty, J.; Polacek, M.: The stability of machine tools against self-excited vibrations in machining (1963), pp. 465–474.

TOBIAS & FISHWICK 1958

Tobias, S. A.; Fishwick, W.: Theory of regenerative machine tool chatter. Engineering 205 (1958).

TØFFNER-CLAUSEN 1996

Tøffner-Clausen, S.: System Identification and Robust Control: A Case Study Approach. London: Springer 1996. ISBN: 9781447115137. Advances in Industrial Control.

TÖNSHOFF ET AL. 2002

Tönshoff, H. K.; Denkena, B.; Götz, T.: Piezoelectric Actuator Based Preload Control Unit for Machine Tool Spindles. WGP Annals IX (2002) 1, pp. 117–122.

TRAVERSTOOL 2020

TraversTool: Variable Helix End Mill. https://www.travers.com/variable-helix-end-mill/p/20-452-462/ - 31.3.2020.

TUYSUZ & ALTINTAS 2017

Tuysuz, O.; Altintas, Y.: Frequency Domain Updating of Thin-Walled Workpiece Dynamics Using Reduced Order Substructuring Method in Machining. Journal of Manufacturing Science and Engineering 139 (2017) 7, pp. 071013–1–16.

UHLMANN ET AL. 2017

Uhlmann, E.; Kushwaha, S.; Mewis, J.; Richarz, S.: Automatic design and synthesis of control for a plug and play active vibration control module. Journal of Vibration and Control 24 (2017) 11, pp. 2261–2273.

UNBEHAUEN 2009

Unbehauen, H.: Zustandsregelungen, digitale und nichtlineare Regelsysteme. 9th edition. Wiesbaden: Vieweg+Teubner 2009. ISBN: 978-3-528-83348-0. Automatisierungstechnik.

URBIKAIN ET AL. 2015

Urbikain, G.; Campa, F.-J.; Zulaika, J.-J.; López de Lacalle, L.-N.; Alonso, M.-A.; Collado, V.: Preventing chatter vibrations in heavy-duty turning operations in large horizontal lathes. Journal of Sound and Vibration 340 (2015), pp. 317–330.

VAN DIJK ET AL. 2012

van Dijk, N. J. M.; van de Wouw, N.; Doppenberg, E. J. J.; Oosterling, H. A. J.; Nijmeijer, H.: Robust Active Chatter Control in the High-Speed Milling Process. IEEE Transactions on Control Systems Technology 20 (2012) 4, pp. 901–917.

VDI 2062-1 2011

VDI 2062-1: Vibration insulation - Terms and methods. Berlin: Beuth 2011.

VDI 3833-1 2014

VDI 3833-1: Dynamic damper and dynamic vibration absorber - Dynamic damper - Fundamentals, characteristics, implementation, application. Berlin: Beuth 2014.

VOGEL ET AL. 2019

Vogel, F. A.; Berger, S.; Özkaya, E.; Biermann, D.: Vibration Suppression in Turning TiAl6V4 Using Additively Manufactured Tool Holders with Specially Structured, Particle Filled Hollow Elements. Procedia Manufacturing 40 (2019), pp. 32–37.

WAIBEL 2012

Waibel, M.: Aktive Zusatzsysteme zur Schwingungsreduktion an Werkzeugmaschinen. PhD Thesis. TU München (2012). Munich, Germany: Utz 2012. ISBN: 978-3-8316-4250-2. (Forschungsberichte IWB 273).

WECK & BRECHER 2006a

Weck, M.; Brecher, C.: Werkzeugmaschinen 2: Konstruktion und Berechnung. 8th edition. Berlin, Heidelberg: Springer 2006. ISBN: 3-540-22502-1.

WECK & BRECHER 2006b

Weck, M.; Brecher, C.: Werkzeugmaschinen 3: Mechatronische Systeme, Vorschubantriebe, Prozessdiagnose. 6th edition. Berlin, Heidelberg: Springer 2006. ISBN: 3-540-22506-5.

WECK & BRECHER 2006c

Weck, M.; Brecher, C.: Werkzeugmaschinen 5: Messtechnische Untersuchung und Beurteilung, dynamische Stabilität. 7th edition. Berlin, Heidelberg: Springer 2006. ISBN: 3-540-32951-0.

WELCH 1967

Welch, P.: The use of fast Fourier transform for the estimation of power spectra: a method based on time averaging over short, modified periodograms. IEEE Transactions on audio and electroacoustics 15 (1967) 2, pp. 70–73.

WEREMCZUK ET AL. 2015

Weremczuk, A.; Rusinek, R.; Warminski, J.: The Concept of Active Elimination of Vibrations in Milling Process. Procedia CIRP 31 (2015), pp. 82–87.

WERNER 2017

Werner, H.: Optimal and Robust Control - Lecture Notes. https://www.tuhh.de/t3resources/ics/PDFs/Opt_Robust_Ctrl/orc.pdf - 31.3.2020.

WERNTZE 1973

Werntze, G.: Dynamische Schnittkraftkoeffizienten: Bestimmung mit Hilfe des Digitalrechners und Berücksichtigung im mathematischen Modell zur Stabilitätsanalyse. PhD Thesis. RWTH Aachen (1973). Aachen, Germany 1973.

WITT 2007

Witt, S. T.: Integrierte Simulation von Maschine, Werkstück und spanendem Fertigungsprozess. PhD Thesis. RWTH Aachen (2007). Aachen, Germany: Shaker 2007. ISBN: 978-3-8322-6810-7. (Berichte aus der Produktionstechnik 31/2007).

WORONKO ET AL. 2003

Woronko, A.; Huang, J.; Altintas, Y.: Piezoelectric tool actuator for precision machining on conventional CNC turning centers. Precision Engineering 27 (2003) 4, pp. 335–345.

YAMATO ET AL. 2018

Yamato, S.; Ito, T.; Matsuzaki, H.; Kakinuma, Y.: Programmable Optimal Design of Sinusoidal Spindle Speed Variation for Regenerative Chatter Suppression. Procedia Manufacturing 18 (2018), pp. 152–160.

YANG ET AL. 2010

Yang, Y.; Muñoa, J.; Altintas, Y.: Optimization of multiple tuned mass dampers to suppress machine tool chatter. International Journal of Machine Tools and Manufacture 50 (2010) 9, pp. 834–842.

ZAEH & PIECZONA 2018

Zaeh, M.; Pieczona, S.: Adaptive inverse control of a galvanometer scanner considering the structural dynamic behavior. Cirp Annals 67 (2018) 1, pp. 385–388.

ZAEH ET AL. 2009

Zaeh, M. F.; Waibel, M.; Baur, M.: A Computational Approach to the Integration of Adaptronical Structures in Machine Tools. In: Yuan, Y.; Cui, J. (Editor): Computational structural engineering. New York, NY: Springer 2009. pp. 1017–1028.

ZAEH ET AL. 2017, publication ⑤

Zaeh, M. F.; Kleinwort, R.; Fagerer, P.; Altintas, Y.: Automatic tuning of active vibration control systems using inertial actuators. CIRP Annals 66 (2017) 1, pp. 365–368.

ZATARAIN ET AL. 2005

Zatarain, M.; Ruiz de Argandoña, I.; Illarramendi, A.; Azpeitia, J. L.; Bueno, R.: New Control Techniques Based on State Space Observers for Improving the Precision and Dynamic Behaviour of Machine Tools. CIRP Annals 54 (2005) 1, pp. 393–396.

ZATARAIN ET AL. 2008

Zatarain, M.; Bediaga, I.; Muñoa, J.; Lizarralde, R.: Stability of milling processes with continuous spindle speed variation: Analysis in the frequency and time domains, and experimental correlation. CIRP Annals 57 (2008) 1, pp. 379–384.

ZHANG ET AL. 2001

Zhang, M.; Lan, H.; Ser, W.: Cross-updated active noise control system with online secondary path modeling. IEEE Transactions on speech and audio processing 9 (2001) 5, pp. 598–602.

ZHANG & SIMS 2005

Zhang, Y.; Sims, N. D.: Milling workpiece chatter avoidance using piezoelectric active damping: a feasibility study. Smart Materials and Structures 14 (2005) 6, pp. N65–N70.

ZHOU ET AL. 1996

Zhou, K.; Doyle, J. C.; Glover, K.: Robust and Optimal Control. Upper Saddle River, NJ: Prentice Hall 1996. ISBN: 0-13-456567-3.

ZHU & LIU 2020

Zhu, L.; Liu, C.: Recent progress of chatter prediction, detection and suppression in milling. Mechanical Systems and Signal Processing 143 (2020), pp. 106840–1–37.

ZULAIKA ET AL. 2011

Zulaika, J. J.; Campa, F. J.; Lopez de Lacalle, L.N.: An integrated process–machine approach for designing productive and lightweight milling machines. International Journal of Machine Tools and Manufacture 51 (2011) 7-8, pp. 591–604.

List of Supervised Student Theses

In the course of writing this dissertation, the following student theses were written at the *Institute for Machine Tools and Industrial Management* of the Technical University of Munich (TUM) in the years from 2014 to 2018 under essential scientific, technical and content-related guidance of the author. Among other things, these theses examined questions on the dimensioning and commissioning of active vibration control systems. Some of the results have been incorporated into this document. The author would like to thank all students for their commitment in supporting this scientific work.

Student	**Title of the Thesis**
Cavalié Jaramillo, Sebastian Benedict	Implementation of a simulation method to predict the increase of the energy efficiency for an active damped milling machine (submission: March 2015)
Kapfinger, Philipp	Implementation of a milling process simulation for an energy demand analysis (submission: April 2015)
Merz, Maximilian	Study of different filter strategies for active vibration damping of machine tools (submission: April 2015)
Yilmaz, Mustafa	Experimental modal analysis of a five axis milling machine (submission: May 2015)
Schweizer, Martin	Design and implementation of model based control strategies for active damping of milling machines (submission: June 2015)
Wankmiller, German	Implementation and analysis of modern filter strategies for active vibration control of machine tools (submission: February 2016)
Wirtz, Stefanie	Analysis and evaluation of the performance of different control strategies for active damping (submission: May 2016)
Fagerer, Peter	Automatic system identification using a proof-mass actuator (submission: October 2016)
Sellemond, Markus	Extension of an active damping controller for multi-axis machining (submission: October 2016)
Platz, Jonathan	Methodological optimization of an adaptive controller for active damping of machine tools (submission: November 2016)
Herb, Johannes	Automatic calibration of a robust controller for active damping using an proof-mass actuator (submission: May 2017)
Weishaupt, Philipp	Methodology for a simulation-based design of proof mass actuators for active vibration control of machine tools (submission: July 2017)
Platz, Jonathan	Implementation of an adaptive active vibration control system on a Programmable Logic Controller (submission: August 2017)
Kapfinger, Philipp	Evaluation of the robustness of an active vibration control system in the industrial application (submission: September 2018)